P450 BM3 ELECTROCHEMISTRY AND ELECTROCATALYSIS

Thesis by

Andrew K. Udit

In Partial Fulfillment of the Requirements for the

Degree of

Doctor of Philosophy

CALIFORNIA INSTITUTE OF TECHNOLOGY

Pasadena, California

2005

(Defended May 9, 2005)

ACKNOWLEDGEMENTS

My tenure at Caltech has been filled with collaborative efforts and fruitful interactions. Accordingly, there are a number of people who need to be acknowledged.

First, I would like to acknowledge my two advisors, Frances Arnold and Harry Gray. This pairing of advisors may seem odd: Frances's interest in engineering and biocatalysis is in stark contrast to Harry's endeavors into fundamental electron transfer. However, with a thesis entitled "P450 BM3 Electrochemistry and Electrocatalysis," you can imagine how this would appeal to both. Harry's enthusiasm was offset by Frances's practicality, giving me a balanced perspective and unique insights into the research. Most important, I would like to thank them for allowing me to freely pursue my own scientific endeavors.

Mike Hill taught me everything I know about electrochemistry. Over the years he has become a mentor and a wonderful friend. Carlos Martinez was the first person I worked with at Caltech. Carlos taught me all the basic tools and tricks of molecular biology. To this day, he too remains a great friend.

Susan Schofer kindly gave much of her time to help me synthesize my cobalt molecule. Steve Contakes provided many unique insights and discussions. Wendy, Yen, and Phoebe dragged me into the world of NOS; I'm glad they did – we had a lot of fun with the so-called "two-day paper." Katsumi Niki introduced me to SAMs, and provided many stimulating conversations. I feel honored to have had the opportunity to work with Katsumi; his recent passing is a great loss to the field of protein electrochemistry. Joff Silberg, Edgardo Farinas, Pat Cirino, and Daisuke Umeno provided thought-provoking scientific discussions, and invaluable assistance in the lab.

I am fortunate to have had the experience of working with some very talented undergraduates; Nareen Hindoyan and Bridget Sabat from Occidental College, and Nick Halpern-Manners and Kevin Peng from Caltech were all fantastic. Others that deserve to be mentioned: Geethani Bandara for helping with various things, from protein purification to finding me bench space; Pat Farmer and Emek Blair at UCI for invaluable assistance in protein electrochemistry; Tom Poulos and Yerga Meharenna at UCI for helpful discussions; Dave Goodin at Scripps for his insights into NOS; Pat Collier and Garrett Bittner for allowing me to participate in their interesting research; NSERC for kindly granting tenure of my scholarship outside of Canada for all four years.

The personal acknowledgements follow. First, I have a great group of friends who have been with me from the start: Rebecca, Jeremy, and Susanna have provided both amusement and support. My fondest memories are of those early years, particularly Happy Hour at McCormick's: you can't beat a $3 martini.

Jolene Fernandes: surely, anything I say here will not do her justice. Over the last three years she has been a constant source of love and compassion. It's amazing she has put up with me for this long.

Finally, whatever success I have in life is due to the unwavering love and support of my family. My parents, David and Carmelita, have guided me through all of life's challenges. My sister, Jessica, is both a headache and a source of joy. My grandmother (Nan) and my aunt Lolita (Aunty) have always supported me, and cooked for me whenever Mom was away. Because of them, I have no fear of pushing forward in life; if I fall, they will always be there to catch me. But then, I don't intend to fall.

ABSTRACT

Cytochromes P450 catalyze monooxygenations of relatively inert substrates. The significance of this activity in physiology and industry has inspired many to capture this activity *in vitro*. However, practical applications of P450s will continue to be hindered by the need for reducing equivalents from NAD(P)H. While electrochemical methods provide a potential solution, the difficulty in achieving good electronic coupling to the heme remains an enormous obstacle.

Flavocytochrome P450 BM3 is soluble, well-characterized, and easily manipulated, making it a good target for *in vitro* applications. Bioelectrocatalysis was first attempted with holo BM3 using a novel electrochemical mediator, 1,1'-dicarboxycobaltocene (M_{red}). Absorption spectroscopy confirmed electron transfer (ET) from M_{red} to the cofactors, while electrolyses resulted in M_{red}-mediated hydroxylation of lauric acid by both the holo (16.5 nmol product / nmol enzyme / min) and heme proteins (hBM3) (1.8 nmol product / nmol enzyme / min).

Subsequent bioelectrocatalysis was attempted with the more stable hBM3. We achieved direct electrochemistry of hBM3 by wiring it through engineered surface Cys^{387} to a basal plane graphite electrode (BPG) with 1-pyreneiodoacetamide (Py). AFM images revealed that only pyrene-wired enzyme molecules adsorb to BPG. k^o for the BPG-Py-hBM3 system was 650 ± 50 s^{-1}. Rotated-disk electrode (RDE) experiments show that the BPG-Py-hBM3 system catalyzes the four-electron reduction of dioxygen to water. Analogous experiments were performed with enzyme labeled at Cys^{62}, which is spatially adjacent to Cys^{387} but does not provide a similar well-coupled through-bond pathway to the heme. Surprisingly, the Cys^{62} mutant showed similar electrode kinetics,

demonstrating that the pyrene tether does not provide a unique pathway, but probably anchors the protein onto the electrode surface in a favorable docking mode for ET.

Extensive electrochemical characterization of hBM3 was conducted in various surfactant films on BPG. Cyclic voltammetry of hBM3 in SDS films revealed the $Fe^{III/II}$ redox couple at -330 mV (vs. Ag/AgCl, pH 7.4), and k^o of 40 s^{-1}. Although voltammetry confirmed catalytic dioxygen reduction by Fe^{II}, substrate oxidation was not observed.

Voltammetry of hBM3 mutant 1-12G in DDAPSS films revealed $Fe^{III/II}$ (-202 mV) and $Fe^{II/I}$ (-1082 mV) redox couples of the heme (pH 7). Catalytic activity included dioxygen reduction by Fe^{II}, and reductive dehalogenation by Fe^{I}. Voltammetry on hBM3 in DDAPSS revealed that hBM3 and 1-12G display distinct redox properties. Absorption spectra in solution showed the Fe^{III} Soret at 418 nm for hBM3, and a split Soret for 1-12G at 390 and 418 nm. Voltammetry of the proteins within DDAPSS films revealed nearly identical $Fe^{III/II}$ potentials (~ -200 mV), but significant differences in k^o, 250 vs. 30 s^{-1}, and $Fe^{III/II}$ – CO potentials, -140 vs. -115 mV, for hBM3 vs. 1-12G. Catalytic dioxygen reduction by the proteins on RDEs was analyzed using Levich and Koutecky-Levich treatments. Calculated values of n, 2.7 vs. 4.7, and k_{obs}, 1.4 x 10^6 vs. 1 x 10^5 $M^{-1}s^{-1}$, for hBM3 vs. 1-12G suggest that the two proteins differ strikingly in their reaction with dioxygen.

Using the prototypical cytochrome P450 CAM (CAM), we attempted to generate high-valent species of P450 in DDAB films. Performing rapid-scan (50 V/s) voltammetry revealed a couple (**E**) at 831 mV. **E** was not observed at scan rates less than 30 V/s at room temperature; however, at 4^{o}C **E** could be reversibly generated at 1 V/s. **E** was found to be sensitive to imidazole in solution and to variations in pH, suggesting that

the redox reaction is occurring at the metal center (i.e., $Fe^{IV/III}$) rather than at the porphyrin macrocycle. Electrolyses revealed that the electrochemically generated high-valent species is only capable of performing S-oxidation, converting thioanisole to methyl phenyl sulfoxide.

TABLE OF CONTENTS

LIST OF TABLES, SCHEMES, AND FIGURES

Chapter 1

Introduction and Background

Abbreviations: ET, electron transfer; P450, cytochrome P450; BM3, cytochrome P450 from *Bacillus megaterium*; CAM, cytochrome P450 from *Pseudomonas putida*.

Enzymes as Commercial Tools

The field of biocatalysis is constantly growing as scientists continue to search for industrial catalysts with minimal environmental consequences. In this regard, enzymes have already demonstrated their enormous commercial utility (e.g., in the synthesis of chiral compounds for use in pharmaceutical, agricultural, and food industries[1]). However, the relative complexity, instability, and (for some) slow reaction rates has limited the use of biocatalysts. Despite these drawbacks, popular demand for cleaner synthetic schemes utilizing environmentally friendly (so-called "green") catalysts will continue to fuel research into biological alternatives for chemical synthesis.

The group of proteins known as oxidoreductases has received special attention from industry for its ability to perform regio- and stereospecific reactions under physiological conditions. *In vivo*, oxidation reactions are critical for a broad range of biological processes, from hormone synthesis[2,*] to pro-drug activation.[3,†] Certainly, capturing oxidoreductase activity *in vitro* would facilitate medicinal fields by aiding in drug discovery and elucidating *in vivo* drug interactions.[4,5] In addition to medicinal chemistry, exploiting oxidoreductase activity would also greatly contribute to the stereo- and regiospecific synthesis of high-value molecules. In particular, achieving selective oxidation of alkanes is of considerable interest and worth.[6] While the inert nature of

[*] Hydroxylation of androgens to estrogens by oxidoreductases is essential for development of female sexual characteristics.
[†] Site-specific hydroxylation of the anticancer pro-drug cyclophosphoamide is required to generate the bio-active molecule

alkanes limits their use largely to combustion, selective functionalization results in molecules that can be used as building blocks for more complex structures.[7,‡] Oxidoreductase activity also has applications in bioremediation.[8]

Typically, commercial chemical oxidations require the use of powerful catalysts (e.g., Cr^{VI}, Mn^{VII}). Use of such catalysts has several drawbacks, including uncontrolled (over-) oxidation, poor regio- and stereoselectivity, toxicity (requiring proper handling and disposal), poor efficiency, and various side reactions.[9,10] Indeed, the harsh conditions required to drive these chemical conversions can also lead to degradation of the desired products (particularly true for medicinal compounds that likely have multiple functionalities). Thus, biocatalytic oxidation systems seem to be the clear choice for achieving selective oxidations. Unfortunately, exploiting oxidoreductase activity for commercial and medical applications has proven difficult, due in large part to the complexity of biological systems. For many oxidoreductases, this complexity often includes lengthy electron transfer (ET) chains that utilize several intermediate proteins and cofactors, each of which makes a specific interaction in order to achieve the required ET for subsequent catalysis. Consequently, these enzymes have realized only a small fraction of their potential.

The Cytochromes P450: Potential Tools

The superfamily of enzymes called cytochromes P450 (P450s) are heme-containing oxidoreductases that perform highly regio- and stereospecific reactions under physiological conditions. First discovered in 1960, to date more than 500 different P450s

‡ As an example, hydroxylated alkanes can be used to synthesize surfactants. The physical and chemical properties of the surfactant will be entirely dependent on the site of oxidation and the nature of the subsequent chemical modifications.

have been identified, cloned, and sequenced, resulting in a plethora of information on P450 structure, function, and biochemistry.[11-13] The diverse repertoire of reactions catalyzed by P450s is shown in **Table 1.1.** The hallmark reaction of this enzyme class is catalytic hydroxylation of hydrocarbons:

$$R\text{-}H + NAD(P)H + H^+ + O_2 \xrightarrow{P450} R\text{-}OH + NAD(P)^+ + H_2O$$

In vivo, P450s are critical for the biosynthesis of various hormones, eicosanoids, and prostaglandins.[5] In addition to catabolism, P450s also perform crucial oxidation reactions that determine the ultimate fate of many drugs and xenobiotics; for example, human microsomal P450s are known to metabolize more than 90% of all marketed drugs.[14] *In vitro*, P450s are capable of catalyzing many industrially valuable oxidation reactions, converting inert hydrocarbons into alcohols and ketones that can be used as precursors for more complex molecules.[6]

Broadly, P450s can be divided into two categories, mammalian and bacterial. Key differences between the two forms are found in solubility and electron transfer partners. Bacterial forms are soluble proteins that receive electrons from cytosolic ferredoxins (Fe-S proteins) and ferredoxin reductases. In contrast, mammalian forms are membrane-bound, and are reduced by membrane-associated flavin-containing reductases. In addition to these differences, the two classes also display low sequence identity (e.g., 16% amino acid identity between human cytochrome P450 1A2 and bacterial P450 BM3[15]); indeed, even closely related P450s are known to be somewhat divergent in sequence (e.g., 63% amino acid identity between *Bacillus* P450 homologs 102A1 and 102A2[16]). Despite this low sequence identity, all P450s do share a similar overall fold. Most contain heme domains that are 40-60 kDa with an approximate triangular prism

shape. In particular, the structure around the heme is known to be highly conserved, with all P450s possessing a thiolate ligand in the heme iron proximal coordination site.

Mechanism

The characteristic common to all P450s is the Soret band at ~ 450 nm of the $Fe^{II} - CO$ complex, which is diagnostic of a cysteinate ligand bound to the heme iron in a trans orientation relative to the carbon monoxide ligand.[17] Thiol ligation to the heme iron is postulated to be the critical factor that separates P450-type reactivity from other heme proteins (like myoglobin, which has a histidine-ligated heme) by modulating the heme redox properties to activate dioxygen for substrate oxidation.[18] Indeed, mutating this cysteine to another amino acid abolishes the unique chemistry catalyzed by P450.[19]

The scheme shown in **Figure 1.1** represents the generally accepted catalytic mechanism for P450.[12] The resting state is the six-coordinate low spin Fe^{III} (E^o between -330 and -370 mV vs. NHE, depending on the P450), with the porphyrin occupying the four planar positions and the axial positions occupied by a cysteine (proximal) and water (distal). Catalysis is initiated by substrate binding in the protein active site and displacement of the axial water, causing the six-coordinate low spin Fe^{III} to convert to five-coordinate high spin Fe^{III}. This shift in spin state is accompanied by a change in heme potential (substrate-dependent, but generally greater than +100 mV), which has been shown to initiate ET to the heme from native reductase proteins.[20] Reduction to Fe^{II} allows dioxygen to bind to the iron, forming the $Fe^{II} - O_2$ complex. A second reduction followed by protonation creates the peroxy complex, $Fe^{III} - OOH^-$, which is further protonated to yield a molecule of water and a high valent iron-oxo complex. The nature of this iron-oxo complex, formally referred to as compound I, is not definitively known.

Currently, there is no solid experimental evidence for the precise identity of this species. Two possibilities are generally considered: one is $Fe^{V} = O$, while the other is $Fe^{IV} = O(P^{+})$, where P^{+} represents a porphyrin cation radical. Whatever the true nature of compound I, it is believed that this species is responsible for substrate oxidation, producing the oxidized product and regenerating the P450 resting state.

Notably, an alternative catalytic pathway termed the "peroxide shunt" also exists. In this pathway, reduced dioxygen is supplied in the form of peroxide, which can enter the catalytic cycle and directly generate the $Fe^{III} - OOH^{-}$ complex in **Figure 1.1**.

Electrons and P450

NAD(P)H

Arguably, the key to the catalytic mechanism in **Figure 1.1** is ET. *In vivo*, the ultimate source of electrons for P450 catalysis is NAD(P)H: this requirement for NAD(P)H is perhaps the greatest obstacle standing in the way of commercial use of P450s for selective oxidations. NAD(P)H is expensive, decomposes over time, and is difficult to recover once oxidized. This has resulted in several investigations aimed at regenerating NAD(P)H. The most obvious regeneration method is to utilize an electrode. However, electrochemical regeneration of NAD(P)H proceeds through two one-electron transfer steps, which competes unfavorably with a pathway that forms biologically inactive dimers between the one-electron reduced form of the cofactor.[21] Chemical reductants for NAD(P)H have the additional drawback of either not being reusable or requiring regeneration themselves (which would typically utilize a negatively polarized electrode that can lead to NAD(P)H dimers).[22] Enzymatic recycling systems provide an

efficient way of regenerating NAD(P)H *in vitro*,[23] but having additional proteins in the system introduces several problems: 1) optimal conditions for the different proteins may not be compatible; 2) having other enzymes in solution could lead to unforeseen competing reactions; 3) additional reaction components can lead to greater difficulty in recovering the products. Finally, *in vivo* recycling systems that utilize whole-cell machinery for NAD(P)H regeneration usually suffer from poor reaction rates, in addition to the usual problems associated with whole-cell reactions (e.g., poor cell permeability of substrates/products, poor product recovery).[24]

Direct P450 Electrochemistry

An alternative approach for supplying reducing equivalents to P450 bypasses the NAD(P)H requirement altogether by delivering electrons to the protein directly with an electrode. Generally, direct protein electrochemistry has proven difficult: the intervening peptide medium results in relatively weak electronic coupling between buried cofactors and external reductants.[25-27] For P450, the heme is buried deep within the polypeptide, which means that success of an electrochemical method is going to depend on finding a way to increase electronic coupling between the heme and the electrode. Notably, direct electrochemistry at an unmodified edge-plane graphite electrode has been achieved with P450 from *Pseudomonas putida* (CAM); however, the study revealed that the system displayed poor electronic coupling, as evidenced by the slow and quasi-reversible ET.[28]

A survey of the available literature reveals several techniques for direct electrochemical reduction of P450. The first, and perhaps most general method for P450 reduction at an electrode utilizes surfactant films to confine the protein to the electrode surface.[29,30] The surfactant forms bilayers and micelles on the electrode, and has been

shown to provide a favorable environment for ET to the P450 heme. A second, similar method utilizes polyelectrolyte films that are co-adsorbed with P450.[31,32] Both types of films result in good electronic coupling, with standard rate constants (k^o, $\Delta G^o = 0$) typically between 100 - 300 s^{-1}. The ability of these films to electronically couple the P450 heme to the electrode has been rationalized in the following ways: 1) the films block adsorption of contaminants that would foul the electrode surface; 2) the films provide an environment that retains the native protein conformation at the surface, preventing non-specific adsorption and denaturation.[33] In both film systems, immobilized P450s were able to catalytically epoxidize styrene to styrene oxide (1 - 6 mols substrate / mols enzyme / hr). The mechanism was found to operate through the peroxide shunt, with peroxide being generated from electrochemically-mediated P450-catalyzed dioxygen reduction.

The third successful method achieved electrochemistry with CAM by using sodium montmorillite (carbon-based polyanionic clay) to coat the surface of an electrode.[34] The anionic clay was proposed to interact electrostatically with a region on the surface of CAM that was positively charged; this region is also presumed to be the binding site of the native reductase for CAM. Rapid, reversible ET was observed (k^o approximately 150 s^{-1}), as well as catalytic reduction of dioxygen. However, substrate turnover was not reported.

A fourth method for electrochemical P450 reduction utilized self-assembled mercaptan films on gold to achieve ET with mammalian P450 2E1.[35] Indeed, alkanethiol monolayers on gold electrodes are commonly used to provide surfaces that interact favorably with various proteins to achieve ET.[36] For P450 2E1, the critical step was to

further derivatize the gold-mercaptan surface, using either maleimide or poly(diallyldimethylammonium chloride); without this second coating, ET was not observed. While electronic coupling was not as efficient as the aforementioned systems (k^o between 2 and 10 s^{-1}), catalytic substrate oxidation was observed. Although this type of system is not practical for large-scale substrate turnover,[§,37] it shows promise for biosensing.

Finally, Shumyantseva *et al.* reported a technique where they covalently attached a synthetic flavin cofactor to the surface of two mammalian P450s, 2B4 and 1A2.[38] The flavin was meant to act as an electronic relay, mimicking the contact that the natural reductase would make with the heme domains. Reduction of the flavin at the electrode resulted in ET through the protein sheath and into the heme. Although ET rates were not reported, they did report catalytic rates of approximately 1 nmol product / nmol enzyme / minute (similar to reactions conducted with NAD(P)H). Drawbacks of this system include the slow rates and the need for covalent modification of the protein.

Clearly, P450 electrochemistry is not straightforward. Electrode or protein modifications are often required to achieve the desired ET. In addition, as demonstrated in the examples above, achieving good electronic coupling will not necessarily produce systems competent for catalytic substrate oxidation, while those that are catalytic generally do not function at practical rates.

[§] There are several difficulties with scaling up this system, most of which are related to properly preparing the gold surface. See Tanimura *et al* for a discussion on this.

Cytochrome P450 BM3

Of the numerous P450s, the variant isolated from the bacterium *Bacillus megaterium* (BM3) is a good candidate for commercial applications. Credit goes to Fulco's group at UCLA for initially identifying and characterizing BM3.[39,40] The protein is comprised of a heme domain and a flavin-containing reductase domain fused together on a single polypeptide chain. The enzyme catalyzes the sub-terminal hydroxylation of long-chain fatty acids (10-16 carbons), and has catalytic rates up to 1000 times faster than most other P450s. BM3 possesses several ideal characteristics for biocatalysis: the enzyme 1) is soluble; 2) can be expressed in large quantities in *E. coli*; 3) has relatively broad substrate specificity, while 4) mutants of BM3 are even more active and have broader substrate specificity;[6] 5) has a partial crystal structure available;[41] 6) can be easily assayed for activity.[42]

Structure

BM3 is 119 kDa and consists of two domains: 1) a reductase domain (66 kDa) at the carboxy end of the polypeptide contains FAD and FMN cofactors, and is responsible for mediating ET from NADPH in solution to the heme domain; 2) an amino-terminal heme domain (55 kDa) that contains protoporphyrin IX with Fe^{III} (resting state) in the cavity.[43] This arrangement makes BM3 more similar to mammalian P450s, which utilize flavin containing reductases, than to the ferredoxin-mediated bacterial variants. Indeed, based on sequence identity, BM3 shows greater similarity to the eukaryotic P450s. The primary amino acid sequence of the BM3 reductase and heme domains are approximately 35% and 30% identical to their eukaryotic microsomal counterparts, while the bacterial forms share as little as 15% identity with BM3.[41] The similarity of BM3 to the little-

understood mammalian P450s has led many to consider it a good candidate for modeling the eukaryotic variants.[44]

To date, the crystal structure of the full-length BM3 has not been solved. However, crystal structures of the heme domain[41] and the heme domain complexed with the adjacent FMN domain[45] do exist. **Figure 1.2** shows the crystal structure of the BM3 heme domain with N-palmitoylglycine (yellow) bound in the active site over the heme (red).[46] In the absence of substrate, the distal axial position is occupied by a water molecule coordinated to the heme iron. The protein is approximately 65 Å in diameter. The heme lies deeply buried within the protein matrix, with no part of it directly exposed to bulk solvent. The active site is accessible to external molecules through a long substrate access channel, ~ 8-10 Å, lined mostly with non-aromatic, hydrophobic amino acids. In **Figure 1.2**, this channel is occupied by the tail end of N-palmitoylglycine.

Several key amino acid residues have been identified in the BM3 heme domain (**Figure 1.2**). Most notably, Cys^{400} ligates the heme iron directly and, as described above, is responsible for the unique oxidation chemistry catalyzed by all P450s. Phe^{87} lies directly over the heme and is one of the most extensively characterized amino acids in BM3. When substrate binds, Phe^{87} "flips" from a horizontal to a perpendicular orientation relative to the heme.[47] This residue has a significant effect on the peroxide shunt activity of BM3: while the wild type enzyme has no activity with the peroxide shunt, mutating Phe^{87} to smaller amino acids (most notably F87A) has been shown to confer shunt acitivity.[48] A third important amino acid is Phe^{393}, which has been shown to have a significant effect on the heme redox potential. Mutating Phe^{393} to other amino acids resulted in variants with significantly altered heme reduction potentials, electron

transfer rates, and catalytic rates.[49] Finally, Thr[268] has been shown to be conserved throughout the P450 superfamily and is thought to play a critical role in the catalytic cycle by providing protons for dioxygen reduction (ultimately to water) by the heme.[41]

Redox Chemistry and Electron Transfer

ET in BM3 begins with NADPH in solution (E^o = -340 mV vs. NHE) transferring hydride to the FAD in the reductase domain.[20] A single electron is then transferred to the second flavin in the reductase, FMN, resulting in semi-quinone forms of each flavin. Reduction of the heme by the FMN semi-quinone can only occur with substrate bound: substrate binding converts the heme from low spin (E^o = -370 mV) to high spin (E^o approximately -250 mV), with the resulting shift in potential now favoring ET from the FMN semi-quinone to the heme. The second electron in the FAD is then transferred to the FMN, which in turn reduces the heme a second time at the appropriate moment according to the scheme in **Figure 1.1**.

The crystal structure of the heme domain complexed with the FMN domain is shown in **Figure 1.3**. Since the inter-domain contact forms the relevant complex for ET between the FMN (blue) and the heme (red), the structure in **Figure 1.3** provides key insights into the native ET pathway in BM3. As mentioned above, the heme is deeply buried within the protein matrix. Isolation of the heme in this way would make it difficult for an external source to reduce the iron, as is required for P450 oxidation chemistry. Thus, proper positioning and docking of the FMN domain directly underneath the heme is likely to be crucial for efficient ET.

Unlike the CAM-ferredoxin docking interaction, where electrostatics are the key force driving proper orientation of the two domains for ET,[50] BM3 likely uses a

combination of forces. Electrostatic interaction between the two domains is proposed to be relatively weak: analysis of the structure revealed two direct hydrogen bonds, one salt bridge (His^{100} and Glu^{494}), and several water-mediated contacts.[45] Given that the contact interface spans some 967 $Å^2$, these relatively few electrostatic interactions suggest that these forces contribute minimally. Most likely, the electrostatics act in combination with the orientation effect supplied by the short peptide linker between the heme and FMN domains to synergistically orient the two for ET. Indeed, reconstitution experiments that utilize separately expressed reductase and heme domains result in poor substrate turnover rates in the presence of NADPH.[51]

The isoalloxazine ring of the FMN has its methyl groups pointing directly to the heme binding loop (residues 382 – 400, highlighted in yellow in **Figure 1.3**); without the heme domain, this part of the FMN would be solvent-exposed. Thus, the methyl groups likely act as a bridge, providing an inter-domain pathway for ET. Indeed, distance calculations put the 7-methyl group at only 4 Å from the amide nitrogen of Gln^{387}.[45] It has been suggested that this precise positioning indicates the two domains form a specific complex for ET.

Objective: NADPH Alternatives for BM3

In summary, exploiting P450 oxygenase activity would greatly facilitate many areas of fundamental medical research and have invaluable potential in industrial processes. BM3 in particular possesses many of the characteristics that the ideal P450 biocatalyst should have. However, the need for reducing equivalents from NADPH will continue to hinder practical uses of BM3. The NADPH requirement is best dealt with by

finding alternative sources of electrons; this can be accomplished with a reductant that can transfer electrons through the reductase to the heme, or by utilizing a method that delivers electrons directly to the heme, thereby eliminating the reductase domain. The principal question explored in this thesis can now be stated: how can we efficiently deliver an electron from an external source, either from a soluble reductant or directly from an electrode, through the protein sheath and to the heme in a fashion that sufficiently mimics the native system in order to achieve catalytic substrate oxidation? The pages that follow describe efforts to utilize an electrode as the ultimate source of electrons for BM3 catalysis, providing lessons and insights for *in vitro* electrochemical systems exploiting P450 oxidative catalysis.

References

(1) Kirk, O.; Borchert, T. V.; Fuglsang, C. C. *Curr. Opin. Biotechnol.* **2002**, *13*, 345-351.

(2) Simpson, E. R.; Mahendroo, M. S.; Means, G. D.; Kilgore, M. W.; Hinshelwood, M. M.; Graham-Lorence, S.; Amarneh, B.; Ito, Y.; Fisher, C. R.; Michael, M. D.; Mendelson, C. R.; Bulun, S. E. *Endocr. Rev.* **1994**, *15*, 342-355.

(3) Erion, M. D.; Reddy, K. R.; Boyer, S. H.; Matelich, M. C.; Gomez-Galeno, J.; Lemus, R. H.; Ugarkar, B. G.; Colby, T. J.; Schanzer, J.; van Poelje, P. D. *J. Am. Chem. Soc.* **2004**, *126*, 5154-5163.

(4) Guengerich, F. P. *Nature Reviews: Drug Discovery* **2002**, *1*, 359-366.

(5) Guengerich, F. P. *Molecular Interventions* **2003**, *3*, 194-204.

(6) Glieder, A.; Farinas, E. T.; Arnold, F. H. *Nature Biotechnology* **2002**, *20*, 1135-1139.

(7) Lange, K. R., Ed. *Surfactants: A Practical Handbook*; Hanser Gardner Publications, Inc.: Cincinnati, 1999.

(8) Blair, E.; Greaves, J.; Farmer, P. J. *J. Am. Chem. Soc.* **2004**, *126*, 8632-8633.

(9) Labinger, J. A.; Bercaw, J. E. *Nature* **2002**, *417*, 507-514.

(10) Mayer, J. M. *Acc. Chem. Res.* **1998**, *31*, 441-450.

(11) Lewis, D. F. V. *Guide to Cytochromes P450: Structure and Function*; Taylor and Francis: New York, 2001.

(12) Ortiz de Montellano, P. R., Ed. *Cytochrome P450: Structure, Mechanism, and Biochemistry*; 2nd ed.; Plenum Press: New York, 1995.

(13) Phillips, I. R.; Shephard, E. A., Eds. *Cytochrome P450 Protocols*; Humana Press: Totowa, 1998; Vol. 107.

(14) Williams, P. A.; Cosme, J.; Vinkovic, D. M.; Ward, A.; Angove, H. C.; Day, P. J.; Vonrhein, C.; Tickle, I. J.; Jhoti, H. *Science* **2004**, *305*, 683-686.

(15) Sieber, V.; Martinez, C. A.; Arnold, F. H. *Nature Biotechnology* **2001**, *19*, 456-460.

(16) Otey, C. R.; Silberg, J. J.; Voigt, C. A.; Endelman, J. B.; Bandera, G.; Arnold, F. H. *Chem. Biol.* **2004**, *11*, 309-318.

(17) Yu, C.-A.; Gunsalus, I. *The Journal of Biological Chemistry* **1974**, *249*, 106-106.

(18) Green, M. T.; Dawson, J. H.; Gray, H. B. *Science* **2004**, *304*, 1653-1656.

(19) Yoshioka, S.; Takahashi, S.; Hori, H.; Ishimori, K.; Morishima, I. *Eur. J. Biochem.* **2001**, *268*, 252-259.

(20) Daff, S.; Chapman, S.; Turner, K.; Holt, R.; Govindaraj, S.; Poulos, T.; Munro, A. *Biochemistry* **1997**, *36*, 13816-13823.

(21) Schmakel, C. O.; Santhanam, S. V.; Elving, P. J. *J. Am. Chem. Soc.* **1975**, *97*, 5083-5092.

(22) Wienkamp, R.; Steckhan, E. *Angew. Chem. Int. Ed.* **1982**, *21*, 782-783.

(23) Seelbach, K.; Riebel, B.; Hummel, W.; Kula, M.-R.; Tishkov, V. I.; Egorov, A. M.; Wandrey, C.; Kragl, U. *Tetrahedron Lett.* **1996**, *37*, 1377-1380.

(24) Schneider, S.; Wubbolts, M.; Sanglard, D.; Witholt, B. *Appl. Environ. Microbiol.* **1998**, *64*, 3784-3790.

(25) Gray, H. B.; Winkler, J. R. *Quart. Rev. Biophys.* **2003**, *36*, 341-372.

(26) Gray, H. B.; Winkler, J. R. *Annu. Rev. Biochem.* **1996**, *65*, 537-561.

(27) Hawkridge, F. M.; Taniguchi, I. In *The Porphyrin Handbook*; Kadish, K. M., Smith, K. M., Guilard, R., Eds.; Academic Press: San Diego, CA, 2000; Vol. 8.

(28) Kazlauskaite, J.; Westlake, A. C. G.; Wong, L.-L.; Hill, A. O. *Chem. Commun.* **1996**, 2189-2190.

(29) Fleming, B. D.; Tian, Y.; Bell, S. G.; Wong, L.; Urlacher, V.; Hill, H. A. O. *Eur. J. Biochem.* **2003**, *270*, 4082-4088.

(30) Zhang, Z.; Nassar, A.-E.; Lu, Z.; Schenkman, J. B.; Rusling, J. F. *J. Chem. Soc., Faraday Trans.* **1997**, *93*, 1769-1774.

(31) Munge, B.; Estavillo, C.; Schenkman, J. B.; Rusling, J. F. *ChemBioChem* **2003**, *4*, 82-89.

(32) Lvov, Y. M.; Lu, Z.; Schenkman, J. B.; Zu, X.; Rusling, J. F. *J. Am. Chem. Soc.* **1998**, *120*, 4073-4080.

(33) Rusling, J. F. *Acc. Chem. Res.* **1998**, *31*, 363-369.

(34) Lei, C.; Wollenberger, U.; Jung, C.; Scheller, F. W. *Biochem. Biophys. Res. Comm.* **2000**, *268*, 740-744.

(35) Fantuzzi, A.; Fairhead, M.; Gilardi, G. *J. Am. Chem. Soc.* **2004**, *126*, 5040-5041.

(36) Niki, K. *Electrochemistry* **2002**, *70*, 82-90.

(37) Tanimura, R.; Hill, M. G.; Margoliash, E.; Niki, K.; Ohno, H.; Gray, H. B. *Electrochem. Solid State Lett.* **2002**, *5*, E67-E70.

(38) Shumyantseva, V.; Bulko, T.; Bachmann, T.; Bilitewski, U.; Schmid, R.; Archakov, A. *Arch. Biochem. Biophys.* **2000**, *377*, 43-48.

(39) Ruettinger, R. T.; Fulco, A. J. *The Journal of Biological Chemistry* **1981**, *256*, 5728-5734.

(40) Narhi, L. O.; Fulco, A. J. *J. Biol. Chem.* **1986**, *261*, 7160-7169.

(41) Ravichandran, K. G.; Boddupalli, S. S.; Hasemann, C. A.; Peterson, J. A.; Deisenhofer, J. *Science* **1993**, *261*, 731-736.

(42) Schwaneberg, U.; Otey, C.; Cirino, P. C.; Farinas, E.; Arnold, F. H. *J. Biomol. Screen.* **2001**, *6*, 111.

(43) Narhi, L. O.; Fulco, A. J. *J. Biol. Chem.* **1987**, *262*, 6683-6690.

(44) Munro, A.; Leys, D.; McLean, K.; Marshall, K.; Ost, T.; Daff, S.; Miles, C.; Chapman, S.; Lysek, D.; Moser, C.; Page, C.; Dutton, P. *Trends Biochem. Sci.* **2002**, *27*, 250-257.

(45) Sevrioukova, I. F.; Li, H.; Zhang, H.; Peterson, J. A.; Poulos, T. L. *Proc. Natl. Acad. Sci. USA* **1999**, *96*, 1863-1868.

(46) Haines, D. C.; Tomchick, D. R.; Machius, M.; Peterson, J. A. *Biochemistry* **2001**, *40*, 13456-13465.

(47) Li, H.; Poulos, T. L. *Nat. Struct. Biol.* **1997**, *4*, 140-146.

(48) Li, Q.-S.; Ogawa, J.; Shimizu, S. *Biochem. Biophys. Res. Comm.* **2001**, *280*, 1258-1261.

(49) Ost, T. W. B.; Clark, J.; Mowat, C. G.; Miles, C. S.; Walkinshaw, M. D.; Reid, G. A.; Chapman, S. K.; Daff, S. *J. Am. Chem. Soc.* **2003**, *125*, 15010-15020.

(50) Roitberg, A. E.; Holden, M. J.; Mayhew, M. P.; Kurnikov, I. V.; Beratan, D. N.; Vilker, V. L. *J. Am. Chem. Soc.* **1998**, *120*, 8927-8932.

(51) Boddupalli, S. S.; Oster, T.; Estabrook, R. W.; Peterson, J. A. *J. Biol. Chem.* **1992**, *267*, 10375-10380.

Table 1.1. P450-catalyzed reactions.

C-H Bond hydroxylation	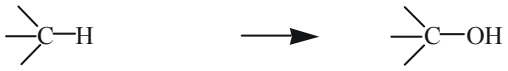
Epoxidation	
	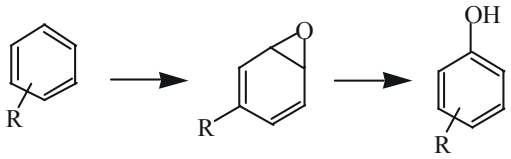
Oxidative N-dealkylation	
Oxidative O-dealkylation	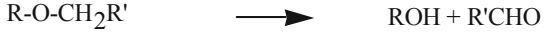
N-Hydroxylation	
Sulfoxidation	
Peroxidase-type oxidation	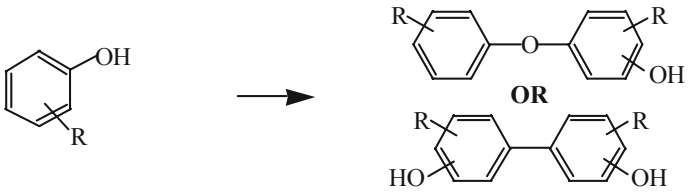
NO Synthase-type oxidation (C=N bond cleavage)	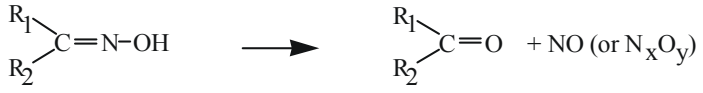
Oxidative deformylation	
Dehydrogenation	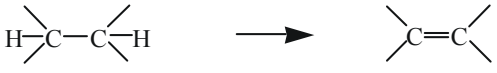

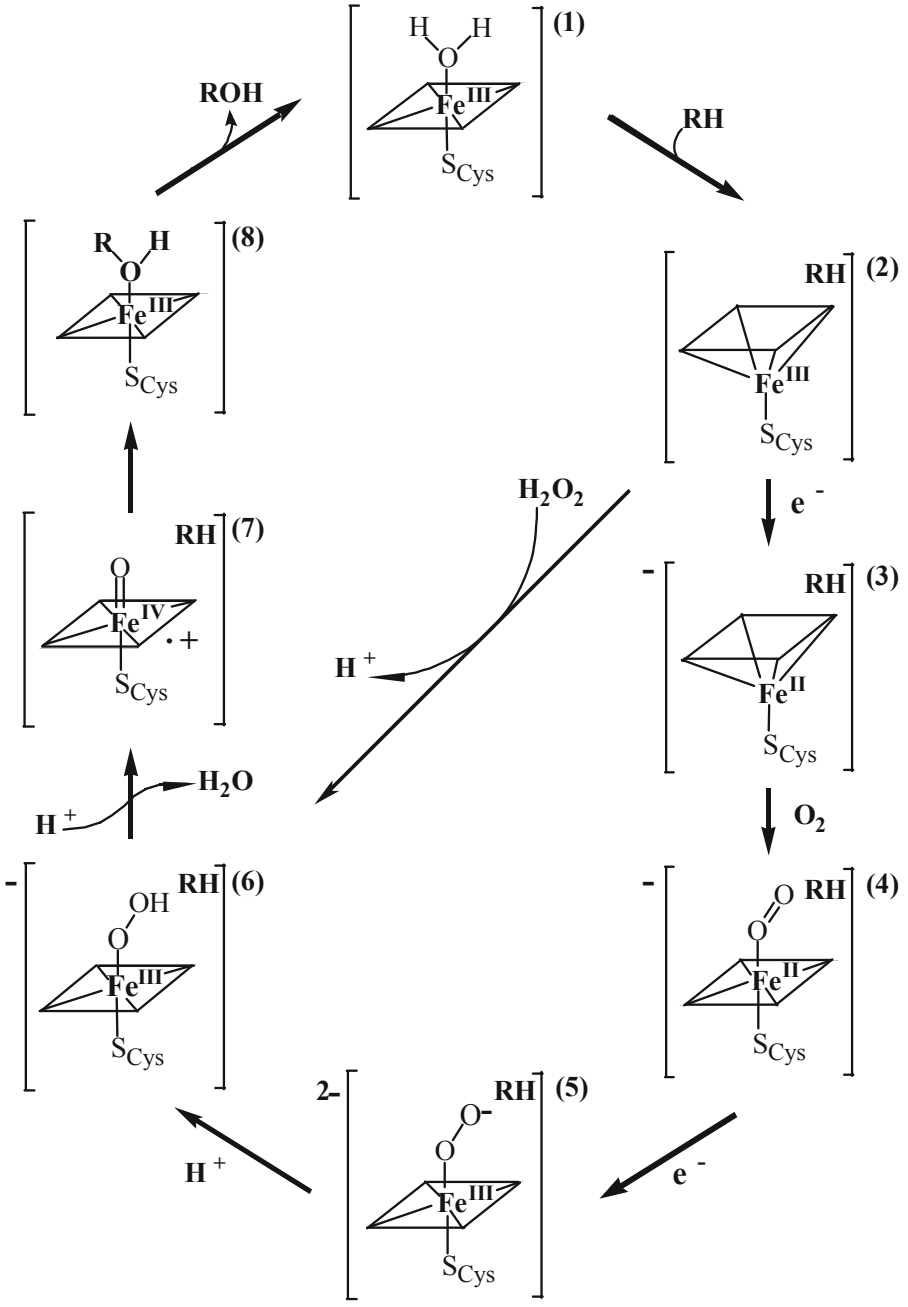

Figure 1.1. The canonical mechanism of cytochrome P450 is shown.

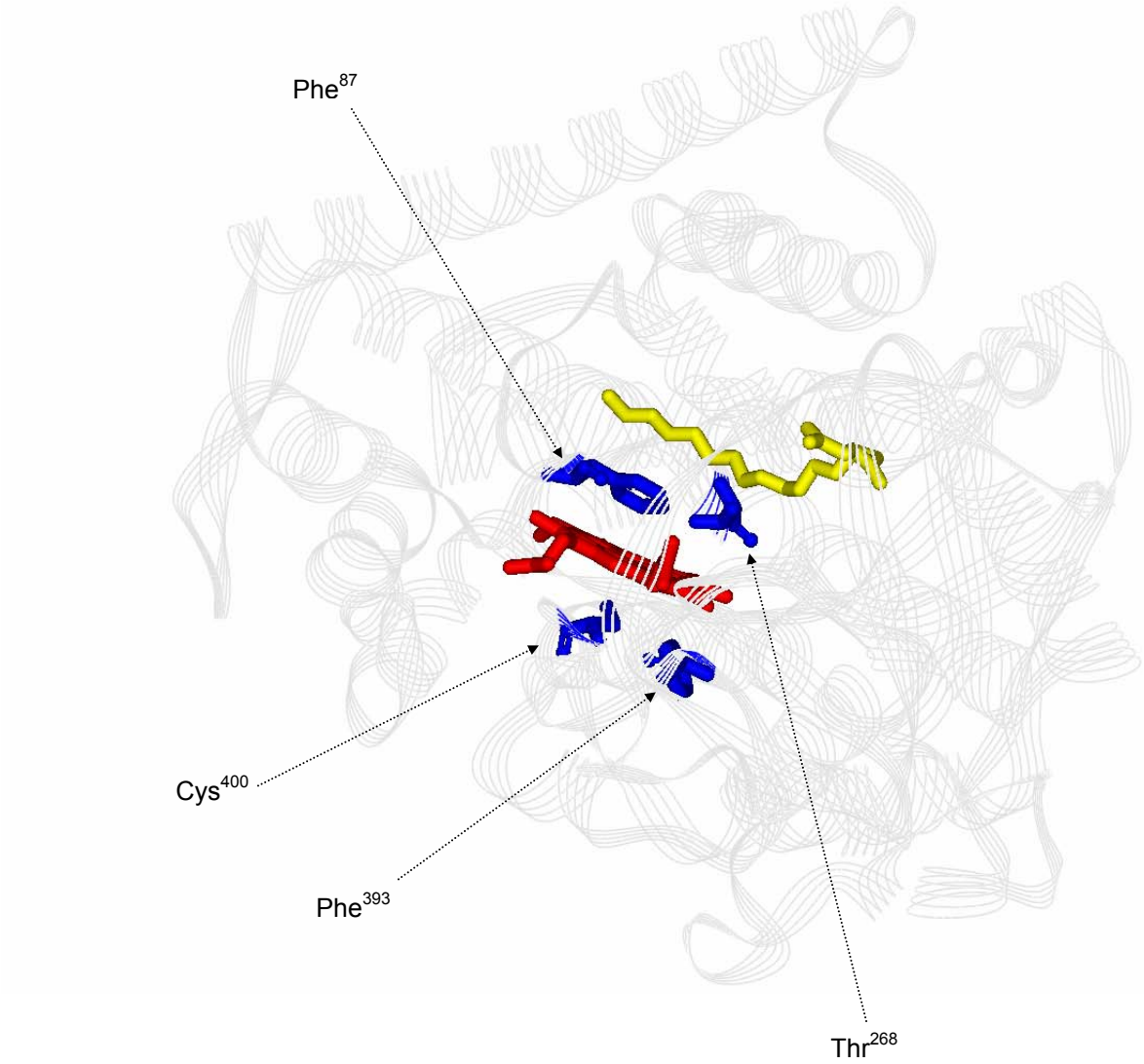

Figure 1.2. The crystal structure of the cytochrome P450 BM3 heme domain is shown. The substrate N-palmitoylglycine (yellow) is bound in the substrate access channel directly above the heme (red). Key amino acids (blue) are labeled.

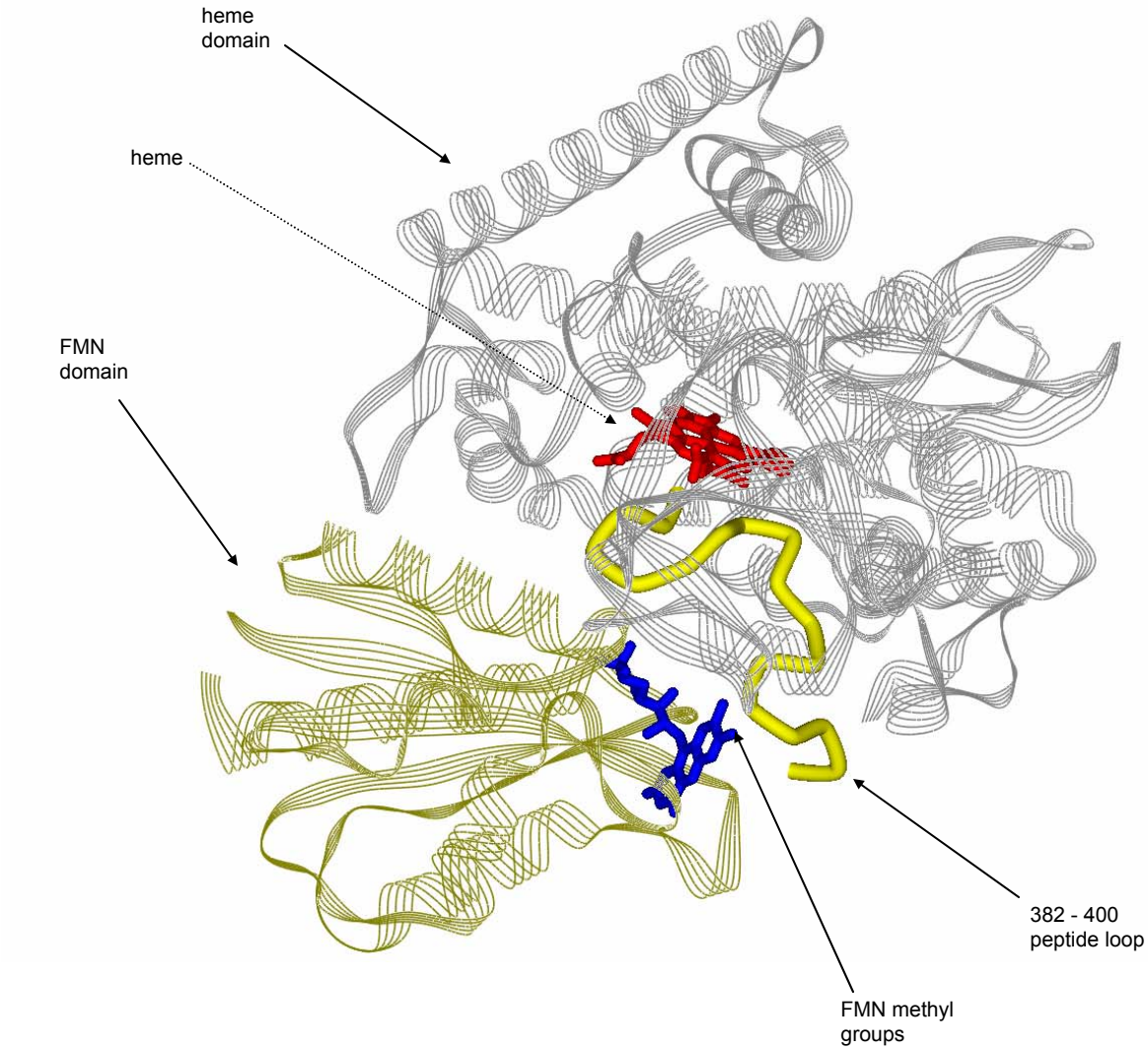

Figure 1.3. The crystal structure of the cytochrome P450 BM3 heme domain complexed with the native FMN domain is shown. The heme (red) and FMN (blue) cofactors are presumed to be electronically coupled through the 382 – 400 peptide loop (yellow).

Chapter 2

Cobaltocene-Mediated Catalytic Monooxygenation Using Holo and Heme Domain Cytochrome P450 BM3*

*Adapted from Udit, A. K.; Arnold, F. H.; Gray, H. B. *J. Inorg. Biochem.* **2004**, *98*, 1547-1550.

Acknowledgements: Susan Schofer (Caltech) for assistance with the chemical synthesis; Mike Hill (Occidental College) for helpful discussions; NSF (HBG) and NSERC (Canada) (AKU) for research support.

Abstract

The feasibility of replacing NADPH with 1,1'-dicarboxycobaltocene in the catalytic cycle of cytochrome P450 BM3 has been explored. Using the holoprotein, the surrogate mediator was observed to reduce both the FAD and FMN in the reductase domain, as well as the iron in the heme domain. In an electrochemical system, the mediator was able to support lauric acid hydroxylation at a rate of 16.5 nmol product / nmol enzyme / minute. Similar electron transfer and catalysis were observed for the heme domain alone in the presence of the metallocene; the turnover rate in this case was 1.8 nmol product / nmol enzyme / minute. Parallel studies under the same conditions using a previously reported cobalt sepulchrate mediator showed that the two systems give similar results for both the holoenzyme and the heme domain.

Abbreviations: BM3, flavocytochrome P450 BM3; ET, electron transfer; Co(sep), cobalt(III) sepulchrate; M_{ox}, 1,1'-dicarboxycobaltocenium hexafluorophosphate; M_{red}, 1,1'-dicarboxycobaltocene; hBM3, heme domain P450 BM3

Introduction

The ability of the cytochromes P450 to catalyze challenging oxidation reactions under physiological conditions has made them attractive targets for *in vitro* applications.[1,2] Of the P450s, flavocytochrome P450 from *Bacillus megaterium* (BM3) is particularly appealing for commercial use, owing to its ease of handling and the ability to create mutants with altered substrate specificity.[3(and references therein)] Capturing BM3 activity *in vitro* would be greatly facilitated if reductants other than NAD(P)H could be found. One way to replace NADPH in the catalytic cycle of BM3 would be to use the holo protein in an electrochemical system that employed a small molecule mediator as an electron shuttle. The mediator, after transferring electrons to the BM3 reductase domain, would be regenerated at the electrode. Electron transfer (ET) through the protein can then occur via the native pathway, FAD → FMN → heme, culminating in catalytic substrate oxidation.

Among the investigations seeking alternative reductants for P450,[4,5] the most successful utilized a platinum electrode and cobalt(III) sepulchrate (Co(sep)) as the electron shuttle (**Figure 2.1a**).[6] Co(sep) is a water soluble cobalt cage complex that has a $Co^{III/II}$ redox couple at -550 mV (vs. Ag/AgCl). Co(sep)-mediated catalysis was demonstrated with a variety of P450s, with rates approaching that of NAD(P)H-driven systems (for BM3 with lauric acid, 110 min^{-1} cf. 900 min^{-1} for Co(sep) cf. NADPH).[6]

However, practical limitations of the Co(sep) system include production of reactive oxygen species,[7] difficulty in synthetically manipulating Co(sep) to tune the mediator to different reaction conditions (e.g., solvent, pH), and aggregation and precipitation at functional Co(sep) concentrations (typically, 1-10 mM).[8]

We endeavored to find a better mediator for BM3. Previous work with glucose oxidase utilized a ferrocene derivative to mediate enzyme oxidation,[9] demonstrating the idea of designing a mediator for a given application. For BM3 reduction, we decided to use the analogous reductant cobaltocene as a scaffold to construct a suitable mediator. In the hope that the dicarboxy derivative of cobaltocene could improve water solubility and disfavor aggregation, as well as raise the redox potential so the mediator would not be as air-sensitive, we synthesized 1,1'-dicarboxycobaltocenium hexafluorophosphate (M_{ox}) (**Figure 2.1b**) and evaluated this molecule for its efficacy as a mediator for bioelectrochemical catalysis with BM3.

Results and Discussion

The synthetic scheme for M_{ox} is shown in **Scheme 2.1**. At physiological pH (7-8), the carboxyls are fully deprotonated,[10] greatly enhancing water solubility. Cyclic voltammetry with a glassy carbon electrode in 0.1 M phosphate buffer pH 8 revealed that the Co^{III}/Co^{II} couple is fully reversible with an $E_{1/2}$ of -830 mV (vs. Ag/AgCl); this value is 320 mV more positive than that of unmodified cobaltocene, owing to the electron withdrawing nature of the carboxyl groups. Chemical reduction to the active Co^{II} form, 1,1'-dicarboxycobaltocene (M_{red}), was achieved with zinc dust.

Absorption spectra were recorded to observe flavin reduction by the putative mediator. The flavins are the most readily reduced centers: FAD is rapidly reduced by soluble reductants (e.g., NADPH), and ET between the two flavins is fast.[11] In **Figure 2.2**, the shoulder between 440 and 490 nm is characteristic of oxidized flavins in BM3;[12] this shoulder disappears upon reduction by NADPH. As can be seen from **Figure 2.2**, adding M_{red} to a solution of BM3 results in a spectrum similar to that obtained after adding NADPH. This confirms flavin reduction by M_{red}, and suggests that M_{red} can indeed function in place of NADPH.

Addition of M_{red} to a solution of BM3 saturated with CO gave a peak at 448 nm (**Figure 2.3**), characteristic of the Fe^{II}-CO species.[13] Notably, heme reduction by M_{red} occurs in the absence of substrate, unlike in the native system where ET from flavins to the heme requires substrate at the active site.[14] Substrate displaces water from the heme pocket, converting Fe^{III} from low to high spin. This conversion is accompanied by a positive shift in the heme potential (> 100 mV) that favors ET from FMN to the heme. It appears that M_{red} reduces the heme directly, bypassing the reductase pathway. To test this, M_{red} was added to a CO-saturated solution of the isolated BM3 heme domain (hBM3). As can be seen in **Figure 2.3**, the Soret band at 448 nm shows that M_{red} reduced the heme iron. The hydrophobic substrate access channel[15] and the -2 charge on M_{red} make it unlikely that heme reduction occurs by direct interaction of the mediator with the active site. Apparently, M_{red} takes an alternative ET pathway, thereby opening the way for catalysis without the reductase domain.

Enzyme activity assays were performed with lauric acid (K_m = 100 μM with BM3[16]). Thirty-minute reactions in air were conducted with 1 μM BM3 or hBM3, 1 mM

lauric acid, and 1 mM reductant (M_{red} or NADPH) in a final volume of 1 mL at room temperature. The reactions were quenched with 5 drops of concentrated HCl, and then samples were prepared for GC/MS analysis as described.[17] Negative controls lacking one component (substrate, mediator, or enzyme) were also carried out. The negative controls gave no product, while the NADPH and M_{red} samples for both BM3 and hBM3 yielded the expected hydroxylated compounds. The resulting product distribution of the M_{red} reactions, 36:28:36 for ω-1:ω-2:ω-3 hydroxy laurate, was similar to that of the NADPH-driven reaction.[16] To test if the observed products are a consequence of the peroxide shunt (from oxygen reduction to peroxide by M_{red}), reactions with M_{red} were also carried out in the presence of catalase. The resulting product profile was similar to that without catalase,[†] indicating that the reaction was metallocene-mediated: this was expected as previous work has shown that wild type BM3 does not have significant peroxide shunt activity.[17]

Next, we developed an electrochemical system where the soluble mediator provides electrons to the enzyme and is continuously regenerated at an electrode.[‡] Co(sep) reactions were run in parallel with M_{red} reactions in order to compare the two mediators. The results in **Table 2.1** reveal that the two mediator systems perform similarly under the conditions used. Notably, the rate shown in **Table 2.1** for Co(sep) with BM3 is less than that previously reported (38 vs. 110 min^{-1}); this probably results from continuously bubbling air into solution, which removes both dioxygen and the mediator from the reaction as they react with one another. The hBM3 results are intriguing: to our knowledge, this is the first report of mediated electrochemical catalysis

[†] See Experimental Methods for details of the catalase control reaction.
[‡] See Experimental Methods for details of the electrochemical reaction setup.

with the heme domain. Although the reaction proceeds slowly, it nevertheless occurs and opens the possibility of performing the reaction with the heme domain alone, which could be advantageous given the propensity of the reductase to become inactivated through over-reduction.[14]

The difference in rate between the mediated reactions and the native system can be partially understood by examining the current function. A typical current function from an M_{ox}-BM3 reaction is shown in **Figure 2.4**. Initially, the reaction solution contains only M_{ox}. Applying a reducing potential results in a current that decays from an initial value of 4 mA to one that is near zero as M_{ox} is converted to M_{red}. Addition of the oxygenated enzyme-substrate solution followed by bubbling air into the reaction causes a spike and subsequent limiting current of 3 mA. From this limiting current, the coupling between total current passed by the electrode and total product formed can be calculated:[§] this yields a coupling efficiency of only 2% for the M_{red}-BM3 bioelectrochemical system. A similar calculation for hBM3 reactions yields only 0.3%. These poor efficiencies attest to the acute sensitivity of cobaltocene to dioxygen.[18] Bubbling air into the reaction leads to rapid M_{red} oxidation, removing both dioxygen and the reduced mediator from the reaction as it becomes substrate limited; this undoubtedly contributes to the difference in rate between the mediated and native systems.

[§] Using the limiting current, the coupling between product formation and total charge passed can be calculated. From Table 2.1, 224 nmols of product are formed in the BM3 reaction. From Figure 2.4, the total charge passed by the electrode during the biocatalytic reaction at the onset of the limiting current is 2.7 Coulombs. Applying the Faraday constant, the degree of coupling is calculated as the number of moles of product divided by half the number of moles of electrons (two electrons per product).

Summary

In conclusion, we have shown that the dicarboxy derivative of cobaltocene can function as an electrochemical mediator of P450 catalytic reactions. The main limitation of the M_{ox} system is its poor coupling efficiency, owing largely to the sensitivity of M_{red} to dioxygen. Although the overall kinetics and turnover of Co(sep) with P450 are slightly better, M_{ox} can be modified more readily to optimize reaction parameters, providing a more versatile mediator.

Experimental Methods

Protein Expression

Expression, purification, and quantification of BM3 and hBM3 for use with the mediator were performed as described.[17]

Synthesis of 1,1'-dicarboxycobaltocenium hexafluorophosphate (M_{ox})

Lithium methylcyclopentadienide (LiMeCp) and cobalt(II) acetylacetone (2:1 molar ratio) were added to THF in a dry ice/acetone bath under argon. The mixture was left to stir overnight at room temperature. The solvent was removed under vacuum, and the dark brown product Co(II)$(MeCp)_2$ was isolated by sublimation for 2 hours at 85°C. The product was mixed with $AgPF_6$ (1:1 molar ratio) and was left overnight to stir in CH_2Cl_2 under argon at room temperature. After filtering the solution to remove the silver, the solvent was removed under vacuum, leaving behind the yellow-green product Co(III)$(MeCp)_2PF_6$. This product was mixed with NaOH pellets and $KMnO_4$ (1:2:3 molar ratio, respectively). The mixture was refluxed in water for 4 hours, filtered hot through Celite, and an equimolar amount (cf. Co(III)$(MeCp)_2PF_6$) of $NaPF_6$ was added.

The solvent was then removed on a rotovap and the solid was washed repeatedly with acetone. The final product, $Co(III)(CpCOOH)_2PF_6$ (M_{ox}), was a bright yellow powder (λ_{max} = 410 nm).

Chemical reduction was achieved by adding 500 mg of zinc dust to 15 mg of M_{ox} and 8 mL of degassed buffer (25 mM Tris hydroxymethylaminoethane-HCl, 25 mM potassium phosphate, 250 mM KCl, pH 8.0). This mixture was stirred under argon for 4 hours and then filtered to remove the zinc dust. The result was a dark red solution (λ_{max} = 490 nm) of M_{red} solubilized in a buffer that could be readily used in an enzymatic reaction.

Catalase Control

Analogous to the reaction conditions described in the main text, a thirty-minute reaction in air was conducted with 1 μM BM3 or hBM3, 1 mM lauric acid, and 1 mM reductant (M_{red}) in a final volume of 1 mL that also contained 2 μL of a 2.42 x 10^3 Unit/μL solution of catalase. The reaction was conducted at room temperature. The sample was then prepared for analysis by GC/MS[17] (described in detail in the next section). The product profile was found to be similar for reactions with or without catalase. Negative controls (reactions lacking either enzyme, metallocene, or substrate) did not result in any observable products.

Bioelectrochemical Cell

All electrochemical reactions were carried out at room temperature. A mini-bioreactor was constructed using a stirred two-compartment cell, separating the working and Ag/AgCl reference electrodes from the Pt wire auxiliary with a glass frit. The working electrode was a 2 cm x 2 cm carbon cloth (ElectroChem, Inc.) that covered the

bottom of the cell. A CH Instruments Electrochemical Workstation consisting of a potentiostat and software was used for the electrochemical reactions. The cell was first purged with a stream of argon, which was left on during the entire reaction. To the sample chamber, 2 mL of degassed buffer (170 mM KCl, 10 mM $MgCl_2$, 57 mM Tris-HCl pH 7.4) were added, as well as 2 mL of a degassed 5 mM solution of mediator (M_{ox} or Co(sep)) in the same buffer. 4 mL of degassed buffer were also added to the auxiliary chamber. A potential of -0.9 V was applied, and the mixture was stirred for 6 minutes. At this point, 1 mL of a solution containing protein and 5 mM lauric acid were added to the working chamber, and air was bubbled into the reaction at a rate of 1 bubble/second using a Pasteur pipette. Final concentrations and volumes were 1 mM lauric acid, 2 mM mediator, 1 μM BM3 or 1.5 μM hBM3, and 5 mL reaction volume.

Determination of Enzyme Activity in the Electrochemical System

0.5 mL aliquots were removed from the electrochemical cell at various time points and added to 3 drops of concentrated HCl to quench the reaction. The samples were then prepped for analysis using GC-FID as described.[17] Briefly, 5 μL of 50 mM 10-OH capric acid in DMSO (internal standard, described below) were added, and the reactions were then extracted three times with an equivolume of ethyl acetate. The ethyl acetate extracts were dried with sodium sulfate, followed by evaporation under vacuum. The samples were derivatized by adding 100 μL of a 1:1 mixture of pyridine:BSTFA, and then incubating at 80^{o}C for 20 minutes. 2 μL of these samples were then injected into the GC-FID with an HP-5 column.

A calibration curve was created to quantify the amount of product formed. Wild type BM3 sub-terminally hydroxylates lauric acid at the ω-1, ω-2, and ω-3 positions.[16]

Since authentic standards for these compounds are not available, 12-OH-lauric acid was used to make the calibration curve with the assumption that the position of the hydroxyl group does not affect the FID response. An internal standard, 10-OH-capric acid, was used to aid quantification by adding a known amount to the samples, and then correlating the relative areas of 12-OH- to 10-OH-laurate to the amount of 12-OH-laurate initially present.

The reported rates in **Table 2.1** were sustained for the initial 10 minutes of the reaction, after which a decrease in rate was observed (likely due to enzyme denaturation from excessive bubbling of air into solution). Total turnover numbers were determined after 45 minutes of reaction, after which it was found that no further significant turnover occurred.

References

(1) Urlacher, V. B.; Lutz-Wahl, S.; Schmid, R. D. *Appl. Microbiol. Biotechnol.* **2004**, *64*, 317-325.

(2) Urlacher, V.; Schmid, R. D. *Curr. Opin. Biotechnol.* **2002**, *13*, 557-564.

(3) Munro, A.; Leys, D.; McLean, K.; Marshall, K.; Ost, T.; Daff, S.; Miles, C. S.; Chapman, S.; Lysek, D.; Moser, C.; Page, C.; Dutton, P. *Trends Biochem. Sci.* **2002**, *27*, 250-257.

(4) Fang, X.; Halpert, J. R. *Drug Metab. Dispos.* **1996**, *24*, 1282-1285.

(5) Reipa, V.; Mayhew, M. P.; Vilker, V. L. *Proc. Natl. Acad. Sci. USA* **1997**, *94*, 13554-13558.

(6) Estabrook, R.; Faulkner, K.; Shet, M.; Fisher, C. *Methods Enzymol.* **1996**, *272*, 44-51.

(7) Faulkner, K.; Shet, M.; Fisher, C.; Estabrook, R. *Proc. Natl. Acad. Sci. USA* **1995**, *92*, 7705-7709.

(8) Schwaneberg, U.; Appel, D.; Schmitt, J.; Schmid, R. *J. Biotechnol.* **2000**, *84*, 249-257.

(9) Heller, A.; Degano, Y. *J. Am. Chem. Soc.* **1988**, *110*, 2615-2620.

(10) Murr, N. E. *Transition Met. Chem.* **1981**, *6*, 321-324.

(11) Roitel, O.; Scrutton, N. S.; Munro, A. W. *Biochemistry* **2003**, *42*, 10809-10821.

(12) Li, H.; Darwish, K.; Poulos, T. L. *J. Biol. Chem.* **1991**, *266*, 11909-11914.

(13) Narhi, L.; Fulco, A. *J. Biol. Chem.* **1986**, *261*, 7160-7169.

(14) Daff, S.; Chapman, S.; Turner, K.; Holt, R.; Govindaraj, S.; Poulos, T.; Munro, A. *Biochemistry* **1997**, *36*, 13816-13823.

(15) Ravichandran, K. G.; Boddupalli, S. S.; Hasemann, C. A.; Peterson, J. A.; Deisenhofer, J. *Science* **1993**, *261*, 731-736.

(16) Shirane, N.; Sui, Z.; Peterson, J. A.; Ortiz de Montellano, P. R. *Biochemistry* **1993**, *32*, 13732-13741.

(17) Cirino, P. C.; Arnold, F. H. *Adv. Synth. Catal.* **2002**, *344*, 1-6.

(18) Sheats, J.; Hlatky, G. *J. Chem. Educ.* **1983**, *60*, 1015-1016.

Table 2.1. Rates and total turnovers for the electrochemical biocatalytic reactions.

Enzyme	**Mediator**	**Rate (nmol product / nmol enzyme / min)**	**Total Turnover (nmols product / nmols enzyme)**
BM3	Cobaltocene cation	16.4 ± 0.6	224 ± 7
BM3	Cobalt(III) sepulchrate	37.8 ± 0.3	835 ± 7
hBM3	Cobaltocene cation	1.8 ± 0.5	58 ± 7
hBM3	Cobalt(III) sepulchrate	2.2 ± 0.1	76 ± 7

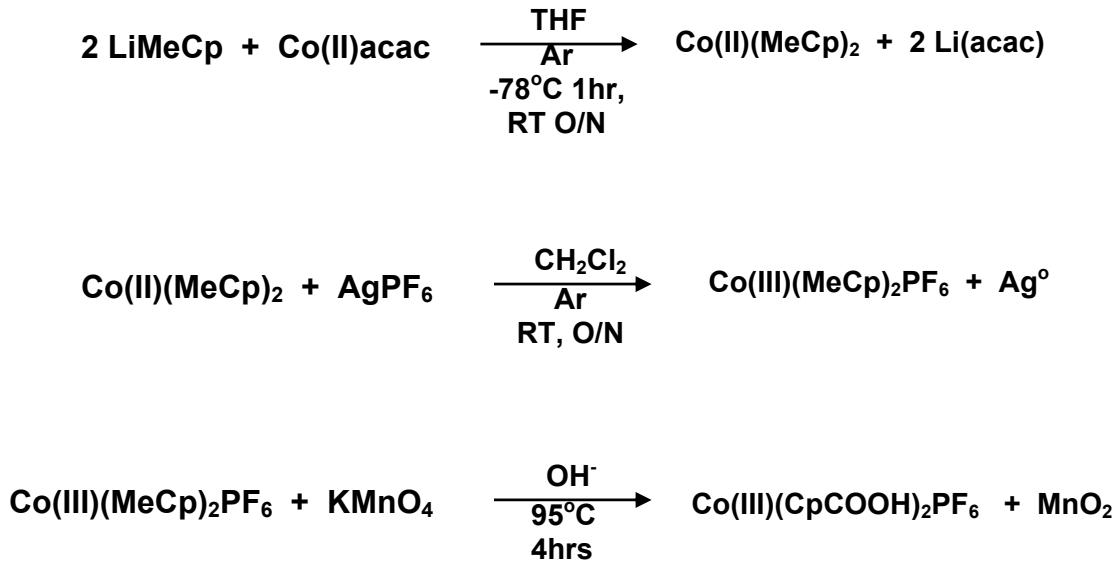

Scheme 2.1. Synthesis of 1,1'-dicarboxycobaltocenium hexafluorophosphate (M_{ox}).

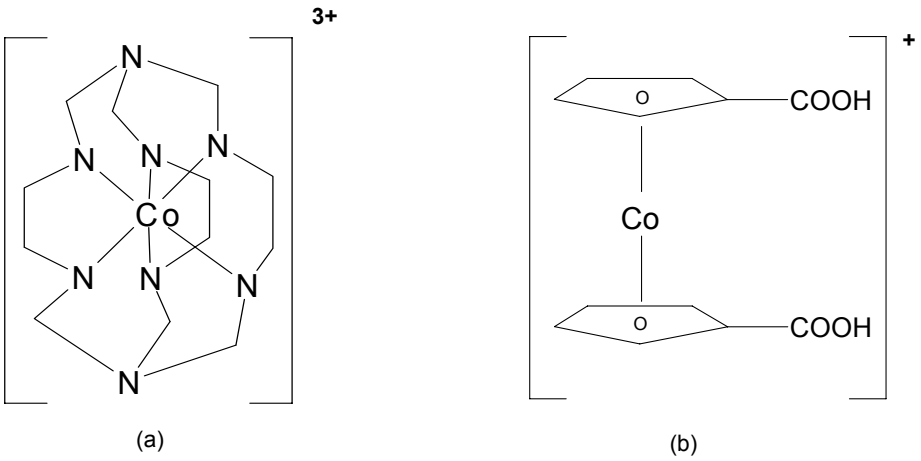

Figure 2.1. Structures of (a) cobalt(III) sepulchrate and (b) 1,1'-dicarboxycobaltocene cation.

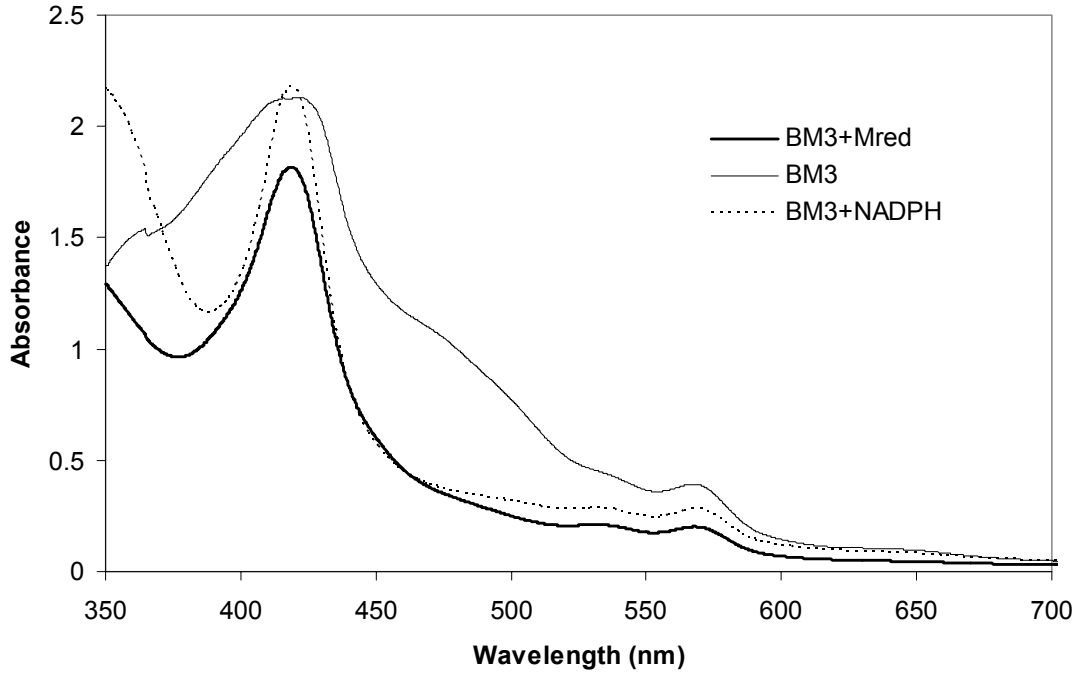

Figure 2.2. BM3 absorption spectra (oxidized and reduced proteins): the shoulder between 440 and 490 nm attributable to oxidized flavins disappears upon reduction by NADPH and M_{red}.

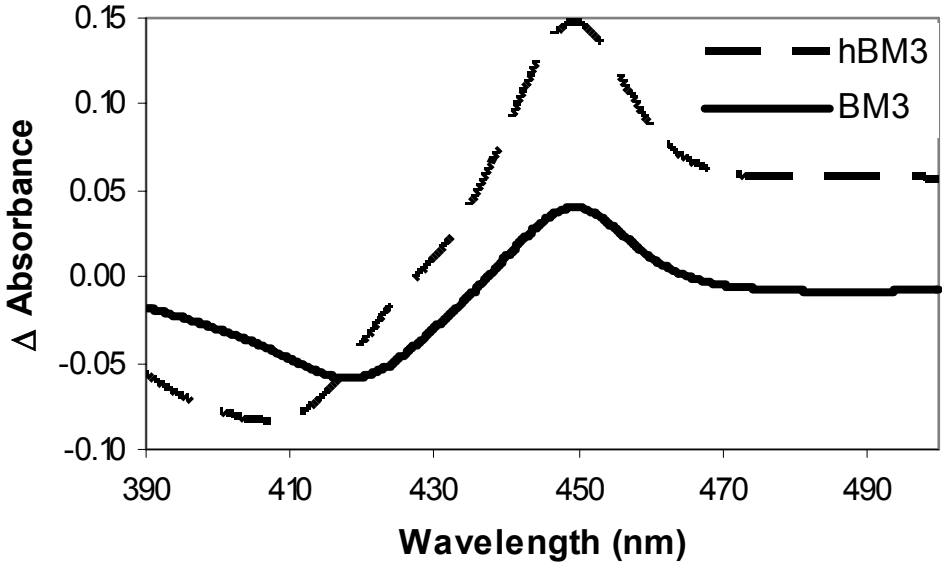

Figure 2.3. Spectra of both holo (BM3) and heme domain (hBM3) BM3 in the presence of carbon monoxide and M_{red}: the peaks at 448 nm indicate heme reduction by M_{red} and formation of an Fe^{II}-CO complex.

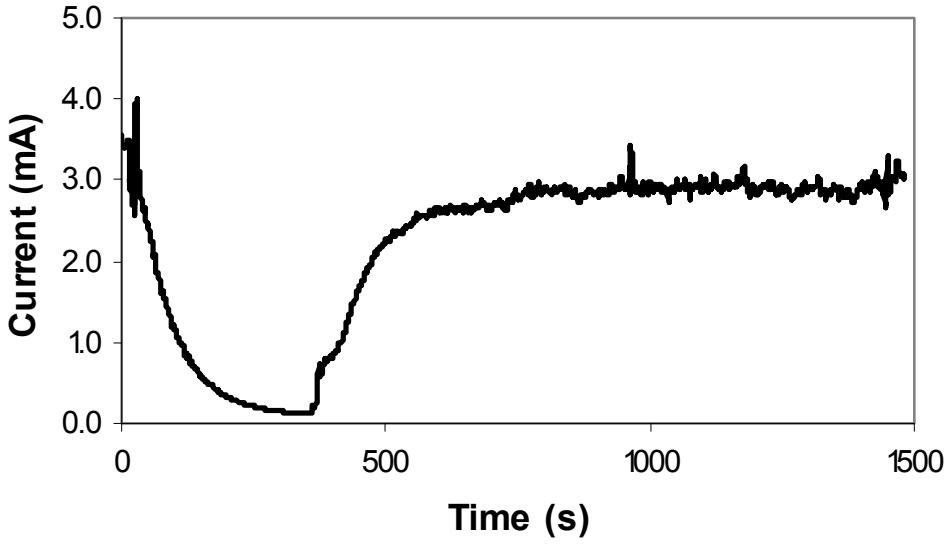

Figure 2.4. Current versus time for the electrochemical biocatalytic reaction: the initial decay represents anaerobic electrochemical reduction of M_{red}; this decay is followed by a spike in the current resulting from addition of oxygenated enzyme-substrate solution; a steady-state condition is established after 600 s (plateau region).

Chapter 3

Pyrene-Wired Heme Domain Cytochrome P450 BM3 Electrodes*

*Reproduced in part with permission from *J. Am. Chem. Soc.* **2004**, *126*, 10218-10219.

Acknowledgments: This work was in collaboration with M. G. Hill (Occidental College) and V. G Bittner (Caltech). We thank J. S. Magyar and J. R. Winkler (Caltech), T. L. Poulos (U.C. Irvine), and E. M. Spain (Occidental College) for helpful discussions; C. P. Collier (Caltech) for assistance with the AFM; NSF (HBG), NSERC (Canada) (AKU), and the David and Lucile Packard Foundation (MGH) for research support.

Abstract

We have electronically wired the cytochrome P450 BM3 heme domain through surface Cys^{387} to a graphite electrode with the use of a pyrene-terminated tether. AFM images clearly reveal that pyrene-wired enzyme molecules are adsorbed to the electrode surface. The enzyme-electrode system undergoes rapid and reversible electron transfer, displaying a standard rate constant higher than that of any other P450-electrode system. We also show that the graphite-pyrene-BM3 system catalyzes the four-electron reduction of dioxygen to water. Analogous experiments were also conducted with enzyme labeled at Cys^{62}, which is situated spatially adjacent to Cys^{387} but does not provide a similar well-coupled through-bond pathway to the heme. Surprisingly, the Cys^{62} mutant showed similar electrode kinetics. This demonstrates that the pyrene tether does not provide a unique through-bond pathway, but rather anchors the protein onto the electrode surface in a favorable docking mode for rapid heme reduction.

Abbreviations: P450, cytochrome P450; ET, electron transfer; BM3, cytochrome P450 from *Bacillus megaterium*; Py, N-(1-pyrene)iodoacetamide; BPG, basal plane graphite; hBM3, cytochrome P450 BM3 heme domain; AFM, atomic force microscopy; RDE, rotated-disk electrode; 12-pNCA, 12-p-nitrophenylcarboxylic acid; pNP, p-nitrophenol; HOPG, highly-oriented pyrolytic graphite

Introduction

The cytochromes P450 (P450s) are ubiquitous heme monooxygenases that catalyze a wide range of reactions under physiological conditions.[1] The value of their oxidative activity in both fine chemicals (e.g., alkane hydroxylation) and medical (e.g., pro-drug activation) industries has fueled research into capturing this activity *in vitro*. Of the P450s, flavocytochrome P450 from *Bacillus megaterium* (BM3) is particularly appealing for commercial use, owing to its ease of handling and the ability to create mutants with altered substrate specificity.[2]

Exploiting BM3 activity *in vitro* would be greatly facilitated if reductants other than NADPH could be found. While an electrode is perhaps the most attractive source of electrons, direct BM3 electrochemistry has been elusive, owing largely to poor electronic coupling to the deeply buried heme. An excellent example of a system highly coupled for electron transfer (ET) was presented by Sevrioukova *et al*: they achieved rapid heme reduction of BM3 photochemically (2.5×10^6 s^{-1} and 4.6×10^5 s^{-1} with and without substrate) by covalently tethering a ruthenium diimine to an engineered cysteine (N387C) on the heme domain of BM3 (hBM3).[3] The positioning of the Ru complex was meant to mimic the interaction between hBM3 and its reductase; indeed, the rapid rates suggest

that the complex was attached at a position that was well coupled to the heme. It occurred to us that "wiring" the N387C hBM3 mutant to an electrode through the engineered cysteine could also yield high electron tunneling rates. Previously, Katz utilized N-(1-pyrene)iodoacetamide (Py) (thiol specific) to anchor and electronically connect a photosynthetic reaction center to a basal plane graphite (BPG) electrode.[4] Thus, we made the hBM3 single surface cysteine mutant at position 387, attached Py to the cysteine, and successfully achieved rapid ET with the use of a BPG electrode. Wiring the enzyme in this way creates a system where the electrode mimics the reductase, leaving the active site accessible to molecules in solution.

Results and Discussion

Mutant Cys^{387}

Protein integrity after labeling with Py was confirmed by observing the Soret band of the reduced heme at 448 nm in CO-saturated buffer. Labeled protein (Py-hBM3) was verified by observing fluorescence of Py (~ 50% labeled). The protein film was prepared by suspending a BPG electrode in a ~ 20 μM Py-hBM3 solution. Cyclic voltammetry on the resulting film (**Figure 3.1**) revealed a couple centered at -340 mV. Neither unmodified enzyme nor Py alone produced a similar couple. The observed $E_{1/2}$ is assigned to the $Fe^{III/II}$ redox couple of the heme.[5,6] Compared to the native enzyme in its resting state (six-coordinate heme, low spin) as measured by redox titration, this potential is shifted approximately +230 mV.[7] As previously suggested, local electrostatic effects (e.g., solvation, surface interactions) likely contribute to the altered potential.[5]

The cathodic to anodic peak-current ratio in **Figure 3.1** is approximately 1.05, indicating a chemically reversible system.[8] A plot of the cathodic peak current versus the scan rate is linear, characteristic of a surface-confined species.[8] This plot also indicates the number of electrons transferred: the slope of the line divided by the area under the voltammogram at any sweep rate (39 nC) is equal to nF/4RT.[9] Performing this operation yields n = 1.2 ± 0.1, fully consistent with one-electron transfer.

Voltammetry in CO-saturated buffer shifted $E_{1/2}$ by +35 mV, as found for other P450 electrochemical systems (+45 mV to +80 mV).[6,10,11] The $E_{1/2}$ was also found to vary linearly with pH according to

$$E_{1/2} = 56 \text{ mV} - 58 \text{ mV/pH}$$

This indicates proton-coupled electron transfer.[12,13]

To characterize the surface, protein films were cast onto highly oriented pyrolytic graphite (HOPG) and imaged using atomic force microscopy (AFM) in tapping mode. **Figure 3.2a** shows a section of HOPG (800 nm x 800 nm) soaked in a Py-hBM3 solution, revealing a series of small islands (dark spots) ranging from 2-5 nm in height. Given that hBM3 is ~ 65 Å in diameter, it can be inferred that these islands represent protein clusters on the surface. **Figure 3.2b** shows the corresponding image of HOPG soaked in unlabeled hBM3. Clearly, no surface features are visible; this image is identical with HOPG soaked in buffer alone, and implies that only the Py-hBM3 conjugate adsorbs to the surface. Regarding surface coverage, **Figure 3.2a** suggests that there is sub-monolayer coverage. Cyclic voltammetry experiments on HOPG (0.25 cm^2) with a Py-hBM3 film (hBM3 monolayer = 1.4 x 10^{-12} mols) confirm this finding:

integrating under the cathodic peak yielded 6.2 x 10^{-13} mols of electroactive protein, or ~ 44% surface coverage.

The standard rate constant (k^o, $\Delta G^o = 0$) for the BPG-Py-hBM3 system was evaluated using Laviron's theory,[14] yielding a value of 650 ± 50 s^{-1}, which is the fastest electrode kinetics reported for any P450 system (**Table 3.1**). ET rates for photochemical reduction of the Fe^{III} heme[3] were used to estimate rates at zero driving force ($\Delta G^o = 0$) for substrate-free and substrate-bound hBM3: these were found to be 280 and 3300 s^{-1}.* As can be seen, k^o from our electrochemical experiments falls within this range.

The BPG-Py-hBM3 system is an excellent catalyst for dioxygen reduction (**Figure 3.3**). Negative controls (Py or hBM3 on BPG only) reveal slow dioxygen reduction at more negative potentials. Possible fates of dioxygen are reduction to peroxide (directly or through superoxide decomposition) or to water. To determine the number of electrons transferred to dioxygen, Py-hBM3 films were cast onto a BPG rotated-disk electrode (RDE). Using the Levich equation for an RDE,[8]

$$i_L = 0.62nFAD_o^{2/3}\omega^{1/2}v^{-1/6}C$$

theoretical lines for the one-, two-, and four-electron reduction of dioxygen were generated (**Figure 3.4**).† RDE experiments were conducted by performing electrolysis at -0.5 V and determining the limiting current for each rotation rate. The results of these experiments (solid points, **Figure 3.4**) scatter around the theoretical line for n = 4, suggesting that the BPG-Py-hBM3 system converts dioxygen primarily to water. Our proposal of an efficient four-electron reduction pathway is further supported by results

* See Experimental Methods for details on the calculation.

† The variables for air saturated water are: limiting current (i_L,A), electrode area (A, cm^2), diffusion coefficient (D_o, 1.7 x 10^{-5} cm^2/s for O_2 in water), angular velocity (ω, s^{-1}), kinematic viscosity (v, 0.01 cm^2/s for water), bulk concentration (C, 2.5 x 10^{-7} mol/cm^3 for O_2 in air saturated buffer at 25°C).

from an Amplex Red fluorescence assay for hydrogen peroxide, which revealed that only a small fraction of the current (< 17%) was used to generate the two-electron reduction product. This is in stark contrast to other P450 electrochemical systems, where peroxide is the primary product of dioxygen reduction.[10,12] Conceivably, dioxygen reduction to water can occur if ET is fast enough such that, after initial reaction to form a peroxy complex, the final two electrons arrive at the active site before peroxide dissociation. A precedent for this can be found in previous work with ruthenium-modified cobalt porphyrins:[15] π-backbonding by the ruthenium ligands increased the ET rate, creating a catalyst that reduced dioxygen primarily to water. For the BPG-Py-hBM3 system, the estimated k^o is so high that applying a potential of -0.5 V apparently leads to rapid reduction of dioxygen to water.

Mutant Cys^{62}

In the study reported by Sevrioukova *et al.*,[3] two single-surface-cysteine mutants were examined, Cys^{387} and Cys^{62}. Attaching the Ru complex to Cys^{62} did not result in observable ET. We found this intriguing: as shown in **Figure 3.5**, both positions are on the proximal side of the heme on the protein surface. Cys^{62} is spatially closer to the heme (15 Å), while Cys^{387}, although farther (19 Å), provides a potential through-bond pathway for heme reduction. The fact that the photochemical experiments with Cys^{62} resulted in no ET suggests that the Ru complex was not able to dock with the protein in a favorable orientation for ET. However, it is possible that anchoring Cys^{62} with Py onto BPG would allow the protein to optimally position itself on the electrode surface for rapid heme reduction.

We created the single-surface-cysteine mutant Cys^{62}, modified it with Py, and anchored it onto the surface of BPG. As can be seen from the voltammogram in **Figure 3.6**, this construct also appears to be electrochemically active and yields a voltammogram similar to Cys^{387}. However, although the $E_{1/2}$ for both mutants is similar, the voltammograms do differ in their peak separation ($E_{p,c} - E_{p,a}$): 55 ± 1 mV for Cys^{387} and 98 ± 3 mV for Cys^{62}. Increased peak separation for a surface bound species is indicative of greater resistance to charge transfer,[8] implying that electronic coupling between the electrode and the heme in Cys^{62} is less efficient compared to Cys^{387}.

The appropriate parameter for comparing the ET is k^o, which is estimated using Laviron's theory at scan rates where the peak separation is greater than 200 mV.[14] However, the smaller surface coverage (39 nC for Cys^{387} cf. 24 nC for Cys^{62}) made it difficult to record interpretable voltammograms at scan rates higher than 12 V/s for Cys^{62}. Laviron's theory does permit an estimation of k^o at scan rates where the limiting forms of the theoretical equations cannot be used; however, under these conditions there is a significant dependence of k^o on the scan rate, and so comparisons between the two mutants must be made at the same scan rate and should only be considered as a relative comparison within the context of the system. With this in mind, k^o evaluated at 8 V/s for Cys^{387} and Cys^{62} are 197 ± 12 s^{-1} and 84 ± 5 s^{-1}, respectively. Thus, although Cys^{62} appears to have slower ET kinetics compared to Cys^{387}, clearly Cys^{62} can still participate in rapid ET with the electrode.

Oxidative Catalysis

To test for hydroxylation acitivity, the substrate 12-p-nitrophenylcarboxylic acid (12-pNCA) was used. Hydroxylation at the carbon adjacent to the phenoxy group

produces a hemiacetal that rapidly decomposes to p-nitrophenol (pNP).[16] The product pNP can be readily detected spectrophotometrically at 400 nm, or electrochemically by looking for oxidation of pNP to the phenoxy radical at ~ 890 mV.[17]

Catalysis experiments were performed by sweeping the potential continuously at 20 mV/s between -250 mV and -600 mV for two hours. Experiments were performed this way because it was unclear at precisely what potential the reaction would be optimal; conceivably, performing bulk electrolysis at the wrong potential could result in ET being too fast or slow, leading to uncoupling. For all reactions, both positive (Py-hBM3 films) and negative (BPG only) controls were performed. Once completed, the reactions were immediately assayed electrochemically for pNP, after which they were concentrated ten times and then assayed spectrophotometrically.

Catalysis experiments were performed with both Cys^{62} and Cys^{387}. However, pNP could not be definitively detected using either the electrochemical or absorption assays. The inability of the Py-BM3-BPG system to support oxidative catalysis is probably due to improper protein folding on the electrode surface. This supposition is supported by two observations. First, there is the small shift in $E_{1/2}$ (+35 mV) when voltammograms are recorded in CO-saturated buffer. For comparison, the redox potential of the $Fe^{III/II}$ couple in native rabbit liver P450 in the presence of CO is shifted +180 mV.[18] Thus, the small shift in the BM3 heme potential in the presence of CO likely indicates a perturbed heme environment on the electrode. Second, once immobilized on the surface, the protein probably loses much of its flexibility due to aggregation. This is supported by the AFM image in **Figure 3.2a**, which suggests that the protein adsorbs onto the graphite surface in clusters. P450s are known to undergo large conformational

changes upon substrate binding;[19,20] restricting this motion by confining the protein to the electrode surface could very well abolish the enzyme's catalytic activity.

Experimental Methods

Electrode Preparation

Pyrolytic graphite electrodes (0.07 cm^2) were used for voltammetry with the basal plane exposed. The electrodes were sanded to expose a fresh surface, and then they were sonicated briefly in water. Next, the electrodes were polished sequentially with 0.3 μm and then 0.05 μm alumina slurries, followed by sonication and drying in air. HOPG electrodes were cleaned by removing a few layers from the surface with adhesive tape prior to use.

Mutagenesis and Protein Expression

The single surface cysteine mutants at positions 62 and 387 were constructed as previously described.[3] During cloning, a 6-His tag was introduced at the C-terminus of the protein after Thr^{464}, followed by a stop codon. Cloning, expression, purification, and quantification of the protein proceeded as previously described.[21]

Protein and Electrode Modification

N-(1-pyrene)iodoacetamide (Py) was purchased from Molecular Probes. A 20 μM stock solution of the Py probe was made in DMSO. A solution containing 50 μM protein in 30 mM KP_i pH 7.4 buffer was partially degassed by blowing Ar over it for 20 minutes. Next, 15 μL of the Py solution was slowly added to the protein solution while being stirred. This mixture was protected from light with aluminum foil and left stirring in the dark under a constant stream of argon at room temperature. After two hours, the

solution was passed over a PD 10 column (Pharmacia) equilibrated with 30 mM KP_i pH 7.4 to separate the unreacted probe from the Py-hBM3 conjugate. Electrodes were filmed by suspending them in 200 µL of the Py-hBM3 solution in a refrigerator (~ 10°C) overnight.

Fluorescence of the pyrene probe was used to confirm labeling of the protein, as described by Molecular Probes. Emission spectra of the purified pyrene-protein conjugate were recorded after excitation at 340 nm. For the assay, the protein solution was diluted to 2.6 µM with 30 mM KP_i pH 7.4.

The labeling efficiency was determined using Ellman's reagent, 5,5'-dithio-bis-(2-nitrobenzoic acid), for quantifying free sulfhydryl groups as described by Pierce Biotechnology. A purified solution of the protein-pyrene conjugate was diluted to 0.4 µM with 50 mM KP_i pH 8 to a final volume of 1 mL. 50 µL of a 4 mg/mL solution of Ellman's reagent were added to the diluted protein, and the absorption spectrum was recorded. The number of free cysteines was calculated using an extinction coefficient of 14,150 $M^{-1}cm^{-1}$ at Abs_{412}. Based on this, the labeling efficiency was determined to be 50%.

Voltammetry

A CH Instruments Electrochemical Workstation system was used for all electrochemistry. Voltammetry was performed in a three compartment cell, with a frit and Luggin capillary separating the Pt wire auxiliary and Ag/AgCl reference, respectively. The buffer solution, 50 mM KP_i / 20 mM KCl / pH 7, was thoroughly degassed by bubbling argon through it for at least 20 minutes. After degassing, argon

was continuously blown through the headspace of the cell to maintain an anaerobic environment.

Rotated-Disk Electrode Experiments

A 0.13 cm^2 pyrolytic graphite electrode with the basal plane exposed was used. The electrode was sanded, polished sequentially with 0.3 μm and 0.05 μm alumina slurries, sonicated, and dried. Experiments were carried out in a two compartment cell, with the working electrode separated from the Ag/AgCl reference and Pt auxiliary electrodes. The solution was approximately 30 mL of 50 mM KP_i / 20 mM KCl / pH 7. All experiments involving oxygen reduction were carried out in air saturated buffer ($[O_2]$ ~ 250 μM). A Pine Instruments rotator was used to control the rotation rate, while a CH Instruments Electrochemical Workstation was used to apply the potential and monitor the current response.

BPG-RDE experiments with Py-hBM3 films were conducted by performing bulk electrolysis at -0.5 V at different rotation rates. Typically, the limiting current used to make the Levich plot is the steady state value observed during the reaction. However, it was found that decomposition of the films occurred over the course of the experiment. This was illustrated both by the decay of the current response with time during the rotation experiment, and the reduced current response of the film after rotation compared to before rotation as seen by cyclic voltammetry. Thus, the limiting current was taken to be the initial current after the start of electrolysis with rotation. This was done by plotting the log(current) vs. time, and extrapolating the data back to t = 0 s. Rotation rates above 700 rpm resulted in highly irreproducible data due to rapid film decomposition.

Hydrogen Peroxide Assay

Hydrogen peroxide concentrations were determined using the Amplex Red fluorescence assay supplied by Molecular Probes, using the 96-well procedure precisely as described by the company. Based on the standard curve generated, the detection limit was determined to be ~ 30 nM.

Calculation of Electron Transfer Rates

Rates for the photochemical system were calculated using the equation

$$k_{ET} = A \exp[-(\Delta G^o + \lambda)/(4\lambda k_B T)]$$

where λ was approximated to be 0.8 eV at 298 K. The zero-driving force rates ($\Delta G^o = 0$) were calculated by equating the pre-exponential factors (A) for the photochemical experiments with known rate (ΔG^o = -0.98 eV or -1.11 eV for substrate free and substrate bound hBM3, respectively) to the scenario with no driving force and solving for $k_{ET}(\Delta G^o = 0)$.

The standard rate constant (k^o) for the electrochemical system was calculated from Laviron's theory using the theoretical curve for $\alpha = 0.5$. The peak splitting ($E_{p,c} - E_{p,a}$) determined at 100 V/s was 130 mV.

pNP Assays

A 15 mM solution of the substrate 12-pNCA was made in DMSO and dissolved by heating briefly to 80°C. 50 µL of the substrate solution were added to 1 mL of 5 mM KP_i pH 8. This solution was placed into the working compartment of a three compartment cell. The working electrode (Py-hBM3 filmed or un-filmed BPG) was placed into the cell and the potential was cycled between -0.25 V and -0.6 V at 20 mV/s for two hours with slow stirring in air. After the reaction, the working electrode was

replaced with a 1.5 mm diameter glassy carbon electrode that was prepared by polishing with 0.3 um and then 0.05 um alumina, sonicating, and drying. Using this electrode, the potential was swept between 0.6 V and 1.1 V at 50 mV/s to assay for pNP produced, which would be indicated by an oxidation wave at 890 mV (phenoxy radical). The solution was then removed and the solvent was evaporated, followed by resuspending the precipitated salts in 100 μL 50 mM KP_i pH 8. This solution was then analyzed using a spectrophotometer for absorbance at 400 nm.

Electrochemical determination of pNP concentrations utilized the Randles-Sevcik equation, $I_p = (2.687 \times 10^5)n^{3/2}v^{1/2}D^{½}AC$, where n is the number of electrons transferred, v is the scan rate (V/s), D is the diffusion coefficient (cm^2/s), A is the area of the electrode (cm^2), and C is the bulk concentration of pNP. The diffusion coefficient of pNP was experimentally determined to be 2.1×10^{-6} cm^2/s using the Randles-Sevcik equation. Spectrophotometric determination of pNP utilized an experimentally determined molar absorptivity of 13700 $M^{-1}cm^{-1}$ in 50 mM KP_i pH 8.

References

(1) Ortiz de Montellano, P. R., Ed. *Cytochrome P450: Structure, Mechanism, and Biochemistry*; Second Edition; Plenum Press: New York, 1995.

(2) Munro, A.; Leys, D.; McLean, K.; Marshall, K.; Ost, T.; Daff, S.; Miles, C.; Chapman, S.; Lysek, D.; Moser, C.; Page, C.; Dutton, P. *Trends Biochem. Sci.* **2002**, *27*, 250-257.

(3) Sevrioukova, I. F.; Immoos, C. E.; Poulos, T. L.; Farmer, P. *Isr. J. Chem.* **2000**, *40*, 47-53.

(4) Katz, E. *J. Electroanal. Chem.* **1994**, *365*, 157-164.

(5) Lvov, Y. M.; Lu, Z.; Schenkman, J. B.; Zu, X.; Rusling, J. F. *J. Am. Chem. Soc.* **1998**, *120*, 4073-4080.

(6) Lei, C.; Wollenberger, U.; Jung, C.; Scheller, F. W. *Biochem. Biophys. Res. Comm.* **2000**, *268*, 740-744.

(7) Daff, S.; Chapman, S.; Turner, K.; Holt, R.; Govindaraj, S.; Poulos, T.; Munro, A. *Biochemistry* **1997**, *36*, 13816-13823.

(8) Bard, A. J.; Faulkner, L. R. *Electrochemical Methods*; Second Edition; John Wiley & Sons, Inc.: New York, 2001.

(9) Brown, A. P.; Koval, C.; Anson, F. C. *J. Electroanal. Chem.* **1976**, *72*, 379-387.

(10) Fleming, B. D.; Tian, Y.; Bell, S. G.; Wong, L.; Urlacher, V.; Hill, H. A. O. *Eur. J. Biochem.* **2003**, *270*, 4082-4088.

(11) Zhang, Z.; Nassar, A.-E.; Lu, Z.; Schenkman, J. B.; Rusling, J. F. *J. Chem. Soc., Faraday Trans.* **1997**, *93*, 1769-1774.

(12) Munge, B.; Estavillo, C.; Schenkman, J. B.; Rusling, J. F. *ChemBioChem* **2003**, *4*, 82-89.

(13) Aguey-Zinsou, K.; Bernhardt, P. V.; Voss, J. J. D.; Slessor, K. E. *Chem. Commun.* **2003**, 418-419.

(14) Laviron, E. *J. Electroanal. Chem.* **1979**, *101*, 19-28.

(15) Anson, F. C.; Shi, C.; Steiger, B. *Acc. Chem. Res.* **1997**, *30*, 437-444.

(16) Schwaneberg, U.; Otey, C.; Cirino, P. C.; Farinas, E.; Arnold, F. H. *J. Biomol. Screen.* **2001**, *6*, 111.

(17) Dressman, S. F.; Simeone, A. M.; Michael, A. C. *Analytical Chemistry* **1996**, *68*, 3121-3127.

(18) Guengerich, F. P.; Ballou, D. P.; Coon, M. J. *The Journal of Biological Chemistry* **1975**, *250*, 7405-7414.

(19) Poulos, T. L. *Proc. Natl. Acad. Sci.* **2003**, *100*, 13121-13122.

(20) Dunn, A. R.; Dmochowski, I. J.; Bilwes, A. M.; Gray, H. B.; Crane, B. R. *Proc. Natl. Acad. Sci.* **2001**, *98*, 12420-12425.

(21) Cirino, P. C.; Arnold, F. H. *Adv. Synth. Catal.* **2002**, *344*, 1-6.

(22) Liu, H.; Wang, L.; Hu, N. *Electrochimica Acta* **2002**, *47*, 2515-2523.

Table 3.1. Comparison of k^o for various heme protein electrochemical systems.

System	k^o (s^{-1})	Ref.
Pyrene modified heme domain BM3 on graphite	650	This work
CAM on glassy carbon coated with montmorillonite	5-152	6
Heme domain BM3 in a DDAB film	221	10
Hb in DHP-PDDA film	30	22

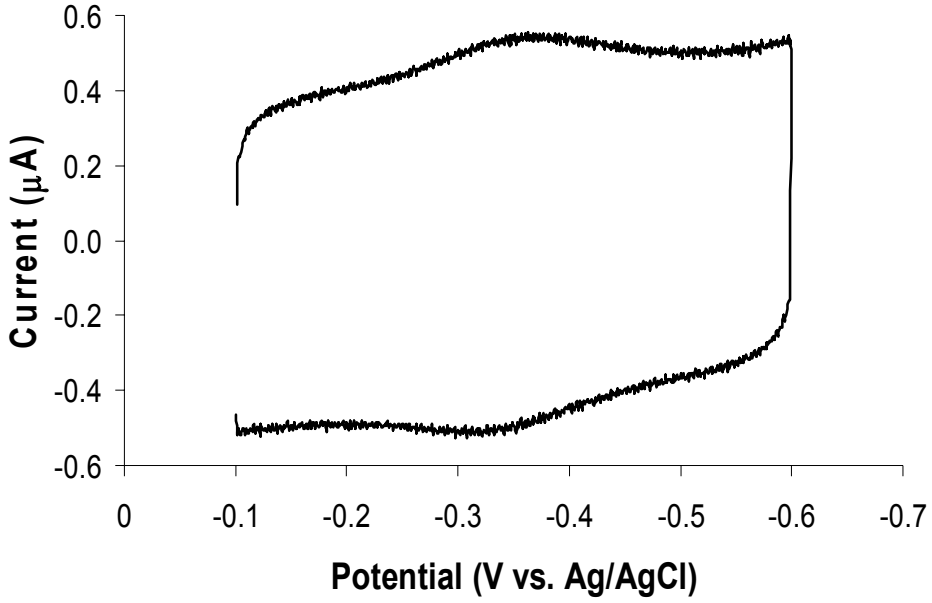

Figure 3.1. Cyclic voltammogram of the Py-hBM3 conjugate on BPG (0.07 cm^2) at 200 mV/s in 50 mM KP_i / 20 mM KCl / pH 7.

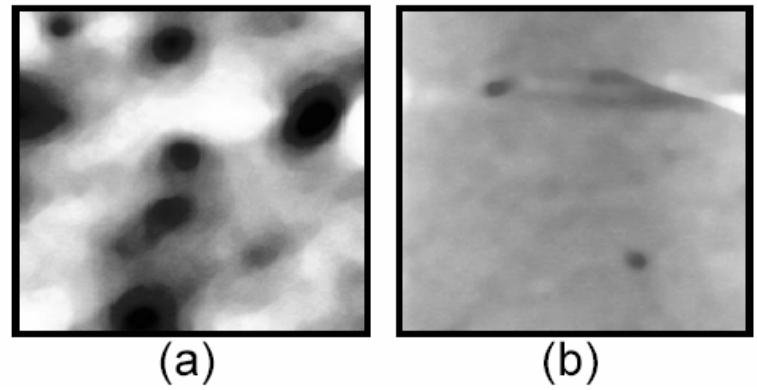

Figure 3.2. 800 nm x 800 nm AFM images of HOPG soaked in (a) Py-hBM3 and (b) hBM3.

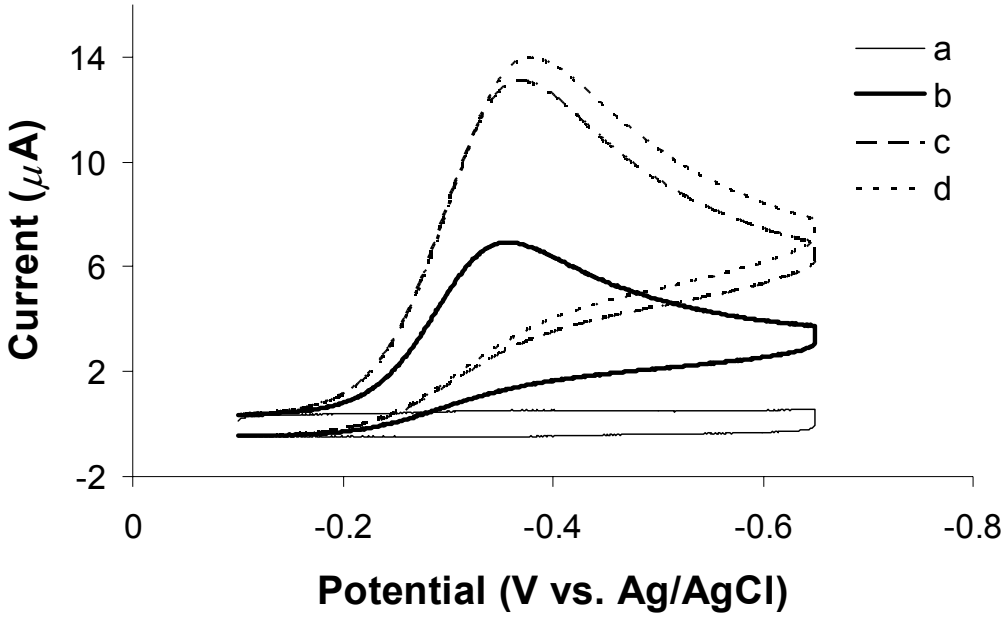

Figure 3.3. Cyclic voltammograms at 200 mV/s of Py-hBM3 on BPG in the presence of increasing amounts of dioxygen: (a) 0 μM, (b) 42 μM, (c) 71 μM, (d) 94 μM.

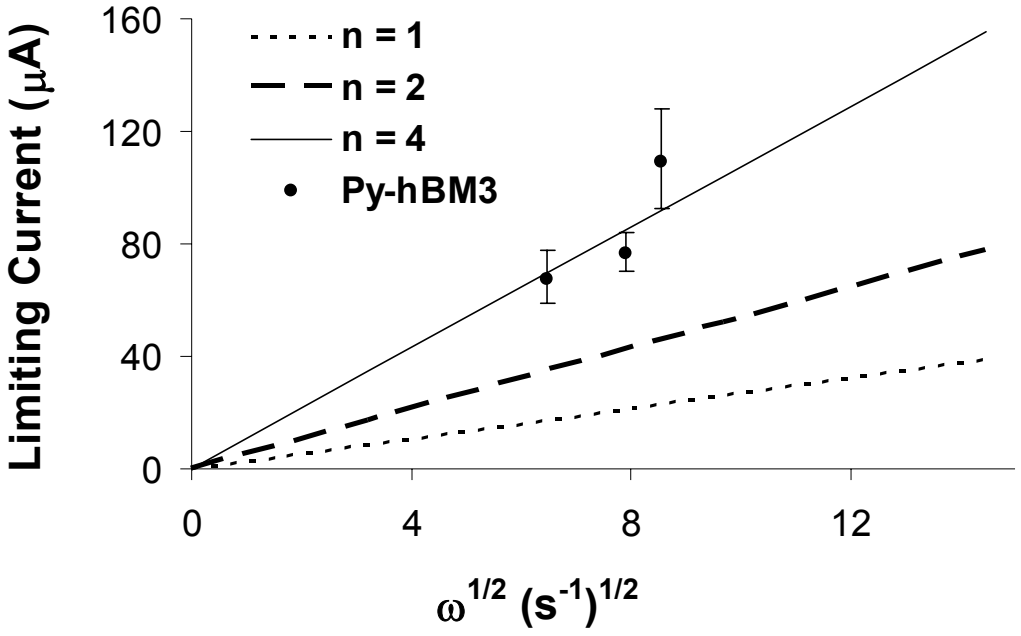

Figure 3.4. Solid lines: Levich plots derived for the one-, two-, and four-electron reductions of dioxygen. The points represent the limiting current at 400, 600, and 700 rpm for Py-hBM3 films on BPG-RDE in the presence of dioxygen (250 μM).

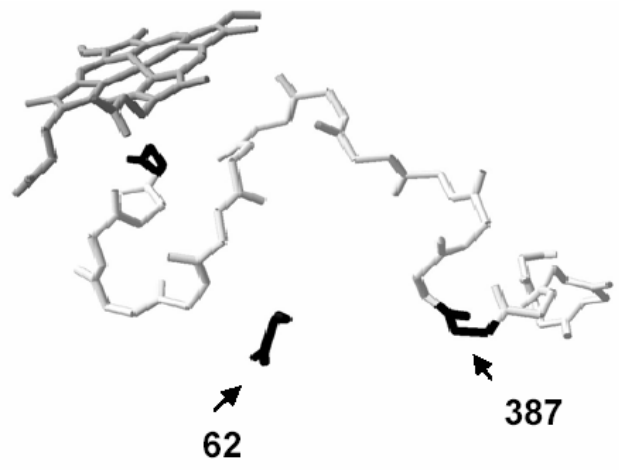

Figure 3.5. The 380-400 peptide loop is shown, as are the positions of residues 62 and 387 relative to the heme.

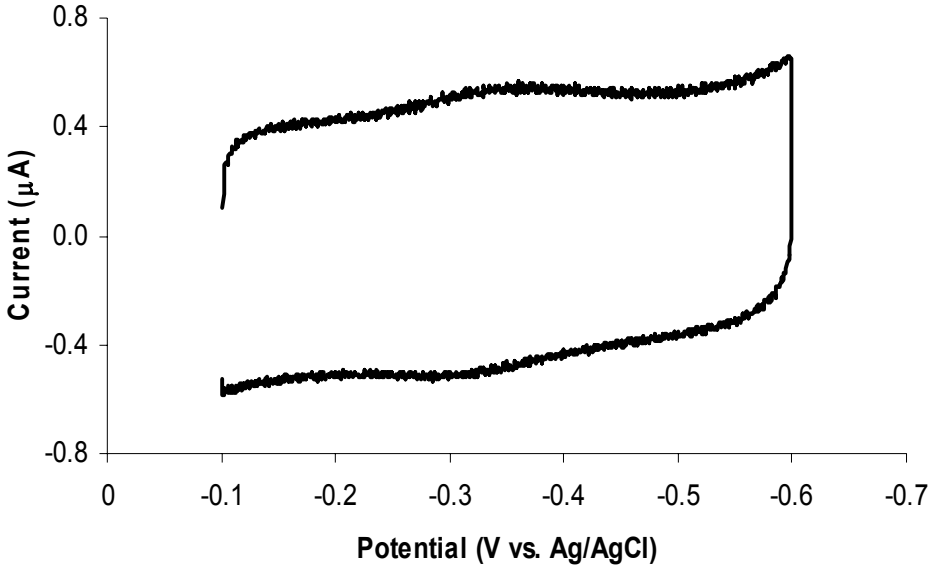

Figure 3.6. Cyclic voltammogram at 200 mV/s of the Cys^{62} mutant modified with Py and filmed onto BPG (0.07 cm^2) in 50 mM KP_i / 20 mM KCl / pH 7.

Chapter 4

Electrochemistry of Cytochrome P450 BM3 in Sodium Dodecyl Sulfate Films

Acknowledgements: This work was in collaboration with M. G. Hill at Occidental College. We thank C. E. Immoos for helpful discussions and NSERC (Canada) (AKU) for research support.

Abstract

Direct electrochemistry of the cytochrome P450 BM3 heme domain was achieved by confining the protein within SDS films on the surface of basal plane graphite electrodes. Cyclic voltammetry revealed a reversible couple due to $Fe^{III/II}$ centered at -330 mV vs. Ag/AgCl at pH 7.4. Laviron's theory was used to estimate a standard rate constant of 40 s^{-1}. Voltammograms in the presence of dioxygen resulted in catalytic waves at the onset of Fe^{III} reduction. Electrolyses performed in the presence of dioxygen and substrates did not result in any products, suggesting that the protein is not capable of catalyzing substrate oxidation within the SDS film.

Abbreviations: hBM3, heme domain cytochrome P450 BM3; ET, electron transfer; SDS, sodium dodecyl sulfate; BPG, basal plane graphite; DDAB, didodecyldimethylammonium bromide.

Introduction

The ability of cytochromes P450 to perform challenging oxidation reactions under physiological conditions makes them attractive targets for *in vitro* applications. As discussed in **Chapter 1**, capturing the activity of cytochrome P450 BM3 *in vitro* would be greatly facilitated if reductants other than NADPH could be found. Following this theme, **Chapter 2** described the application of dicarboxycobaltocene as a recyclable electrochemical mediator for BM3 biocatalysis.

In addition to replacing NADPH, eliminating the BM3 reductase domain would further aid *in vitro* applications by 1) dispensing with the relatively unstable flavin cofactors,[1] 2) avoiding enzyme inactivation by over-reducing the flavins,[2] and 3) eliminating uncoupling of electron transfer (ET) through cleavage of the reductase-heme domain linkage.[3] Direct reduction of the BM3 heme domain (hBM3) with an electrode is perhaps the simplest method of supplying the necessary reducing equivalents for catalysis. In pursuit of this, **Chapter 3** described a novel methodology for achieving direct hBM3 electrochemistry by "wiring" the protein to the electrode surface. However, substrate oxidation was not observed.

Some of the most successful bioelectrochemical systems employ the use of protein films on conductive supports to achieve efficient electronic coupling between the electrode and the enzyme. In particular, Rusling has pioneered the use of surfactant films

on carbon surfaces for direct electrochemistry of heme proteins.[4] The surfactant is deposited onto the electrode, resulting in the formation of bilayers and micelles into which the protein incorporates. The end result is a system that supports rapid and reversible ET between the electrode and the enzyme; this is in sharp contrast to the slow and quasi-reversible electrochemistry of heme proteins in solution.[5] In addition to enhancing ET, the surfactant film also confers stability to the enzyme-electrode system. It has been shown that even after prolonged storage, the enzyme can retain most of its electrochemical activity (e.g., up to 90% active after one month of storage at 4^{o}C).[4] These advantages have led to many studies exploiting this technique, and subsequent comprehensive reviews on thin film electrochemistry.[6,7]

Utilizing the surfactant film methodology, we attempted to create a catalytic system with hBM3 using sodium dodecyl sulfate (SDS) films on the surface of basal plane graphite electrodes (BPG). Notably, SDS films have been successfully used for myoglobin on graphite electrodes:[8] the $Fe^{III/II}$ couple was observed at -232 mV (vs. Ag/AgCl), and ET was rapid and reversible. Thus, based on this prior work, we attempted to develop a similar system for catalysis with hBM3.

Results and Discussion

Protein films were cast onto BPG by applying a solution of hBM3, surfactant, and buffer to the surface, followed by slow evaporation of the water under high humidity. A representative voltammogram of hBM3 in SDS is shown in **Figure 4.1**. Negative controls (no enzyme, no film, or graphite alone) resulted in no observable waves. $E_{1/2}$ was measured to be -330 mV (pH 7.4, vs. Ag/AgCl), consistent with the $Fe^{III/II}$ redox

couple of the heme.[4] Compared to hBM3 in solution (six coordinate heme, low spin), this potential is shifted +237 mV.[9] Typically, potential shifts on electrode surfaces are attributed to effects from the local electrostatic environment (buffer, surfactant, etc.).[10] In this instance, the potential shift is likely a consequence of local electrostatic effects and perturbation of the heme spin state resulting from SDS binding in the active site. SDS is a substrate for BM3 (ω-1 and ω-2 hydroxylation) and causes a low- to high-spin shift of the Fe^{III} heme when bound in the active site, resulting in a higher heme potential. Since a large excess of SDS is present during the filming process, an SDS molecule most certainly binds in the active site and is thus partially responsible for the altered heme potential observed during voltammetry.

Previous work with P450 confined in didodecyldimethylammonium bromide (DDAB) films on graphite revealed that the $Fe^{II/I}$ redox couple is also accessible.[11] However, attempts to access the hBM3 $Fe^{II/I}$ couple in SDS on BPG by scanning to -1.5 V resulted in no observable signals. In addition, scanning in the region of the $Fe^{III/II}$ couple after scanning out to -1.5 V resulted in complete loss of the protein response. Most likely, polarizing the electrode to such a negative potential causes desorption of the negatively charged SDS molecules, with subsequent loss of the protein signal. A related phenomenon has been observed for DDAB films on graphite: polarizing the electrode by applying a positive potential causes a phase transition in this positively charged surfactant to a more liquid-like state.[12] Given the high solubility and relatively high critical micelle concentration of SDS, a similar phase transition would likely cause this surfactant to desorb from the graphite surface.

Up to 10 V/s, the peak current was found to be linear with scan rate, indicating a surface confined system.[13] Analysis of **Figure 4.1** revealed that the cathodic to anodic peak current ratio ($I_{p,c} / I_{p,a}$) was 0.9, which demonstrates electrochemical reversibility: all of the redox active sites that are reduced during the cathodic sweep are re-oxidized on the reverse scan.[13] Regarding surface coverage, the number of moles of electroactive protein reduced during the cathodic sweep can be determined by integrating under the peak in **Figure 4.1**. When this is done, a value of 3 μC is found, which results in a surface coverage (Γ_{P450}) of 2 x 10^{-10} mol/cm^2 and corresponds to approximately 33% of the total protein deposited during filming. Loading more protein onto the surface during filming did not increase the amount that was electroactive. The calculated surface coverage is comparable to other systems (cf. 1 x 10^{-10} mol/cm^2 for hemoglobin[14] and 7 x 10^{-10} mol/cm^2 for P450 CAM[24]).

Laviron's theory was used to estimate the standard rate constant (k^o, $\Delta G^o = 0$).[15] k^o evaluated at 10 V/s was determined to be 40 s^{-1}. For comparison, k^o for hBM3 in DDAB films on pyrolytic graphite is 221 s^{-1}.[16] Thus, although ET for hBM3 in SDS is slow compared to hBM3 in DDAB, it is still much faster than direct electrochemistry of P450 in solution (~ 0.01 s^{-1}).[17]

Catalytic activity was first assessed by observing the response of the system to dioxygen. **Figure 4.2** displays voltammograms of hBM3 in SDS on BPG in the presence of increasing amounts of dioxygen. **Figure 4.2** contains three important observations: 1) the voltammograms become increasingly less reversible as more dioxygen is added, indicating oxidation of the reduced heme by dioxygen; 2) the cathodic peak potential shifts positive with increasing amounts of dioxygen in solution, illustrating the known

potential shift that accompanies dioxygen binding to the heme;[18] 3) the cathodic peak current increases with increasing amounts of dioxygen, indicating catalytic reduction of dioxygen. Voltammograms in the absence of protein result in slow dioxygen reduction occurring at more negative potentials.

Next, the system was assayed for its ability to support catalytic substrate oxidation. For these reactions, films were prepared on larger pieces of graphite or carbon cloth (see Experimental Methods). Electrolysis reactions were conducted at -0.6 V (vs. Ag/AgCl) in a stirred cell in air. Several substrates were tried, including lauric acid, styrene, and oxidation of the SDS film itself. However, no oxidized products were observed using wild type hBM3.

Previous work with P450 CAM suggested that catalysis within films on electrode surfaces occurs through the peroxide shunt: hydrogen peroxide formed by P450-catalyzed reduction of dioxygen is used to support substrate oxidation.[19] This was confirmed by performing control reactions with catalase, which inhibited product formation. To determine if hBM3 is in fact competent for substrate oxidation within the SDS film, catalysis experiments were conducted using hBM3 mutant 5H6, which has enhanced catalytic activity utilizing the peroxide shunt pathway.[20] However, performing electrolysis experiments with 5H6 resulted in no substrate oxidation. The ability of the protein to reduce dioxygen, coupled with an inability to perform substrate oxidation, suggests: 1) the enzyme is not in a conformation that allows substrates to bind; 2) the substrates have a higher affinity for the film, and therefore do not partition into the protein active site; 3) polarizing the electrode negatively for extended periods of time causes film desorption. Evidence for (1) and (2) comes from anaerobic voltammograms

in the presence of substrate: the potential of the $Fe^{III/II}$ couple is insensitive to the presence of substrates, which is in contrast to the known potential shifts that occur upon substrate binding. Evidence to support (3) comes from voltammetry after electrolysis, which reveals that the $Fe^{III/II}$ couple is no longer present. Thus, the inability of hBM3 to perform substrate oxidation in SDS films is likely due in some part to all of these factors.

Experimental Methods

Protein Expression and Purification

Expression and purification of wild type and mutant BM3 heme domains proceeded as previously described.[21]

Electrode Preparation and Voltammetry with hBM3-SDS Films

Electrodes were made using the basal plane of pyrolitic graphite (Union Carbide) (0.2 cm^2). The surfaces were prepared by abrasion with 600-grit sandpaper, followed by brief sonication in ddH_2O and drying with a heat gun. Protein films were applied by placing 20 μL of a solution containing 6 μM hBM3, 15 mM SDS, and 8 mM KP_i pH 7.4 onto the electrode surface. The electrodes were covered under water-saturated air for 6 hours, followed by uncovering and drying in air overnight. Prior to voltammetry, the films were thoroughly dried under vacuum for 1 hour.

A CH Instruments Electrochemical Workstation was used for the reactions. Voltammetry experiments were performed in a three-compartment cell, using a platinum wire auxiliary and a Ag/AgCl reference (BAS). The buffer, 30 mM KP_i / 130 mM NaCl / pH 7.4, was thoroughly degassed by evacuating and backfilling with argon multiple times. All experiments were performed under argon unless otherwise stated.

Electrode Preparation for Bulk Electrolysis with hBM3-SDS Films

Carbon cloth electrodes (ElectroChem, Inc.) were cleaned by soaking in concentrated nitric acid for 1 hr, followed by repeated rinsing with ddH_2O and final drying with a heat gun. Films were cast by soaking the electrode in a solution of 10 mM SDS, 5 μM hBM3, and 6 mM KP_i pH 7.4 for 5 hrs, followed by drying in air overnight.

Pyrolytic graphite for electrolysis was obtained from GE Advanced Ceramics. The surface was prepared by abrading with 600-grit sandpaper, followed by brief sonication in ddH_2O and drying with a heat gun. Protein films were applied by placing 250 μL of a solution containing 6 μM hBM3, 15 mM SDS, and 8 mM KP_i pH 7.4 onto the electrode surface. The electrodes were covered under water-saturated air overnight, followed by uncovering and drying in air overnight.

Electrolysis Protocols and Activity Assays

Electrolysis reactions were performed in a two-compartment cell separated by a glass frit, with the working and reference Ag/AgCl electrodes in one compartment and the Pt auxiliary in the second compartment. The potential was set to -0.6 V, and the cell was stirred in air. The reaction solution typically consisted of 1-5 mM of substrate (lauric acid, styrene) in 30 mM KP_i / 130 mM KCl / pH 7.4 buffer, in a final volume of 10 mL. The reaction was allowed to proceed for 1 hr, after which it was extracted and analyzed by GC/MS. GC/MS protocols for lauric acid and SDS were performed as described[21] (details also in **Chapter 2**).

For styrene reactions, 5 μL of a 5 mM solution of 1-hexanol in methanol (internal standard) were added to the reaction solution after electrolysis, followed by extraction with 400 μL of $CHCl_3$. The extract was then analyzed by GC/MS using an Innowax

column. Styrene, styrene oxide, and benzaldehyde were quantified using a calibration curve constructed from standards, and relating the area of these standards to that of the internal standard.

References

(1) Govindaraj, S.; Poulos, T. *J. Biol. Chem.* **1997**, *272*, 7915-7921.

(2) Munro, A.; Leys, D.; McLean, K.; Marshall, K.; Ost, T.; Daff, S.; Miles, C.; Chapman, S.; Lysek, D.; Moser, C.; Page, C.; Dutton, P. *Trends Biochem. Sci.* **2002**, *27*, 250-257.

(3) Sevrioukova, I. F.; Li, H.; Zhang, H.; Peterson, J. A.; Poulos, T. L. *Proc. Natl. Acad. Sci. USA* **1999**, *96*, 1863-1868.

(4) Rusling, J. F. *Acc. Chem. Res.* **1998**, *31*, 363-369.

(5) Kazlauskaite, J.; Westlake, A. C. G.; Wong, L.-L.; Hill, H. A. O. *Chem. Commun.* **1996**, 2189-2190.

(6) Willner, I.; Katz, E. *Angew. Chem. Int. Ed.* **2000**, *39*, 1180-1218.

(7) Farmer, P.; Lin, R.; Bayachou, M. *Comments Inorg. Chem.* **1998**, *20*, 101-120.

(8) Rusling, J. F.; Nassar, A.-E. F. *J. Am. Chem. Soc.* **1993**, *115*, 11891-11897.

(9) Daff, S.; Chapman, S.; Turner, K.; Holt, R.; Govindaraj, S.; Poulos, T.; Munro, A. *Biochemistry* **1997**, *36*, 13816-13823.

(10) Lvov, Y. M.; Lu, Z.; Schenkman, J. B.; Zu, X.; Rusling, J. F. *J. Am. Chem. Soc.* **1998**, *120*, 4073-4080.

(11) Immoos, C. E.; Chou, J.; Bayachou, M.; Blair, E.; Greaves, J.; Farmer, P. J. *J. Am. Chem. Soc.* **2004**, *126*, 4934-4942.

(12) Boussaad, S.; Tao, N. J. *J. Am. Chem. Soc.* **1999**, *121*, 4510-4515.

(13) Bard, A. J.; Faulkner, L. R. *Electrochemical Methods*; Second Edition; John Wiley & Sons, Inc.: New York, 2001.

(14) Liu, H.; Wang, L.; Hu, N. *Electrochimica Acta* **2002**, *47*, 2515-2523.

(15) Laviron, E. *J. Electroanal. Chem.* **1979**, *101*, 19-28.

(16) Fleming, B. D.; Tian, Y.; Bell, S. G.; Wong, L.; Urlacher, V.; Hill, H. A. O. *Eur. J. Biochem.* **2003**, *270*, 4082-4088.

(17) Lei, C.; Wollenberger, U.; Jung, C.; Scheller, F. W. *Biochem. Biophys. Res. Comm.* **2000**, *268*, 740-744.

(18) Honeychurch, M. J.; Hill, H. A. O.; Wong, L. *FEBS Letters* **1999**, *451*, 351-353.

(19) Munge, B.; Estavillo, C.; Schenkman, J. B.; Rusling, J. F. *ChemBioChem* **2003**, *4*, 82-89.

(20) Salazar, O.; Cirino, P. C.; Arnold, F. H. *ChemBioChem* **2003**, *4*, 891-893.

(21) Cirino, P. C.; Arnold, F. H. *Adv. Synth. Catal.* **2002**, *344*, 1-6.

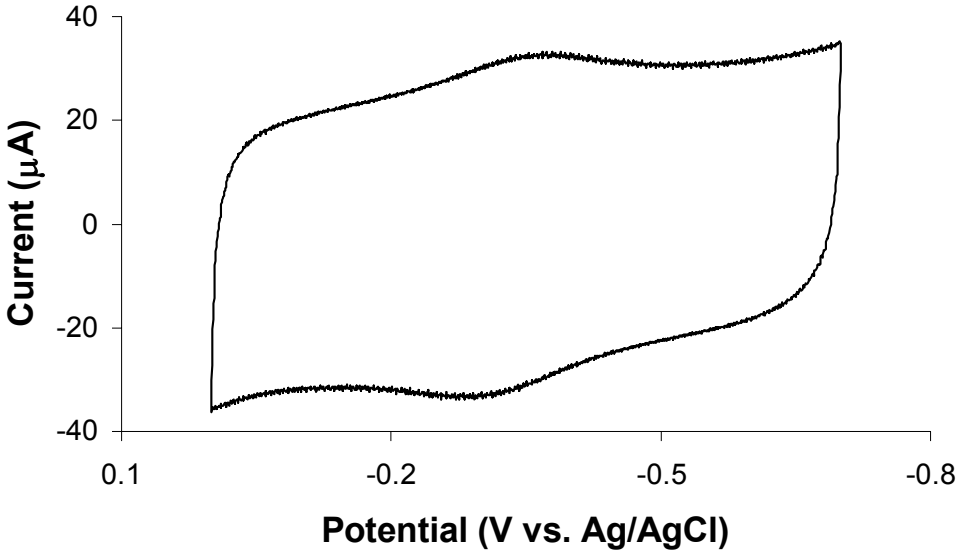

Figure 4.1. Cyclic voltammogram of hBM3 in SDS on BPG (0.2 cm^2) at 200 mV/s in 30 mM KP_i / 130 mM NaCl / pH 7.4.

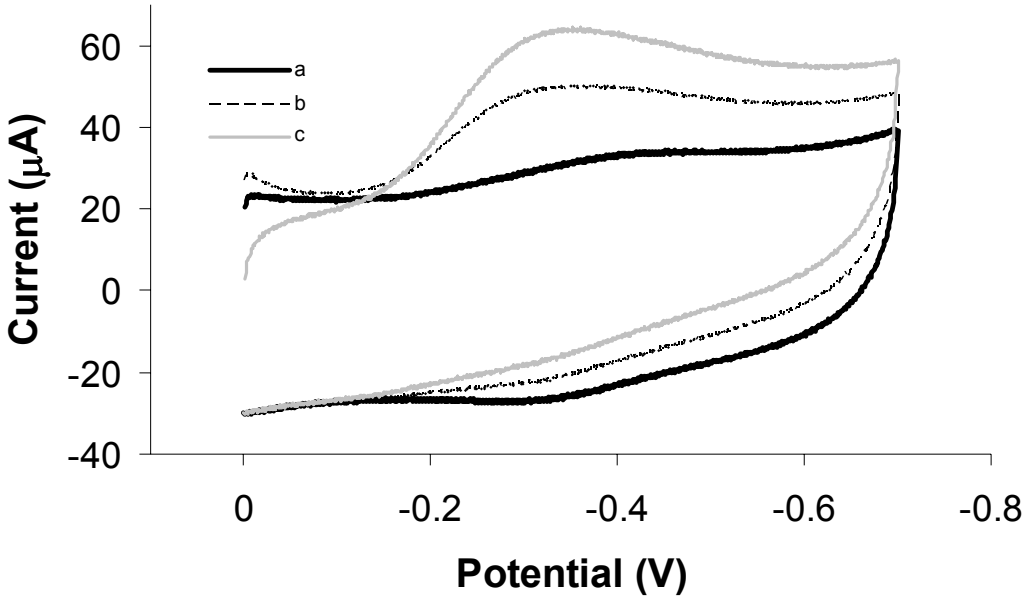

Figure 4.2. Cyclic voltammograms of hBM3 in SDS on BPG in the presence of increasing amounts of dioxygen: (a) 0 μM, (b) 42 μM, (c) 83 μM.

Chapter 5

Voltammetry of Wild Type and Mutant Cytochrome P450 BM3 in DDAPSS Surfactant Films*

Acknowledgements: This work was in collaboration with M. G. Hill and N. Hindoyan at Occidental College. We thank E. Blair and P. J. Farmer (U.C. Irvine) for assistance with film preparation; M. W. Peters and P. Meinhold (Caltech) for helpful discussions; NSERC (Canada) (AKU), NSF (HBG), and the David and Lucille Packard Foundation (MGH) for research support.

Abstract

Voltammetry of mutant cytrochrome P450 BM3 (1-12G) in DDAPSS films on graphite revealed $Fe^{III/II}$ (-202 mV vs. Ag/AgCl) and $Fe^{II/I}$ (-1082 mV) redox couples of the heme. The Fe^{II} species was capable of catalyzing dioxygen reduction, while reductive dechlorination of TCA was catalyzed by Fe^{I}. Performing voltammetry on the wild type (WT) enzyme revealed that WT and 1-12G display distinct redox properties. Absorption spectra in solution showed the Fe^{III} Soret at 418 nm for WT, and a split Soret for 1-12G at 390 and 418 nm. Voltammetry of the proteins within DDAPSS films on the surface of carbon electrodes revealed near identical $Fe^{III/II}$ potentials (~ -200 mV vs. Ag/AgCl), but significant differences in k^o (250 vs. 30 s^{-1}) and $Fe^{III/II}$ – CO potentials (-140 mV vs. -115 mV) for WT vs. 1-12G. Catalytic reduction of dioxygen by the proteins on rotated-disk electrodes was analyzed using Levich and Koutecky-Levich treatments. The data reveal that 1-12G displays n and k_{obs} values that are 1.7 and 0.07 times that of WT, suggesting that the two proteins differ strikingly in their reaction with dioxygen.

Abbreviations: P450, cytochrome P450; WT, wild type heme domain cytochrome P450 BM3; 1-12G, cytochrome P450 BM3 heme domain mutant 1-12G; BPG, basal plane graphite electrode; DDAB, didodecyldimethylammonium bromide; NaPSS, sodium polystyrenesulfonate; DDAPSS, didodecyldimethylammonium polystyrenesulfonate; RDE, rotated-disk electrode; ET, electron transfer; CYP119, cytochrome P450 from *Sulfolobus solfataricus*; CAM, cytochrome P450 from *Pseudomonas putida*; TCA, trichloroacetic acid.

Introduction

Protein-surfactant film voltammetry is a proven technique for achieving good electronic coupling between electrodes and redox enzymes.[1] This methodology has been particularly useful in exploring the redox properties of cytochromes P450.[2-5] In addition to supporting rapid and reversible electron transfer (ET), these systems can also catalyze a limited number of turnovers (e.g., 7.2 turnovers per hour for cytochrome P450 from *Pseudomonas putida* (CAM) with styrene as substrate[6]).

Chapter 4 described the electrochemistry of wild type heme domain cytochrome P450 BM3 (WT) in a sodium dodecyl sulfate (SDS) film on the surface of a basal plane graphite electrode (BPG). Although the system displayed good electronic coupling, catalytic substrate monooxygenation was not observed. Several explanations were suggested for this lack of activity including film desorption, protein misfolding, and hindered substrate access (by SDS occupying the substrate access channel, or substrates preferentially partitioning into the film).

To combat the problems associated with the WT-SDS system, we decided to explore the voltammetry of BM3 heme domain mutant 1-12G (1-12G) in didodecyldimethylammonium polystyrenesulfonate (DDAPSS) films. 1-12G contains 15 amino acid mutations that distinguish it from WT; these mutations are collectively responsible for 1-12G's unique catalytic properties, which include the ability to regio- and stereoselectively hydroxylate linear hydrocarbons (e.g., formation of S-2-octanol at 40% ee), and oxidize small gaseous alkanes (e.g., propane).[7] We hoped that the altered substrate specificity of 1-12G (cf. WT) would allow us to find molecules that could freely diffuse through the surfactant film into the protein active site for protein-catalyzed oxidation.

Regarding the surfactant, heme proteins within DDAPSS films have been shown to retain their spectroscopic properties (cf. in solution), and are active towards dioxygen reduction and reductive dehalogenation.[8,9] Furthermore, DDAPSS films are very stable (cf. SDS), owing to low water-solubility and superior strength against mechanical stresses.[8] Finally, DDAPSS is not a substrate for BM3: absorption spectroscopy reveals that the surfactant does not cause a low- to high-spin shift in the heme Fe^{III} Soret, and NADPH is not consumed in solutions containing the holo enzyme and this surfactant.

Notably, previous work described the redox properties of WT in didodecyldimethylammonium bromide (DDAB) films.[4] The $Fe^{III/II}$ redox potential, standard rate constant (k^o), and dioxygen reactivity of the system were reported. This prior study serves as a convenient point of reference for the present investigation of WT and 1-12G in DDAPSS.

Voltammetry of 1-12G in DDAPSS

Protein films were formed on BPG by adding 1-12G, DDAB, and NaPSS directly to the electrode surface, followed by drying in air. A representative voltammogram at pH 7 for 1-12G in DDAPSS is shown in **Figure 5.1**. We have assigned the two redox processes to the heme $Fe^{III/II}$ (-202 mV vs. Ag/AgCl) and $Fe^{II/I}$ redox couples (-1082 mV), consistent with other studies.[8,10] These assignments are supported by performing voltammetry in the presence of carbon monoxide: with CO present, the $Fe^{III/II}$ couple shifts approximately +87 mV (consistent with other studies[3,4]) while the $Fe^{II/I}$ couple is no longer observed (presumably beyond the solvent window). Notably, the $Fe^{III/II}$ redox potential in the surfactant film is 370 mV more positive than the WT enzyme in solution.[11] As previously suggested, local electrostatic effects probably contribute to the altered potentials on the electrode surface.[12] In particular, the hydrophobic film likely leads to partial dehydration of the protein active site, which would cause a significant positive shift in the observed heme potential.[13]

Catalytic Activity of 1-12G in DDAPSS

Substrate Oxidation

Voltammograms in the presence of dioxygen resulted in large catalytic currents at the onset of Fe^{III} reduction (**Figure 5.2**). This catalytic activity encouraged us to try a series of substrates with the system in the hope of observing catalytic substrate oxidation. Catalytic reactions were conducted in two ways: 1) by performing electrolysis at various potentials (both positive and negative of the $Fe^{III/II}$ $E_{1/2}$); 2) by performing cyclic voltammetry at various scan rates for multiple cycles in a region that included the $Fe^{III/II}$

redox couple. Several substrates were tried, including medium chain (C6 – C10) alkanes and styrene. Unfortunately, no oxidation products were observed.

Reductive Dehalogenation

The ability of 1-12G in DDAPSS to catalytically reduce dioxygen suggested that the system may be capable of performing simple reduction reactions. Thus, we assessed the ability of 1-12G in DDAPSS to reductively dechlorinate trichloroacetic acid (TCA). Reductive dehalogenation is a known P450-catalyzed reaction: previous work demonstrated TCA dechlorination catalyzed by the Fe^{II} heme in CAM within DDAB on graphite,[3] and Fe^{I}-catalyzed dechlorination of carbon tetrachloride by P450 from *Sulfolobus solfataricus* (CYP119) in DDAPSS on BPG.[9] Regarding practical applications, bioelectrochemical systems that catalyze dehalogenation reactions have been investigated with much interest for use in bioremediation.[9,14]

Figure 5.3 overlays voltammograms of BPG with TCA (**a**), BPG with 1-12G in DDAPSS (**b**), and BPG with 1-12G in DDAPSS in the presence of TCA (**c**). The large catalytic current in **Figure 5.3c** indicates protein-mediated dechlorination catalyzed by Fe^{I}. This was confirmed by GC-ECD, which revealed that the mono-dechlorinated product (dichloroacetic acid) is only produced in reactions that contain protein. This result is in accord with CYP119-mediated dechlorination of CCl_4 in DDAPSS; however, this is in stark contrast to CAM in DDAB, which showed CAM-mediated dechlorination of TCA catalyzed by Fe^{II}. Since the $Fe^{III/II}$ redox potentials are similar for the three proteins (-202 mV for 1-12G in DDAPSS, -213 mV for CYP119 in DDAPSS,[9] -191 mV for CAM in DDAB[3]) the differences in catalysis cannot be attributed to different potencies of the Fe^{II} hemes. The commonality for the 1-12G and CYP119 systems is the

DDAPSS film. However, the differential effect of DDAB compared to DDAPSS on the dehalogenation activity of the Fe^{II} heme in P450 is not obvious.

Comparative Voltammetry of WT and 1-12G

As mentioned above, the 15 mutations that distinguish 1-12G from WT are responsible for 1-12G's unique catalytic properties. Conceivably, these differences in catalysis may be due in part to differences in redox properties. Previous work with WT has shown that single point mutations can significantly perturb the heme's redox and catalytic properties.[15] We suspected that the 15 mutations in 1-12G would have a similar effect: indeed, one of the distinguishing features of 1-12G is that, as isolated (heme domain, substrate free), the heme is mixed-spin (absorbance at 390 and 418 nm). This is in stark contrast to WT (**Figure 5.4**), which shows the characteristic low spin absorption spectrum of the hydrated six-coordinate heme (λ_{max} = 418 nm).

The surfactant film methodology provides a simple and sensitive way of probing heme protein redox chemistry. Thus, we decided to use the DDAPSS film system to explore and compare the redox chemistry of WT and 1-12G. Performing voltammetry on the two proteins in DDAPSS films revealed that the two proteins give similar voltammograms with nearly identical half-wave potentials (**Table 5.1**). A representative voltammogram of the $Fe^{III/II}$ couple at pH 7 for 1-12G in DDAPSS is shown in **Figure 5.5**. Notably, the half-wave potential of the $Fe^{III/II}$ couple in **Figure 5.5** is in accord with WT in DDAB (cf. -250 mV vs. SCE).[4]

For both proteins, the peak currents were linear with scan rate (surface bound) up to 14 V/s, after which they became linear with the square root of the scan rate

(diffusive).[16] This is characteristic of thin film electrochemistry,[17] indicative of finite diffusion of the protein within the film. Thus, up to 14 V/s, the systems were treated as surface-confined. Within this diffusionless regime, the ratios of the total charge under the cathodic and anodic peaks ($Q_{p,c}$ / $Q_{p,a}$) approach unity for both proteins, indicating chemically reversible systems.[16]

Voltammetry in the presence of carbon monoxide revealed a 25 mV difference in the $Fe^{III/II}$ potentials of WT and 1-12G (**Table 5.1**). Approximately, this indicates a four-fold difference in $Fe^{III/II}$ – CO binding affinities between WT and 1-12G in the DDAPSS film, and provides further evidence that the two proteins have different heme environments.

Figure 5.6 plots the peak potentials vs. the log of the scan rate for both proteins. Despite nearly identical $Fe^{III/II}$ potentials, **Figure 5.6** demonstrates that the two proteins differ significantly in their electron transfer (ET) properties. Within the diffusionless regime (**Figure 5.6**, vertical line), the theory of Laviron can be used to estimate the standard rate constant k^o ($\Delta G^o = 0$).[18] Assuming a transfer coefficient (α) of 0.5, k^o evaluated at 10 V/s was 250 and 30 s^{-1} for WT and 1-12G, respectively (notably, k^o for WT in DDAB[4] is 221 s^{-1}).

Voltammograms of the two proteins in the presence of dioxygen resulted in catalytic currents at the onset of Fe^{III} reduction. The stability of DDAPSS films to mechanical stress[8] permitted the use of a rotating-disk electrode (RDE) to investigate the dioxygen reaction. The diffusion-convection-limited current at an RDE depends on the angular rotational velocity (ω, s^{-1}), the number of electrons transferred (n), and the bulk concentration of substrate (O_2 in this case) according to the Levich equation:[19,20]

$$i_L = 0.62\ nFAD^{2/3}\,[O_2]\,\nu^{-1/6}\,\omega^{1/2}$$

RDE experiments were carried out at room temperature (20°C) in air-saturated buffer on both WT and 1-12G by performing electrolysis at -0.5 V (vs. Ag/AgCl) and measuring the limiting current for each rotation rate. These data points are plotted in **Figure 5.7** (points), along with theoretical lines for two- and four-electron reduction of dioxygen (solid lines).

For both proteins, the limiting currents in **Figure 5.7** appear to level off at high rotation rates. This indicates that dioxygen reduction is limited by a chemical step preceding the electrode reaction. The Koutecky-Levich treatment was used to analyze the kinetics:[21] plots of i_L^{-1} vs. $\omega^{-1/2}$ were linear for both proteins, with slopes yielding n = 2.7 for WT and n = 4.7 for 1-12G (insets, **Figure 5.7**). The intercepts of the Koutecky-Levich plots were used to calculate the kinetic currents (i_{kin}) that limit the electrode reaction. These currents vary linearly with protein concentration and are given by[22]

$$i_{kin} = nFA\,[O_2]\,\Gamma_{P450}\,k_{obs}$$

(where Γ_{P450} is the surface concentration of protein and k_{obs} is the second-order rate constant that governs the current-limiting reaction). WT and 1-12G gave respective values for k_{obs} of 1.4×10^6 $M^{-1}s^{-1}$ and 1×10^5 $M^{-1}s^{-1}$, a 14-fold difference in reaction rate. The calculated values for n and k_{obs} were used to generate Levich plots for WT and 1-12G (**Figure 5.7**, broken lines).

Chemical fates of dioxygen reduction are one-, two-, and four-electron transfer forming superoxide, peroxide, and water. Our calculated values for n are probably over-estimated: within the hydrophobic film, dioxygen is likely more concentrated compared to in solution.[23] With this in mind, it appears that WT reduces dioxygen primarily by two

electrons to peroxide (as seen before for WT and BM3 point mutants[4,24]), whereas 1-12G apparently reduces dioxygen by an additional two electrons. P450-catalyzed four-electron reduction of dioxygen has been previously observed,[25,26] and is consistent with the canonical P450 mechanism that results in water formation by reducing compound I with two electrons ("oxidase" activity).[27] Dioxygen reduction by 1-12G is also significantly slower (k_{obs}) compared to WT, as evident from the prominent plateau at higher rotation rates for 1-12G where the rate of substrate delivery exceeds that of catalysis.

Results from our electroanalytical treatment can be correlated with the biochemistry of the proteins. First, there is the ten-fold difference in heterogeneous ET rate constants (k^o). Indeed, preliminary stopped-flow experiments using holo proteins and NADPH as the reductant revealed that heme reduction in WT occurred approximately five-fold faster.[28] In addition, substrate turnover rates for WT[29] are generally faster (up to ten-fold) than for 1-12G;[7] since ET is known to be the rate limiting step, then the relative k^o and k_{obs} values are also consistent with the catalytic oxidation rates. Second, there is the striking observation that under similar conditions 1-12G appears capable of reducing dioxygen by four electrons. This difference can be reconciled if the iron-peroxy species is longer-lived in 1-12G. For WT, peroxide apparently dissociates before subsequent conversion to compound I. However, the slower rate of ET in 1-12G, coupled with the observation of catalytic currents corresponding to four-electron transfer to dioxygen, argues for an iron-peroxy complex that is longer-lived in 1-12G relative to WT. This could potentially explain the high degree of stereo- and regioselectivity that 1-12G displays: a longer-lived iron-peroxy

species allows substrates more time to adopt their lowest-energy conformation within the active site and orient a specific C-H bond for subsequent hydroxylation. This argument is in accord with that previously postulated for 1-12G,[7] which reasoned that the mutations (especially A328V and A82L in the active site) kept the substrate in a more fixed orientation, allowing specific products to be generated.

Experimental Methods

Protein Expression and Purification

Expression, purification and quantification of the heme domains of wild type BM3 and mutant 1-12G proceeded as previously described.[30]

Electrode Preparation and Voltammetry

Electrodes for voltammetry (0.07 cm^2) were made using the basal plane of pyrolytic graphite. The surfaces were prepared by sanding briefly with 600-grit sandpaper, followed by polishing with 0.3 and 0.05 μm alumina slurries. The electrodes were then sonicated and dried in air. Protein films were applied by placing 5 μL of 105 μM 1-12G or 21 μM WT in 30 mM KP_i pH 7.4, 5 μL 10 mM DDAB in water, and 5 μL 10 mM NaPSS in 30 mM KP_i pH 7.4 to the electrode surface. The electrodes were covered under water-saturated air overnight, followed by uncovering and drying in air overnight.

A CH Instruments Electrochemical Workstation system was used for the reactions. Voltammetry experiments were performed in a three-compartment cell, using a platinum wire auxiliary and an Ag/AgCl reference (BAS). All experiments were

performed under argon in thoroughly degassed buffer (50 mM KP_i / 20 mM KCl / pH 7) unless otherwise stated.

Activity Assays with 1-12G

Electrolysis reactions were conducted with protein films on pyrolytic graphite plates (2 cm x 1 cm). The plates were sanded, sonicated, and dried in air. Protein films were applied by placing 7 μL of 105 μM 1-12G in 30 mM KP_i pH 7.4, 7 μL 10 mM DDAB in water, and 7 μL 10 mM NaPSS in 30 mM KP_i pH 7.4. The electrodes were covered under water-saturated air overnight, followed by uncovering and drying in air overnight. Electrolyses were conducted in a three-neck flask: working and counter (Pt gauze) electrodes were placed in solution, while the Ag/AgCl reference was housed in a Luggin capillary. The flask contained 6 mL of buffer (50 mM KP_i / 20 mM KCl / pH 7), and typically 1-5 mM of substrate.

Assays for hydroxylated alkanes were conducted as previously described.[7] Styrene assays were conducted as described in **Chapter 4**.

Electrolyses involving TCA were performed anaerobically at -1 V (vs. Ag/AgCl) for 15 minutes with rapid stirring. Dechlorination products were analyzed by first acidifying the electrolyzed solution to pH ~ 1, followed by extraction with 0.5 mL of ethyl acetate. The extract was analyzed using GC with an electron capture detector (ECD).

Rotated-Disk Electrode Experiments

0.5 cm^2 glassy carbon electrodes were used. The electrodes were polished sequentially with 0.3 and 0.05 μm alumina slurries, sonicated, and dried. Experiments were carried out in a two-compartment cell, with the working electrode separated from

the Ag/AgCl reference and Pt auxiliary electrodes. The solution was approximately 30 mL of 50 mM KP_i / 20 mM KCl / pH 7. All experiments involving dioxygen reduction were carried out in air saturated buffer ($[O_2]$ approximately 290 μM at 20°C). Protein surface concentrations on the RDEs were 1.5×10^{-11} and 3.3×10^{-11} mol/cm^2 for WT and 1-12G. A Pine Instruments rotator was used to control the rotation rate, while a CH Instruments Electrochemical Workstation was used to apply the potential and monitor the current response. Protein-DDAPSS films were found to be stable up to 1500 rpm.

RDE experiments were conducted by performing electrolyses at -0.5 V (vs. Ag/AgCl) at different rotation rates. Typically, the limiting current used to make the Levich and Koutecky-Levich plots is the steady state value observed during the reaction. However, it was found that degradation of the protein signal occurred over the course of the experiment (probably through peroxide damage). This was illustrated both by the decay of the current response with time during the rotation experiment, and the reduced current response of the film after rotation compared to before rotation as seen by cyclic voltammetry. Thus, the limiting current was taken to be the initial current after the start of electrolysis with rotation. This was done by plotting the log(current) vs. time, and extrapolating the data back to t = 0 s.

References and Notes

(1) Rusling, J. F. *Acc. Chem. Res.* **1998**, *31*, 363-369.

(2) Aguey-Zinsou, K.; Bernhardt, P. V.; Voss, J. J. D.; Slessor, K. E. *Chem. Commun.* **2003**, 418-419.

(3) Zhang, Z.; Nassar, A.-E.; Lu, Z.; Schenkman, J. B.; Rusling, J. F. *J. Chem. Soc., Faraday Trans.* **1997**, *93*, 1769-1774.

(4) Fleming, B. D.; Tian, Y.; Bell, S. G.; Wong, L.; Urlacher, V.; Hill, H. A. O. *Eur. J. Biochem.* **2003**, *270*, 4082-4088.

(5) Estavillo, C.; Lu, Z.; Jansson, I.; Schenkman, J. B.; Rusling, J. F. *Biophys. Chem.* **2003**, *104*, 291-296.

(6) Zu, X.; Lu, Z.; Zhang, Z.; Schenkman, J. B.; Rusling, J. F. *Langmuir* **1999**, *15*, 7372-7377.

(7) Peters, M. W.; Meinhold, P.; Glieder, A.; Arnold, F. H. *J. Am. Chem. Soc.* **2003**, *125*, 13442-13450.

(8) Ma, H.; Hu, N. *Anal. Lett.* **2001**, *34*, 339-361.

(9) Blair, E.; Greaves, J.; Farmer, P. J. *J. Am. Chem. Soc.* **2004**, *126*, 8632-8633.

(10) Immoos, C. E.; Chou, J.; Bayachou, M.; Blair, E.; Greaves, J.; Farmer, P. J. *J. Am. Chem. Soc.* **2004**, *126*, 4934-4942.

(11) Daff, S.; Chapman, S.; Turner, K.; Holt, R.; Govindaraj, S.; Poulos, T.; Munro, A. *Biochemistry* **1997**, *36*, 13816-13823.

(12) Lvov, Y. M.; Lu, Z.; Schenkman, J. B.; Zu, X.; Rusling, J. F. *J. Am. Chem. Soc.* **1998**, *120*, 4073-4080.

(13) Tezcan, F. A.; Winkler, J. R.; Gray, H. B. *J. Am. Chem. Soc.* **1998**, *120*, 13383-13388.

(14) Walsh, M. E.; Kyritsis, P.; Eady, N. A. J.; Hill, H. A. O.; Wong, L. *Eur. J. Biochem.* **2000**, *267*, 5815-5820.

(15) Ost, T. W. B.; Clark, J.; Mowat, C. G.; Miles, C. S.; Walkinshaw, M. D.; Reid, G. A.; Chapman, S. K.; Daff, S. *J. Am. Chem. Soc.* **2003**, *125*, 15010-15020.

(16) Bard, A. J.; Faulkner, L. R. *Electrochemical Methods*; Second Edition; John Wiley & Sons, Inc.: New York, 2001.

(17) Lin, R.; Immoos, C. E.; Farmer, P. J. *J. Biol. Inorg. Chem.* **2000**, *5*, 738-747.

(18) Laviron, E. *J. Electroanal. Chem.* **1979**, *101*, 19-28.

(19) Levich, V. *Physicochemical Hydrodynamics*; Prentice Hall: Englewood Cliffs, New Jersey, 1962.

(20) F is Faraday's constant, A is the electrode area (cm^2), D is the diffusion coefficient (1.7×10^{-5} cm^2/s for oxygen in water), ν is the kinematic viscosity of the solution (0.01 cm^2/s for water), $[O_2] = 2.9 \times 10^{-7}$ mol/cm^3 for O_2 in air saturated buffer at 20^oC.

(21) Koutecky, J.; Levich, V. *Zh. Fiz. Khim.* **1956**, *32*, 1565.

(22) Andrieux, C.; Saveant, J.-M. *Molecular Design of Electrode Surfaces*; Wiley & Sons: New York, New York, 1992.

(23) Using $[O_2] = 3.3 \times 10^{-7}$ mol/cm^3 results in n values of 4.1 and 2.3 for 1-12G and WT.

(24) Noble, M.; Miles, C.; Chapman, S.; Lysek, D.; Mackay, A.; Reid, G.; Hanzlik, R.; Munro, A. *Biochem. J.* **1999**, *339*, 371-379.

(25) Kadkhodayan, S.; Coulter, E. D.; Maryniak, D. M.; Bryson, T. A.; Dawson, J. H. *J. Biol. Chem.* **1995**, *270*, 28042-28048.

(26) Glieder, A.; Farinas, E. T.; Arnold, F. H. *Nature Biotechnology* **2002**, *20*, 1135-1139.

(27) Wong, L. L.; Westlake, C. G.; Nickerson, D. P. In *Structure and Bonding*; Springer-Verlag: Berlin, 1997; Vol. 88, pp 175-207.

(28) Shoo, J.; Peters, M. W.; Meinhold, P.; Unpublished results*;* California Institute of Technology.

(29) Boddupalli, S.; Estabrook, R.; Peterson, J. *J. Biol. Chem.* **1990**, *265*, 4233-4239.

(30) Cirino, P. C.; Arnold, F. H. *Adv. Synth. Catal.* **2002**, *344*, 1-6.

Table 5.1. Electrochemical parameters determined for WT and 1-12G in DDAPSS on BPG.

	WT	**1-12G**
$\mathbf{E_{1/2}\,(Fe^{III/II})}$	-195 mV	-202 mV
$\mathbf{E_{1/2}\,(Fe^{III/II}}$ **- CO)**	-140 mV	-115 mV
$\mathbf{k^o}$	250 s^{-1}	30 s^{-1}
$\mathbf{k_{obs}}$	1.4 x 10^6 $M^{-1}s^{-1}$	1 x 10^5 M^{-1} s^{-1}

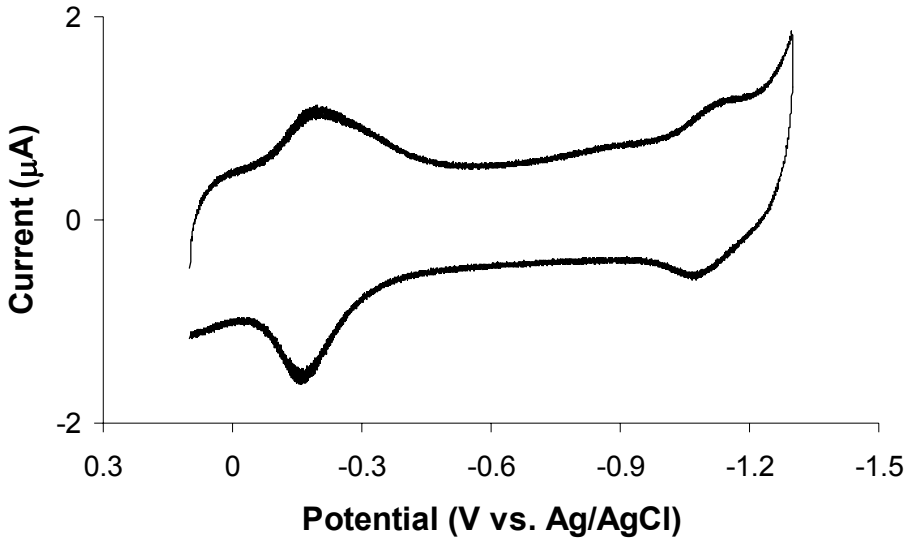

Figure 5.1. Cyclic voltammogram of mutant 1-12G in DDAPSS on BPG at 200 mV/s in 50 mM KP_i / 20 mM KCl / pH 7.

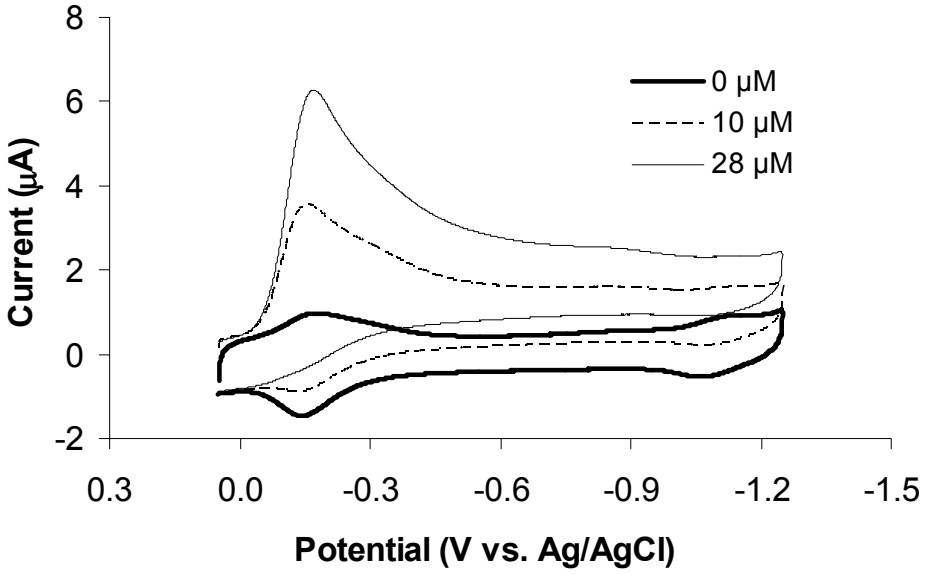

Figure 5.2. Cyclic voltammograms of 1-12G in DDAPSS on BPG in the presence of increasing amounts of dioxygen.

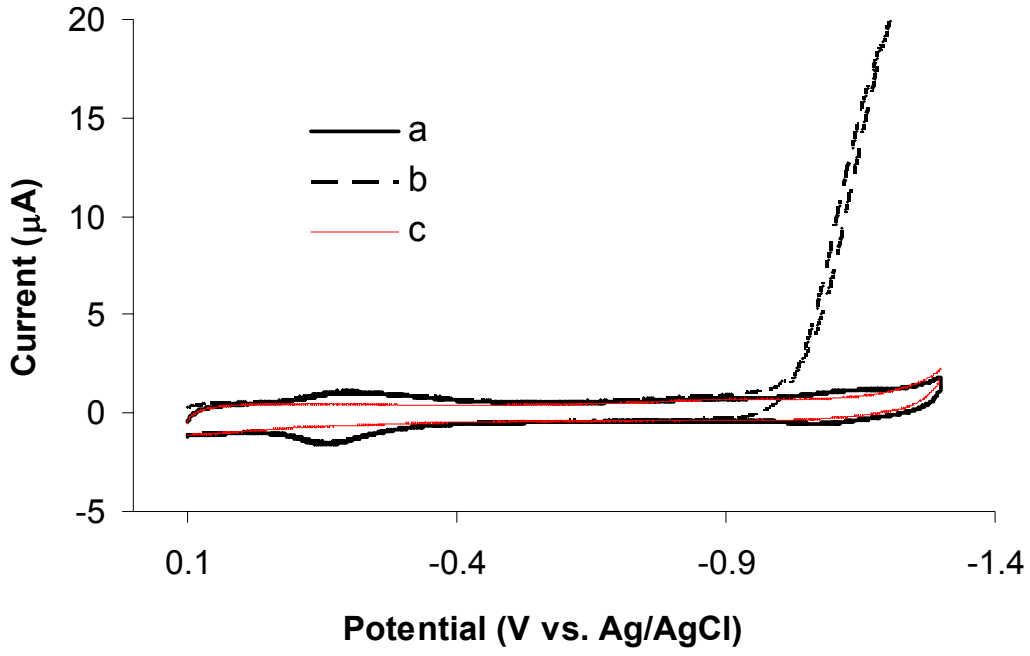

Figure 5.3. Cyclic voltammograms at 200 mV/s with: a) 1-12G in DDAPSS on BPG, b) 1-12G in DDAPSS on BPG with TCA, c) DDAPSS on BPG with TCA.

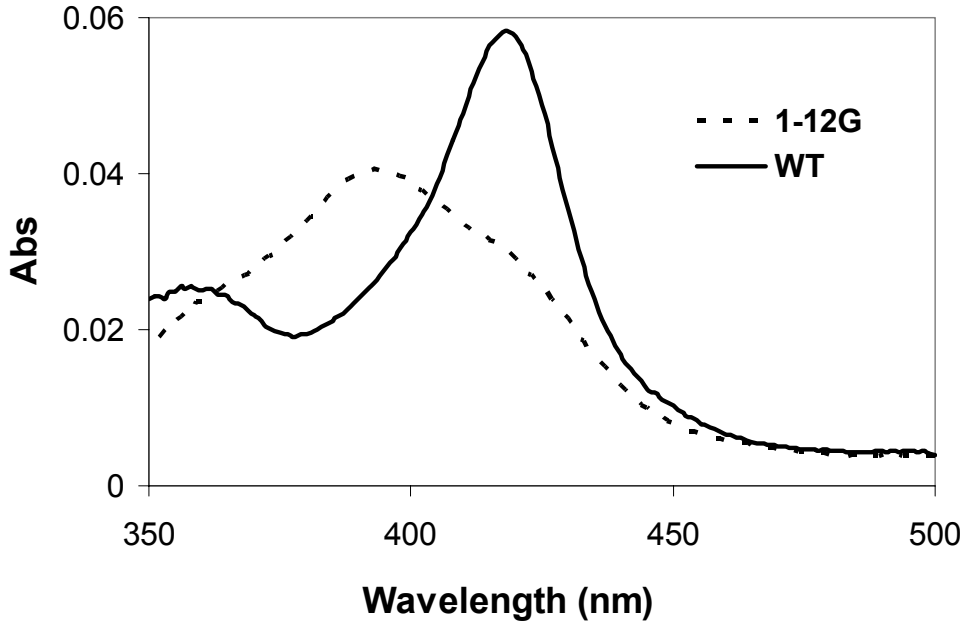

Figure 5.4. Absorption spectra of WT and 1-12G P450 BM3 in the absence of substrate.

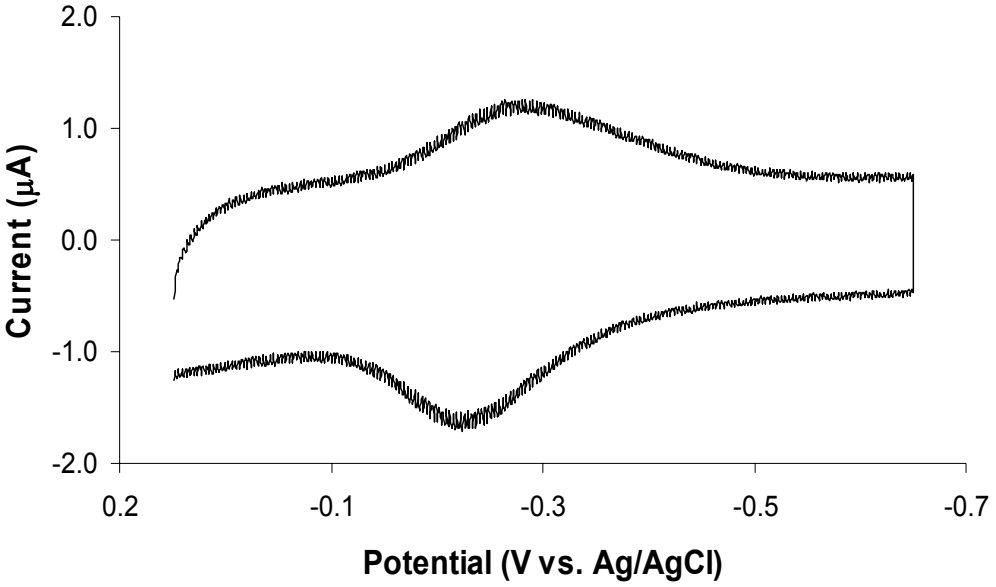

Figure 5.5. Cyclic voltammogram of mutant 1-12G in DDAPSS on BPG at 200 mV/s in 50 mM KP_i / 20 mM KCl / pH 7.

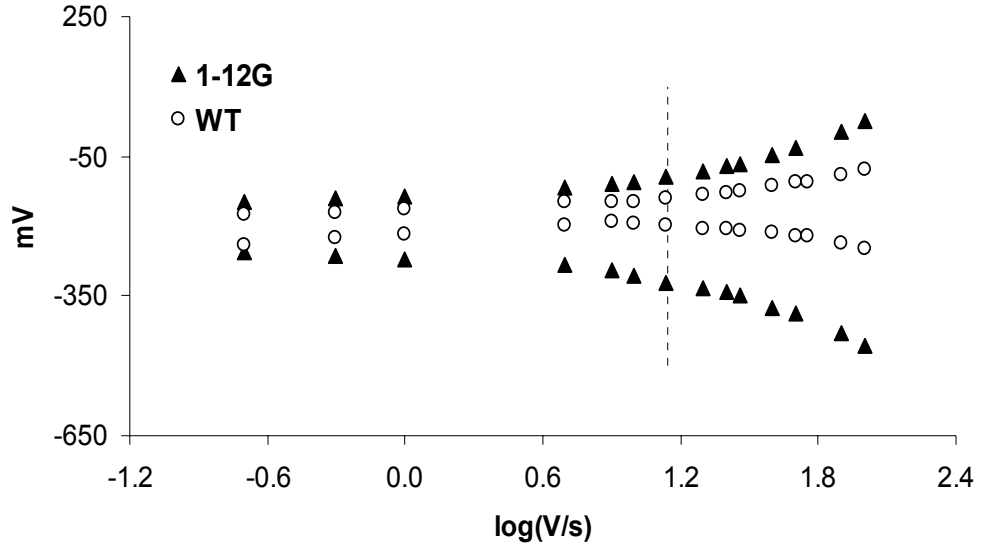

Figure 5.6. Cathodic and anodic peak potentials vs. log of the scan rate for WT and 1-12G are shown. The vertical line represents the transition from surface-bound to diffusive behavior.

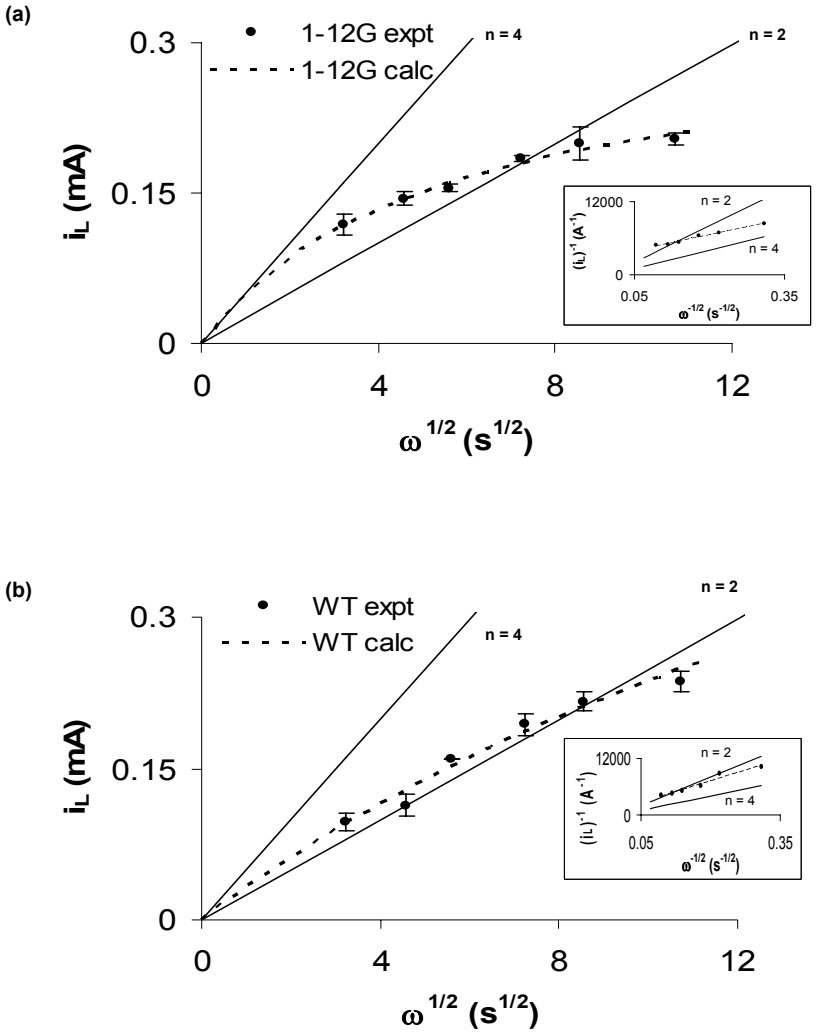

Figure 5.7. Levich plots are shown for a) 1-12G and b) WT. The individual points, solid lines, and broken lines represent the experimental data, the theoretical lines, and the lines derived from the fit of the experimental data, respectively. The insets are the corresponding Koutecky-Levich plots, from which n and k_{obs} were derived. The $[O_2]$ used to generate the lines, 2.9×10^{-7} mol/cm^3, is that of air-saturated buffer at 20^{o}C.

Chapter 6

Electrochemical Generation of a High-Valent State of Cytochrome P450

Acknowledgements: This work was in collaboration with M. G. Hill at Occidental College. We thank P. J. Farmer (U.C. Irvine) and S. Contakes (Caltech) for helpful discussions, N. Halpern-Manners and G. Bandara (Caltech) for assistance with protein purification, and NSERC (Canada) (AKU) for financial support.

Abstract

Cyclic voltammetry performed at rapid scan rates on cytochrome P450 CAM in DDAB films on graphite electrodes revealed a couple (**E**) at 831 mV (vs. Ag/AgCl). **E** was not observed at scan rates less than 30 V/s at room temperature, suggesting that the oxidized species is unstable. The lifetime of **E** could be prolonged at 4^{o}C, which allowed reversible access to **E** at scan rates as low as 1 V/s. **E** was found to be sensitive to imidazole in solution and to variations in pH, suggesting that the redox reaction is occurring at the metal center (i.e., $Fe^{IV/III}$) rather than at the porphyrin macrocycle. Electrolysis reactions with different P450 substrates revealed that the electrochemically generated high-valent species is only capable of performing S-oxidation, converting thioanisole to methyl phenyl sulfoxide.

Abbreviations: CV, cyclic voltammetry; ET, electron transfer; CAM, cytochrome P450 from *Pseudomonas putida.*

Introduction

Heme-thiolate proteins (cytochromes P450, nitric oxide synthase, chloroperoxidase) perform essential functions in biology. The hallmark reaction catalyzed by these enzymes is substrate oxidation, converting R-H to R-OH. Thiol ligation to the heme iron is postulated to be the critical factor that modulates the heme redox properties to activate dioxygen for substrate oxidation:[1,2] two electrons are delivered by native reductase proteins to reduce dioxygen, forming water and a high-valent ferryl species (formally oxidized by two electrons cf. Fe^{III} heme) capable of performing oxygen atom transfer. This ability for oxidative catalysis has led to great interest in capturing heme-thiolate oxygenase activity *in vitro* for both medical and industrial applications.[3,4]

Central to the catalytic cycle of heme-thiolate proteins is electron transfer (ET), leading to several investigations characterizing ET reactions in these enzymes.[5-8] In particular, protein-surfactant film voltammetry has developed into a routine method for achieving direct ET with heme proteins.[9] Using this technique, several studies have electrochemically characterized the $Fe^{III/II}$ redox couple in various heme-thiolate enzymes.[10-12] More recently, a putative $Fe^{II/I}$ couple (~ -1100 mV vs. Ag/AgCl) was observed; in fact, the Fe^{I} species displayed catalytic activity towards reductive dehalogenation.[13,14]

The ability to electrochemically access $Fe^{III/II}$ and $Fe^{II/I}$ redox couples in heme-thiolate proteins within surfactant films led us to wonder if high-valent species could also be generated. Conceivably, one- or two-electron oxidation of the Fe^{III}–OH_2 heme (resting state) should result in rapid conversion to the ferryl species Fe^{IV}=O–H (compound II) or Fe^{V}=O (compound I), as previously observed for horseradish peroxidase[15] and chloroperoxidase.[16] In the presence of substrates, these ferryl species may be capable of performing oxidative catalysis; note that this would occur in the absence of both dioxygen and NAD(P)H, both of which are necessary in the native system.

Previous work has demonstrated that both oxidized and reduced Fe-porphyrin systems can be electrochemically accessed in non-aqueous media.[17,18] Depending on the system, oxidation states from Fe^{I} to Fe^{V} can be generated, as well as porphyrin cations and anions. For P450-type systems, it has been shown that Fe^{III}-porphyrin complexes with basic axial ligands (cf. thiolate in P450) are oxidized first at the metal (Fe^{IV}), and then at the porphyrin macrocycle.[19,20] Indeed, Groves and Gilbert have shown that in the presence of water, these hemes can be electrochemically oxidized to produce ferryl species capable of catalytic epoxidation.[20]

Results and Discussion

We performed cyclic voltammetry (CV) on cytochrome P450 CAM (CAM)* in didodecyldimethylammonium bromide (DDAB) films on the surface of basal plane graphite (BPG) electrodes and looked for evidence of protein and/or heme oxidation.

* The results reported for CAM are also observed in experiments with cytochrome P450 BM3. However, voltammetry with CAM resulted in stronger current responses cf. BM3, making the data easier to interpret.

Preliminary CV experiments were conducted at 200 mV/s and pH 7 at room temperature by beginning at 0 mV, scanning negative to -700 mV, reversing the scan direction to 1300 mV, and then cycling between 1300 mV and -700 mV. In addition to observing the $Fe^{III/II}$ redox couple ($E_{1/2}$ = -227 mV vs. Ag/AgCl), we also observed a large catalytic current corresponding to solvent oxidation at potentials > 900 mV. After scanning beyond this solvent window, subsequent scanning in the region of the $Fe^{III/II}$ couple resulted in no observable signal, suggesting that the heme had been oxidatively damaged.

The above CV experiment was repeated at 50 V/s and pH 8 at room temperature. The resulting voltammogram (**Figure 6.1**) clearly reveals two couples: the $Fe^{III/II}$ redox couple centered at -227 mV, and a second couple (**E**) with $E_{1/2}$ = 831 mV. Accessing **E** was facilitated by scanning faster (> 30 V/s), and performing the experiment at higher pH (best at pH > 8). **E** was found to be reversible above 30 V/s, and multiple CVs could be recorded without any significant loss in signal intensity. Notably, it was possible to reversibly generate **E** at scan rates down to 1 V/s when performed at 4°C (**Figure 6.2**). There are three likely possibilities for the origin of **E**: 1) a porphyrin-centered redox process; 2) an amino acid redox process; 3) an Fe-centered redox process (i.e., $Fe^{IV/III}$).

ET reactions involving the macrocycle of an Fe-porphyrin are relatively insensitive to changes in the iron axial ligands or solution composition.[21] In contrast, CVs recorded under different solution conditions indicated significant perturbations to **E**. First, voltammetry at constant ionic strength and variable pH (6-9) revealed that **E** varied with pH according to -(47 ± 7) mV/pH, indicating proton-coupled ET.[†] Indeed, proton-coupled ET is commonly observed for redox reactions in P450, consistent with a water-ligated heme and the sensitivity of Fe-centered ET reactions to the aquo/hydroxo

[†] Notably, the $Fe^{III/II}$ couple varied similarly with pH according to –(41 ± 3) mV/pH.

equilibrium as the pH is increased. Second, voltammetry in the presence of 500 mM imidazole (**Figure 6.3**) shows that **E** is inhibited. This is in accord with a redox reaction involving a water-ligated Fe^{III} heme: replacing the axial water with another ligand (imidazole in this case) would inhibit ferryl formation, as previously noted.[22]

To be rigorous, the possibility of an amino acid redox process for **E** must also be considered. Likely amino acid candidates for **E** would be tyrosine ($E^{o'}$ = 0.74 V vs. Ag/AgCl) or tryptophan ($E^{o'}$ = 0.85 V) oxidation.[23] Qualitatively, the peak intensities for **E** and the $Fe^{III/II}$ couple (**Figure 6.1**) are similar. CAM contains nine tyrosine and five tryptophan residues. Thus, based on stoichiometry one would expect the signal intensity of **E** compared to $Fe^{III/II}$ to be several times greater if **E** were due to tyrosine or tryptophan; however, this is not the case.

These results lead us to envision the reaction pathway depicted in **Scheme 6.1**. Beginning with Fe^{III}–OH_2 (resting state), oxidation of this species would lead to Fe^{IV}=O–H, which can decay in several ways. First, rapid reduction would regenerate the resting state, Fe^{III}–OH_2. Second, if reduction does not occur fast enough, oxidation of the surrounding protein environment by the ferryl species would likely result in damage to the protein. This is supported by the observation that voltammetry at slower scan rates, or scanning at room temperature (cf. 4°C), results in loss of the $Fe^{III/II}$ couple. Third, it is possible that if a ferryl species is indeed generated, it may be capable of oxidizing substrates and subsequently regenerating the Fe^{III}–OH_2 resting state.

To test if the putative Fe^{IV} species was catalytically active, we performed electrolysis reactions with CAM-DDAB films on graphite electrodes at 0.9 V.[‡] After trying several substrates (e.g., alkanes, styrene), we found that only thioanisole was oxidized by the system. The results listed in **Table 6.1** reveal that reactions with CAM produce significantly more methyl phenyl sulfoxide than control reactions without CAM.[§,24] Additional controls with catalase present,[**] and films made with bovine serum albumin instead of CAM,[††] further support a P450 Fe^{IV}-catalyzed oxidation reaction.

The fact that only thioanisole is oxidized by Fe^{IV}-CAM suggests that the Fe^{IV}=O–H in CAM (within the DDAB film) is not powerful enough to perform more challenging (alkene, alkane) oxidations. The energetics associated with P450-type oxidations can be described in terms of bond dissociation energies (*D(X–Y)*). *D(O–H)* of the electrochemically generated Fe^{IV}=O–H in CAM is related to the measured oxidation potential and the pK_a of the Fe^{III}–OH_2 species,[25,26]

$$D(O–H)\ (\text{kcal/mol}) = 23.06 \times [E^o(Fe^{IV/III})] + 1.37 \times pK_a(Fe^{III}–OH_2) + 57$$

Previous work used this approach to demonstrate that *D(O–H)* at pH 6 for compound I in chloroperoxidase is 98 kcal/mol, making it potent enough to oxidize alkanes (*D(C–H)* ~ 95 - 99 kcal/mol). By contrast, oxidation of thioanisole at the sulfur followed by oxygen rebound (*D(S–O)* ~ 87 kcal/mol) is a more facile reaction. Using the above equation, *D(O–H)* for Fe^{IV}=O–H in CAM in DDAB films at pH 6 is estimated to be 91 kcal/mol;[‡‡]

[‡] Electrolysis at more positive potentials resulted in loss of the protein response, and significantly decreased product formation. There are several possibilities for this, including film desorption and oxidative protein damage.

[§] Direct oxidation of thioanisole to the sulfoxide (E^o = 1.3 V vs. Ag/AgCl) at the electrode can also occur.

[**] Peroxide formed from water oxidation would also oxidize thioansiole.

[††] Films were made with BSA to rule out protein-mediated sequestering of the substrate into the film, followed by oxidation of the substrate directly at the electrode.

[‡‡] E^o at pH 6 is calculated to be 0.93 V vs. NHE; assumed Fe^{III}–OH_2 pK_a = 9

this provides an explanation for the inability of the system to perform reactions more demanding than thioanisole oxidation.

Experimental Methods

Protein Expression and Purification

Expression of CAM proceeded as previously described.[27]

Buffers for protein purification were as follows: Buffer A – 50 mM KP_i pH 7.2, 500 μM camphor, 2 mM DTT; Buffer B – 50 mM KP_i, 1 M KCl pH 7.2, 500 μM camphor, 2 mM DTT; Buffer C – 50 mM KP_i, 30% saturated ammonium sulfate (176 g/L) pH 7.2, 500 μM camphor, 2 mM DTT; Buffer D – 50 mM KP_i, 50 mM KCl pH 7.4, 2 mM DTT, 500 μM camphor. All buffers were filtered and degassed using a vacuum filter.

3 g of cell pellet cell were mixed with 9 mL of Buffer A containing 1 mM phenylmethylsulfonyl fluoride (PMSF, protease inhibitor). Cells were lysed by sonication. The lysate was centrifuged at 24,000 rpm for 30 min at 4°C. The resulting supernatant was filtered using a 0.45 μm filter and then injected onto a 20 mL DEAE Fast Flow column equilibrated with Buffer A. The protein was eluted with a linear gradient of 0 – 500 mM KCl in Buffer A. Fractions containing heme protein (visibly dark red) were pooled. The protein from the pooled fractions was precipitated with 60% ammonium sulfate overnight at 4°C. The mixture was then centrifuged at 12,500 rpm for 25 min at 4°C. The resulting pellet was resuspended in 2 - 5 mL of Buffer C. The solution was loaded onto a phenyl sepharose column equilibrated with Buffer C. Protein was eluted with a linear gradient of ammonium sulfate from 30 – 0 %. Fractions with Abs_{395}/Abs_{280}

> 1 were collected, pooled, and concentrated to ~ 1 mL with a Millipore Centriprep concentrator. The protein solution was injected onto a Sephacryl S200 column equilibrated with Buffer D. The protein was eluted with a constant flow of Buffer D. Fractions with Abs_{395}/Abs_{280} > 1.45 were pooled and concentrated using a Centriprep concentrator.

Preparation of Protein Films for Voltammetry

DDAB films were formed on BPG (0.07 cm^2) by depositing 5 μL of a 10 mM aqueous solution of DDAB on the electrode surface, followed by slow drying overnight. CAM was incorporated into the film by soaking the coated electrode in a solution of enzyme (~ 10 μM in 30 mM KP_i pH 7.4) for 30 minutes.

Voltammetry was conducted in a three-comaprtment cell with an Ag/AgCl reference electrode (BAS) and Pt wire counter electrode. The buffer was 50 mM KP_i / 20 mM KCl / pH 8. Buffers for variable pH measurements were kept at constant ionic strength by adding different proportions of the monobasic and dibasic forms of potassium phosphate salts such that the final concentration was always 50 mM; the resulting pH was determined with a pH electrode.

Voltammetry experiments at 4^oC were performed in an ice-cooled water bath.

Electrolysis and Thioanisole Oxidation

Electrodes for electrolysis were made from pyrolytic graphite plates, 1 cm x 2 cm, 0.025 cm thick. The plates were sanded, sonicated, and dried in air. 20 μL of a 10 mM solution of DDAB in ddH_2O were applied and dried on each side of the graphite plate. Protein was incorporated into the films by soaking the filmed plates in a 5 μM CAM solution for 30 minutes.

Electrolyses were performed in a three-neck flask at room temperature. Working and counter (Pt gauze) electrodes were placed directly into solution, while the reference electrode was housed in a Luggin capillary. Since preliminary experiments revealed that the presence of dioxygen in solution did not affect the electrolysis reaction, degassing the buffers was not necessary. Reactions were performed in 6 mL of 50 mM KP_i / 20 mM KCl / pH 8, with 100 μL thioanisole as substrate. Reactions were conducted at 0.9 V with stirring for 10 minutes. After the reaction, 5 uL of 1 mM 4-chloro-styrene were added (internal standard), followed by extraction of the solution with 0.5 mL $CHCl_3$. The $CHCl_3$ layer was removed and analyzed by GC/MS using an Innowax column. The product methyl phenyl sulfoxide was quantified relative to the internal standard using a calibration curve that was constructed by relating the ratio of the areas of the product to the internal standard.

Control reactions with BSA instead of CAM were conducted by soaking the filmed graphite plate in a solution that contained 6 μM BSA. Control reactions with catalase were performed by adding 2 μL of a 47 mg/mL catalase stock solution to the reaction.

The amount of CAM incorporated into the films from solution was estimated by taking the absorption spectrum of the solution before and after soaking the filmed electrode. The difference in Abs_{416} (ε_{416} = 115 $mM^{-1}cm^{-1}$) was used as the amount of CAM incorporated into the film. Typically, 2 – 2.5 nmols of CAM were incorporated into the films on the PG plates.

References

(1) Green, M. T.; Dawson, J. H.; Gray, H. B. *Science* **2004**, *304*, 1653-1656.

(2) Silaghi-Dumitrescu, R. *J. Biol. Inorg. Chem.* **2004**, *9*, 471-476.

(3) Guengerich, F. P. *Molecular Interventions* **2003**, *3*, 194-204.

(4) Glieder, A.; Farinas, E. T.; Arnold, F. H. *Nature Biotechnology* **2002**, *20*, 1135-1139.

(5) Dunn, A. R.; Dmochowski, I. J.; Winkler, J. R.; Gray, H. B. *J. Am. Chem. Soc.* **2003**, *125*, 12450-12456.

(6) Udit, A. K.; Hill, M. G.; Bittner, V. G.; Arnold, F. H.; Gray, H. B. *J. Am. Chem. Soc.* **2004**, *126*, 10218-10219.

(7) Sevrioukova, I. F.; Immoos, C. E.; Poulos, T. L.; Farmer, P. J. *Isr. J. Chem.* **2000**, *40*, 47-53.

(8) Munge, B.; Estavillo, C.; Schenkman, J. B.; Rusling, J. F. *ChemBioChem* **2003**, *4*, 82-89.

(9) Rusling, J. F. *Acc. Chem. Res.* **1998**, *31*, 363-369.

(10) Fleming, B. D.; Tian, Y.; Bell, S. G.; Wong, L.; Urlacher, V.; Hill, H. A. O. *Eur. J. Biochem.* **2003**, *270*, 4082-4088.

(11) Bayachou, M.; Boutros, J. A. *J. Am. Chem. Soc.* **2004**, *126*, 12722-12723.

(12) Zhang, Z.; Nassar, A.-E.; Lu, Z.; Schenkman, J. B.; Rusling, J. F. *J. Chem. Soc., Faraday Trans.* **1997**, *93*, 1769-1774.

(13) Immoos, C. E.; Chou, J.; Bayachou, M.; Blair, E.; Greaves, J.; Farmer, P. J. *J. Am. Chem. Soc.* **2004**, *126*, 4934-4942.

(14) Blair, E.; Greaves, J.; Farmer, P. J. *J. Am. Chem. Soc.* **2004**, *126*, 8632-8633.

(15) Egawa, T.; Proshlyakov, D. A.; Miki, H.; Makino, R.; Ogura, T.; Kitagawa, T.; Ishimura, Y. *J. Biol. Inorg. Chem.* **2001**, *6*, 46-54.

(16) Berglund, J.; Pascher, T.; Winkler, J. R.; Gray, H. B. *J. Am. Chem. Soc.* **1997**, *119*, 2464-2469.

(17) Kadish, K. M.; Caemelbecke, E. V.; D'Souza, F.; Medford, C. J.; Smith, K. M.; Tabard, A.; Guilard, R. *Inorg. Chem.* **1995**, *34*, 2984-2989.

(18) Kadish, K. M.; Caemelbecke, E. V.; Royal, G. In *The Porphyrin Handbook*; Guilard, R., Ed.; Academic Press: San Diego, CA, 2000; Vol. 8.

(19) Calderwood, T. S.; Lee, W. A.; Bruice, T. C. *J. Am. Chem. Soc.* **1985**, *107*, 8272-8273.

(20) Groves, J. T.; Gilbert, J. A. *Inorg. Chem.* **1986**, *25*, 123-125.

(21) Phillippi, M. A.; Shimomura, E. T.; Goff, H. M. *Inorg. Chem.* **1981**, *20*, 1322-1325.

(22) Immoos, C. E.; Di Bilio, A. J.; Cohen, M. S.; Van der Veer, W.; Gray, H. B.; Farmer, P. J. *Inorg. Chem.* **2004**, *43*, 3593-3596.

(23) Stubbe, J.; van der Donk, W. A. *Chem. Rev.* **1998**, *98*, 705-762.

(24) Baciocchi, E.; Gerini, M. F.; Lanzalunga, O.; Mancinelli, S. *Tetrahedron* **2002**, *58*, 8087-8093.

(25) Bordwell, F. G.; Cheng, J.; Ji, G.; Satish, A. V.; Zhang, X. *J. Am. Chem. Soc.* **1991**, *113*, 9790-9795.

(26) Mayer, J. M. *Acc. Chem. Res.* **1998**, *31*, 441-450.

(27) Gunsalus, I. C.; Wagner, G. C. *Methods Enzymol.* **1978**, *52*, 166-188.

Table 6.1. Results from bioelectrocatalytic oxidation of thioanisole using CAM in DDAB on graphite. Electrolyses were conducted at 0.9 V vs. Ag/AgCl for 10 minutes in 6 mL 50 mM KP_i / 20 mM KCl / pH 8 at ambient temperature.

Reaction	**nmols methyl phenyl sulfoxide**
CAM in DDAB on PG	416 ± 14
CAM in DDAB on PG + catalase	368 ± 20
DDAB on PG	130 ± 14
DDAB on PG + catalase	115 ± 20
BSA in DDAB on PG	92 ± 14

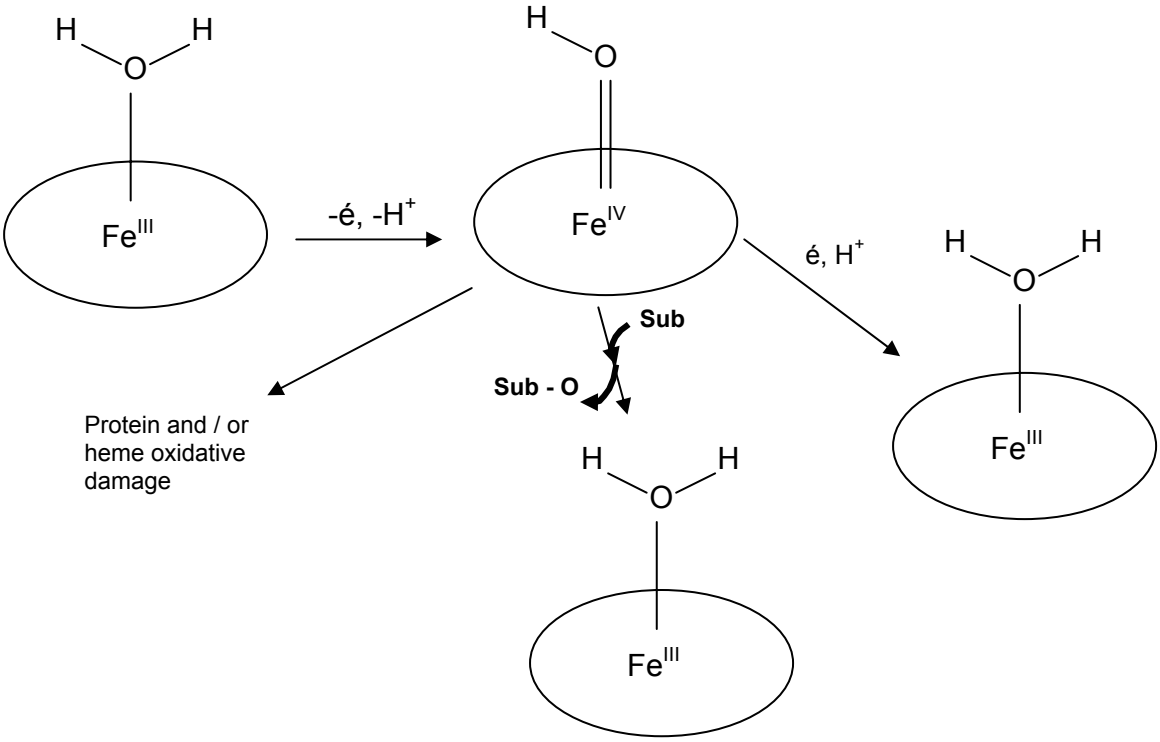
H
O
H
Fe^III
-é, -H^+
H
O
Fe^IV
é, H^+
H
O
H
Fe^III
Sub
Sub - O
Protein and / or
heme oxidative
damage
H
O
H
Fe^III

Scheme 6.1.

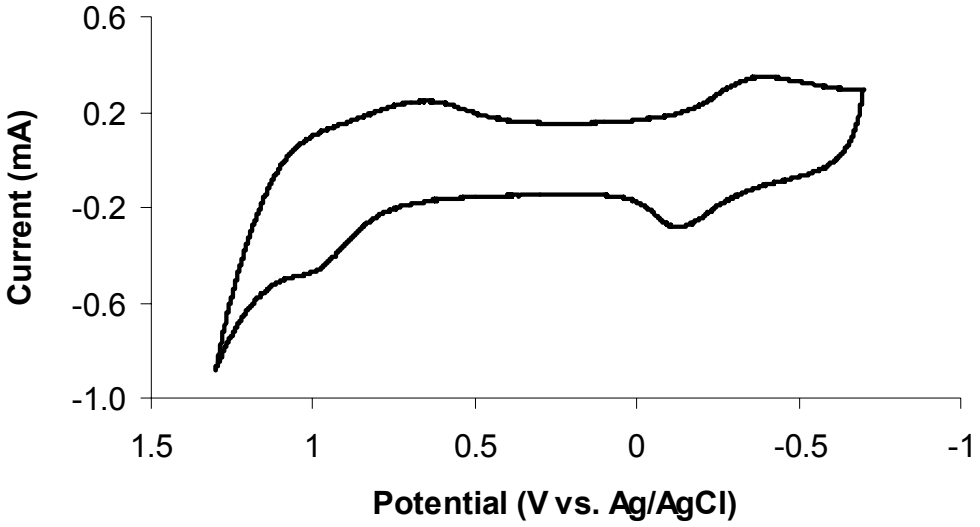

Figure 6.1. Cyclic voltammogram of CAM in DDAB on BPG (0.07 cm^2) at 50 V/s in 50 mM KP_i / 50 mM KCl / pH 8, at ambient temperature.

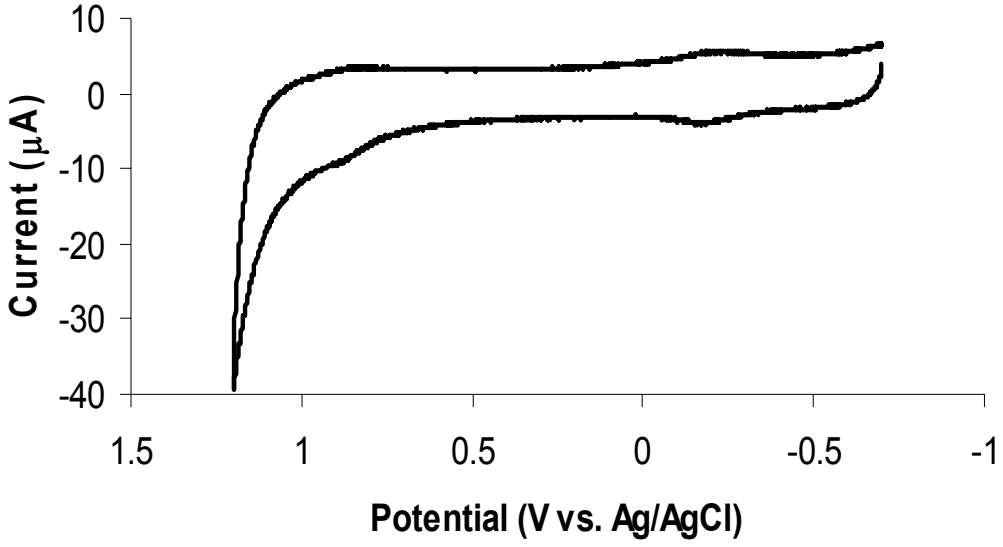

Figure 6.2. Cyclic voltammogram of CAM in DDAB on BPG (0.07 cm^2) at 1 V/s in 50 mM KP_i / 50 mM KCl / pH 8, at 4°C.

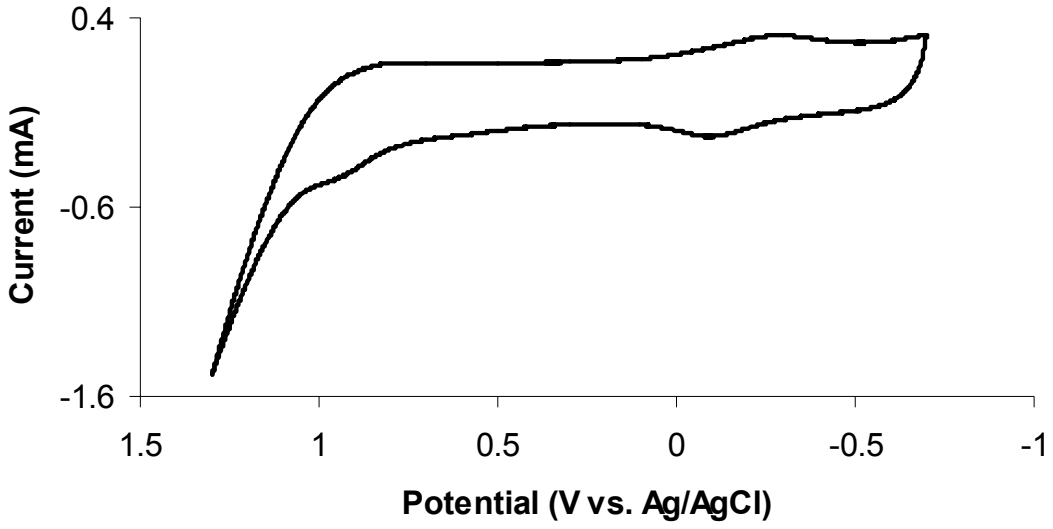

Figure 6.3. Cyclic voltammogram of CAM in DDAB on BPG (0.07 cm^2) at 50 V/s in 50 mM KP_i / 50 mM KCl / pH 8, at ambient temperature in the presence of 500 mM imidazole.

Chapter 7

Concluding Remarks

Abbreviations: BM3, cytochrome P450 BM3; ET, electron transfer;

This thesis details a series of electrochemical systems for cytochrome P450 BM3 (BM3). The primary question originally identified in **Chapter 1** is re-stated here: how can we efficiently deliver an electron from an external source, either from a soluble reductant or directly from an electrode, through the protein sheath and to the heme in a fashion that sufficiently mimics the native system in order to achieve catalytic substrate oxidation? Several different systems were tried with varying degrees of success. Over the course of developing the catalytic systems we discovered several intriguing mechanistic properties of P450, which we further explored and characterized electrochemically. What follows is a summary of what we have learned from our investigations of the different systems.

Summary

The cobaltocene-mediated system for BM3 is an example of an electrochemical mediator designed for a given application (**Chapter 2**). The new mediator was a significant finding, as only cobalt sepulchrate had previously been shown to be capable of supporting catalysis with BM3.[1] Not only was cobaltocene able to mediate catalytic turnover, but we also demonstrated that the molecular scaffold was readily manipulated to suit our purposes (in this case, the added carboxyls raised the redox potential and rendered the mediator water-soluble). Parallel studies with cobalt sepulchrate revealed that the two mediators are comparable in their ability to mediate BM3 bioelectrocatalysis. The primary drawback of cobaltocene, as with cobalt sepulchrate, is its reactivity towards

dioxygen: the active metal complex readily reduces dioxygen in solution, making peroxide and removing dioxygen (a co-substrate) from the reaction.

Next, we attempted to replace the BM3 reductase domain by anchoring the heme domain to an electrode with a pyrene tether (**Chapter 3**). Pyrene was attached to Cys^{387}, which is part of a short peptide (amino acids 382-400) that is proposed to be involved in inter-domain electron transfer (ET).[2] Indeed, the rapid heme reduction rates we achieved are fully consistent with the proposed ET pathway. In fact, heme reduction was so rapid that electrolysis conducted aerobically resulted in four-electron transfer to dioxygen, forming primarily water. Unfortunately, catalytic substrate oxidation was not observed. Several factors likely contribute to this: 1) protein aggregation on the electrode surface, as revealed by AFM; 2) an altered heme environment, as suggested by voltammetry in CO-saturated buffer; 3) unregulated ET that leads to direct dioxygen reduction instead of formation of active iron-oxo intermediates.

Extensive electrochemical characterization of BM3 was made by confining the protein within surfactant films on electrode surfaces (**Chapters 4 and 5**). DDAPSS films proved to be the most effective based on the stability of the voltammetric response. Catalytic activities included dioxygen reduction by Fe^{II} and reductive dechlorination by Fe^{I}; notably, this is the first reported instance of Fe^{I} in BM3. Perhaps most significant was our finding that wild type BM3 and mutant 1-12G display distinct redox properties. The BM3 literature contains many mutagenesis studies that alter the enzyme's substrate and product profiles, with little insight into how these mutations affect the biochemistry and redox chemistry. Our study demonstrates that wild type and 1-12G possess distinct heme environments within the DDAPSS film: the results support a mechanism for 1-12G

that features a longer lived iron-peroxy complex, which can justify 1-12G's superior ability to regio- and stereoselectively hydroxylate linear alkanes.

While useful for mechanistic studies, the surfactant film systems were not capable of supporting substrate oxidation. Several studies have shown that heme proteins within surfactant films retain their solution spectroscopic properties,[3,4] suggesting that they should be able to perform native enzyme chemistry. However, we have found that our P450-surfactant film electrodes are only competent for simple reduction reactions. One possibility for the lack of oxidative activity is that the substrates were not accessible by the protein. It is conceivable that the substrates preferentially partition into the film, or cannot enter the active site because the protein is in a closed conformation within the film. However, the ability of our systems to perform catalytic dechlorination of trichloroacetic acid argues against this point. A second and perhaps more likely possibility is that our systems are not able to reach active iron-oxo intermediates, as direct reduction to peroxide or water is very rapid.

In **Chapter 6**, we utilized the surfactant film methodology to electrochemically access a high-potential redox couple (**E)** in P450. Electrochemical characterization suggests that **E** represents the first observation of a high-valent species in P450, formally a one-electron oxidation of the Fe^{III} resting state. Our data indicate the oxidation reaction is occurring at the metal center, suggesting an $Fe^{IV/III}$ couple. **E** was found capable of catalyzing thioansiole oxidation. The inability of **E** to perform reactions other than S-oxidation suggests that it is not potent enough (within the surfactant film) to catalyze more challenging oxidations. This is not surprising since compound I, the putative

oxidizing species in P450, is two oxidation states higher than Fe^{III} heme, while **E** is only one oxidation state higher.

Perspectives

While electrochemistry in surfactant films does not appear to be viable for bulk oxidation reactions, it has proven to be an invaluable analytical tool. Our work on these systems has shed considerable light on the mechanisms in heme-thiolate proteins (wild type and mutant BM3 in **Chapter 5**, cytochrome P450 CAM in **Chapter 6**, nitric oxide synthase in **Appendix A**). Future endeavors into P450-surfactant film voltammetry should be aimed at spectroelectrochemical experiments, using transparent electrodes to observe the spectral properties of the different heme oxidation states. In particular, it is imperative to provide spectroscopic evidence to confirm the $Fe^{II/I}$ and $Fe^{IV/III}$ redox couples. This can be done with absorption spectroscopy by looking at changes in the heme Soret band during redox cycling, and comparing the results to iron-porphyrin model complexes with known spectra.[5,6]

Only the mediator system was capable of catalytic substrate (C–H) oxidation, while utilizing the holo protein yielded results far superior to the heme domain. These findings are not surprising. Using a soluble mediator with the holo protein most closely resembles the native system, which immediately alludes to two key points. First, allowing the protein to remain in solution permits retention of its native fold and dynamics, which are likely key determinants for catalytic activity. Indeed, this is an inherent failing of the systems that confined the protein to the electrode surface, which may restrict necessary conformational changes for catalysis.[7]

Second, the role of the reductase domain in regulating ET to the heme cannot be underestimated. The pyrene system most clearly demonstrates this point: although we appeared to successfully replace the reductase with an electrode for ET to the heme, the loss of regulation provided by the reductase resulted in heme reduction that was too rapid. As a result, instead of activating dioxygen for subsequent oxygen atom transfer, we achieved rapid four-electron reduction of dioxygen to water.

Of the various challenges associated with using P450s as *in vitro* catalysts, the requirement for reducing equivalents remains the greatest obstacle. Utilizing an electrode is still the simplest and most cost-effective way of replacing NADPH in the catalytic cycle of BM3. The results presented herein indicate that the most promising system for large-scale biocatalysis would be to utilize a small molecule electrochemical mediator with the holo protein. The key is to find a mediator that: 1) is capable of participating in rapid and reversible ET with both the electrode and enzyme; 2) can be electrochemically reduced at moderate potentials, such that the electrode does not need to be polarized too negatively (which would result in solvent reduction, and possibly other side reactions); 3) does not readily reduce dioxygen in solution; 4) is easily manipulated synthetically, permitting versatility (adapt it to different solution conditions, provide a range of redox potentials, etc.). These criteria are in accord with those previously presented for bioelectrochemical mediators.[8]

Future endeavors into this problem should focus on mediators that participate in hydride transfer, such as quinones and certain organometallic complexes. Analogous to cobaltocene, these molecules would have the advantage of synthetic malleability, while displaying significantly decreased reactivity towards dioxygen. Indeed, a hydride

transfer mediator would more closely mimic the native system since NADPH also functions in this manner. Some success with a hydride transfer mediator has already been demonstrated by Witholt's group: they utilized a rhodium complex that was capable of regenerating the flavin cofactors of styrene monooxygenase, resulting in catalytic substrate turnover.[9] Mediator turnover was also shown to be highly coupled to substrate turnover (60%, cf. 2% for cobaltocene), with few electrons wasted on direct reduction of dioxygen in solution. Conceivably, a similar mediator for BM3 would result in a system that could function aerobically at acceptable rates for *in vitro* electrode-driven catalytic substrate oxidation.

References

(1) Estabrook, R.; Faulkner, K.; Shet, M.; Fisher, C. *Methods Enzymol.* **1996**, *272*, 44-51.

(2) Sevrioukova, I. F.; Immoos, C. E.; Poulos, T. L.; Farmer, P. J. *Isr. J. Chem.* **2000**, *40*, 47-53.

(3) Ma, H.; Hu, N. *Anal. Lett.* **2001**, *34*, 339-361.

(4) Blair, E.; Greaves, J.; Farmer, P. J. *J. Am. Chem. Soc.* **2004**, *126*, 8632-8633.

(5) Hawkridge, F. M.; Taniguchi, I. In *The Porphyrin Handbook*; Kadish, K. M., Smith, K. M., Guilard, R., Eds.; Academic Press: San Diego, CA, 2000; Vol. 8.

(6) Kadish, K. M.; Caemelbecke, E. V.; Royal, G. In *The Porphyrin Handbook*; Kadish, K. M., Smith, K. M., Guilard, R., Eds.; Academic Press: San Diego, CA, 2000; Vol. 8.

(7) Poulos, T. L. *Proc. Natl. Acad. Sci.* **2003**, *100*, 13121-13122.

(8) Bartlett, P.; Tebbutt, P.; Whitaker, R. *Prog. Reaction Kinetics* **1991**, *16*, 55-155.

(9) Hollman, F.; Lin, P.-C.; Witholt, B.; Schmid, A. *J. Am. Chem. Soc.* **2003**, *125*, 8209-8217.

Appendix A

Redox Couples of Inducible Nitric Oxide Synthase

Acknowledgements: This work was in collaboration with W. Belliston-Bittner, E. C. Glazer, and Y. H. L. Nguyen from Caltech, M. G. Hill from Occidental College, M. A. Marletta from U.C. Berkeley, and D. B. Goodin from The Scripps Research Institute. We thank NIH (HBG, DBG), NSERC (Canada) (AKU), the David and Lucile Packard Foundation (MGH), and the Parsons Foundation (WBB) for research support; S. Luzzi (U.C. Berkeley) for assistance with protein expression and purification.

Abstract

We report direct electrochemistry of the iNOS heme domain in a DDAB film on the surface of a basal plane graphite electrode. Cyclic voltammetry reveals $Fe^{III/II}$ and $Fe^{II/I}$ couples at -191 and -1049 mV (vs. Ag/AgCl). Added ligands imidazole and carbon monoxide shift the $Fe^{III/II}$ potential by +20 and +62 mV, while the addition of dioxygen results in large catalytic waves at the onset of Fe^{III} reduction. Voltammetry at higher scan rates reveals that the $Fe^{III/II}$ cathodic peak can be resolved into two components, which are attributable to $Fe^{III/II}$ couples of five- and six-coordinate hemes. Scan rate analyses of the five-coordinate iNOS heme indicate an ET rate constant (k^o) of $370 \pm 20\ s^{-1}$.

Abbreviations: NO, nitric oxide; NOS, nitric oxide synthase; ET, electron transfer; H_4B, tetrahydrobiopterin; iNOS, inducible nitric oxide synthase; DDAB, didodecyldimethylammonium bromide; BPG, basal plane graphite; nNOS, neuronal nitric oxide synthase

Introduction

The critical role of nitric oxide (NO) in cellular signaling is now firmly established.[1] In higher animals, NO is synthesized by nitric oxide synthase (NOS), which converts L-arginine to citrulline and NO with NADPH and O_2 as co-substrates.[2] The enzyme consists of a reductase domain where reducing equivalents from NADPH are shuttled through bound flavins FAD and FMN, a calmodulin binding region that controls electron transfer (ET) to the heme, and a heme domain that contains a cysteine-ligated heme and tetrahydrobiopterin (H_4B). Investigations reported here utilize the heme domain of inducible NOS (iNOS), an immune system isoform implicated in a number of diseases in humans.[3]

The complexity of NOS and its impact on human health have thrust work on the NOS mechanism into the spotlight. It is well established that the catalytic cycle involves two turnovers of the enzyme. The first turnover converts L-arginine to N-hydroxyarginine: although envisioned as a P450-like hydroxylation, the reaction is dependent on one-electron oxidation of H_4B.[4] The second turnover is thought to involve a ferric peroxide nucleophile, but H_4B is also required for this turnover in an as yet undetermined role. Although many details of the NOS mechanism remain to be elucidated, it is certain that ET reactions are key steps in the catalytic cycle.

Direct electrochemistry of the iNOS heme domain can be achieved by confining the protein in didodecyldimethylammonium bromide (DDAB) films on the surface of basal plane graphite electrodes (BPG).[5,6] We report reduction potentials for $Fe^{III/II}$ and $Fe^{II/I}$ couples, $Fe^{III/II}$ ET kinetics, catalytic reduction of dioxygen, and evidence for water-free and water-bound forms of the iNOS heme based on scan rate and pH dependence data.

Results and Discussion

DDAB films were formed on BPG (0.07 cm^2) by depositing 5 μL of a 10 mM aqueous solution of DDAB on the electrode surface, followed by slow drying overnight. iNOS was incorporated into the film by soaking the coated electrode in a solution of enzyme (~ 20 μM in 50 mM KP_i, 50 mM KCl, pH 7 buffer) for 30 minutes. A voltammogram of iNOS in DDAB on BPG is shown in **Figure A.1**. We have assigned E_1 (-191 mV) and E_2 (-1049 mV) to heme $Fe^{III/II}$ and $Fe^{II/I}$ couples, consistent with other studies of heme proteins in DDAB films.[7,8] Notably, a couple similar to E_2 was observed for neuronal nitric oxide synthase (nNOS), but was not assigned.[5] Our assignments of E_1 and E_2 are supported by voltammetry in the presence of carbon monoxide: E_1 shifts approximately +62 mV (consistent with other studies),[9,10] while E_2 is not observed (presumably beyond the solvent window). For comparison, redox titrations of iNOS in its resting state (6-coordinate heme, low spin) conducted in solution yield a potential of -544 mV (vs. Ag/AgCl) for $Fe^{III/II}$.[11] As previously suggested, local electrostatic effects likely contribute to the altered potential on the electrode surface.[12]

Besides CO, other molecules in solution also bind the heme. In the presence of 500 mM imidazole, E_1 shifts +20 mV. When dioxygen is added, large catalytic reduction currents at the onset of E_1 are observed (**Figure A.2**).

For E_1, the peak current is linear with scan rate (surface-bound) up to 16.7 V/s, after which it is linear with the square root of the scan rate (diffusive).[13] This behavior is characteristic of thin film electrochemistry and indicates finite diffusion of the protein within the film.[14] Thus, up to 16.7 V/s, we treated the redox system as surface-confined.

Closer inspection of **Figure A.1** reveals that the E_1 cathodic wave is slightly broader than the other waves. Voltammetry at variable scan rates allowed us to resolve this peak into two distinct cathodic processes, $E_{p,c}(1)$ and $E_{p,c}(2)$. **Figure A.3a** shows voltammograms recorded in pH 7 buffer at different scan rates. At high and low scan rates (8 vs. 0.05 V/s) only one cathodic peak ($E_{p,c}(1)$ vs. $E_{p,c}(2)$) is present, while both cathodic processes are observed at intermediate (1 V/s) scan rates. In addition to being scan rate dependent, these cathodic processes are also pH dependent. At pH 5 and 1 V/s (**Figure A.3b**), only one cathodic peak ($E_{p,c}(1)$) is present. Conversely, at pH 9 two distinct cathodic peaks are visible at 1 V/s (**Figure A.3c**); in fact, at higher pH, $E_{p,c}(2)$ is even more prominent. Notably, during the first cathodic sweep $E_{p,c}(2)$ predominates, while in subsequent cathodic sweeps both $E_{p,c}(1)$ and $E_{p,c}(2)$ are resolved.

This pH and scan rate dependence led us to believe that the iNOS heme axial water ligand is involved in an equilibrium that gives rise to $E_{p,c}(1)$ and $E_{p,c}(2)$ (**Scheme A.1**). At pH 7 and 1 V/s, the first cathodic sweep results in $E_{p,c}(2)$: this correlates with initial reduction of $Fe^{III} - OH_2$. The lability of the $Fe^{II} - OH_2$ bond results in rapid conversion to a five-coordinate heme.[15,16] Oxidation of Fe^{II} to Fe^{III}, followed by a second

cathodic sweep at intermediate scan rates (1 V/s, **Figure A.3a**) gives rise to two reduction peaks, corresponding to reduction of water-free ($E_{p,c}(1)$) and water-bound ($E_{p,c}(2)$) Fe^{III} hemes.

Our interpretation is supported by the following observations. First, $E_{p,c}(1)$ and $E_{p,c}(2)$ differ by approximately 133 ± 9 mV, a value consistent with the potential difference between five- and six-coordinate iNOS hemes.[11] Second, voltammetry at low pH results in a single cathodic peak attributable to $E_{p,c}(1)$. Under acidic conditions, disruption of hydrogen bonding in the heme pocket likely leads to dissociation of the axial water, resulting in a five-coordinate heme. Third, voltammetry at high pH (**Figure A.3c**), where the axial water is partially deprotonated, shows that $E_{p,c}(2)$ is more prominent. It is expected that hydroxide will have greater affinity for the cationic metal center, thereby shifting the cathodic peak distribution further to $E_{p,c}(2)$. Fourth, voltammetry with imidazole present yields a single cathodic process, consistent with constant heme ligation as it cycles between oxidation states (**Figure A.4**).[17]

The dependence of the cathodic peak distribution on scan rate can be explained in terms of **Scheme A.1**. At high scan rates, after oxidation of Fe^{II}, reduction of water-free Fe^{III} occurs faster than water ligation to Fe^{III}, yielding only $E_{p,c}(1)$. Conversely, scanning slowly allows water enough time to ligate Fe^{III} before reduction, shifting the cathodic peak distribution to $E_{p,c}(2)$. Thus, intermediate scan rates yield both $E_{p,c}(1)$ and $E_{p,c}(2)$.

Using $E_{p,c}(1)$, k^o ($\Delta G^o = 0$) for ET to the five-coordinate heme evaluated at 16.7 V/s and pH 7 is 370 ± 20 s^{-1}.[18] With this value, we used digital simulation to effectively model the experimental results in **Figure A.3a** (see Experimental Methods). From the simulation, we estimated values for $\boldsymbol{k_1}$, $\boldsymbol{k_2}$, and $\boldsymbol{k_3}$ in **Scheme A.1** to be 1 s^{-1}, 0.5 s^{-1}, and >

100 s^{-1}. As expected,[15,16] water dissociation from Fe^{II} is rapid (k_3), while the kinetics of the Fe^{III} equilibrium with water (k_1, k_2) appear slow. In the catalytic cycle of iNOS, the first ET event is proposed to be the rate-limiting step for substrate turnover, occurring at 1 s^{-1}.[19] Based on our simulation, we suggest that water dissociation from Fe^{III} may function as a potential gating mechanism for the catalytic cycle. Although speculative for iNOS, water-gated ET is consistent with what is known for the similar cytochromes P450.

Proton-coupled ET was observed for nNOS in DDAB films as demonstrated by the variation of $E_{1/2}$ with pH.[5] For comparison, we performed voltammetry on iNOS at 200 mV/s and plotted the variation of $E_{1/2}$ with pH for E_1 (**Figure A.3d**).[20] The data reveal no variation of $E_{1/2}$ for pH < 5, implying simple conversion of five-coordinate Fe^{III} to Fe^{II}. At pH > 7, $E_{1/2}$ varies linearly with pH according to -53 mV/pH unit, as is often found for heme proteins.[21,22] The observation of proton-coupled ET in a pH range where the heme is water-ligated further underscores that the heme axial water ligand plays a significant role in iNOS ET.

Experimental Methods

Protein Expression and Purification

iNOS heme domain was expressed and purified as previously described[23] with the following exceptions. Cells expressing protein were subjected to two rounds of chemical lysis. Cell pellets were resuspended in 40 mL of B-PER lysis buffer (Pierce) with 10 μg/mL benzamidine, 5 μg/mL leupeptin, 1 μg/mL each pepstatin, antipain, and chymotrypsin, ~ 500 μM Pefabloc (Roche), 100 μg/mL DNAse, 100 μg/mL RNAse, ~

500 μg/mL lysozyme, and 20 mM imidazole per liter of cells and shaken for one hour at 4°C. The lysate was then spun down and the supernatant was loaded directly onto a nickel column (5 mL HisTrap, Amersham). The loaded column was washed with 20 column volumes of 20 mM imidazole in 50 mM NaP_i/300 mM NaCl/pH 8. The protein was eluted with 150 mM imidazole, concentrated to ~ 3 mL over an Amicon Ultra filtration device (10,000 MWCO, Millipore) and loaded onto a gel filtration column as previously described.[23] The anion exchange column was omitted when ≥ 95% purity was confirmed by UV-visible spectroscopy and gel electrophoresis.

Electrode Preparation and Voltammetry

Electrodes for voltammetry (0.07 cm^2) were made using the basal plane of pyrolytic graphite. The surfaces were prepared by sanding briefly with 600-grit sandpaper, followed by polishing with 0.3 and 0.05 μm alumina slurries. The electrodes were then sonicated and dried in air. DDAB films were formed by placing 5 μL of 10 mM DDAB in water on the surface of the electrodes, followed by slow drying in air overnight. iNOS was incorporated into the film by soaking the DDAB-filmed electrode in a solution of enzyme (~ 20 μM in 50 mM KP_i pH 7 buffer) for 30 minutes, followed by gentle rinsing with ddH_2O.

A CH Instruments Electrochemical Workstation system was used for the reactions. Voltammetry experiments were performed in a three-compartment cell, using a platinum wire auxiliary and a Ag/AgCl reference electrode (BAS). All experiments were performed under argon in thoroughly degassed buffer (50 mM KP_i, 50 mM KCl, pH 7) unless otherwise stated.

Digital Simulations

Simulations were performed with software from the CH Instruments Electrochemical Workstation. A square scheme was used for the model:

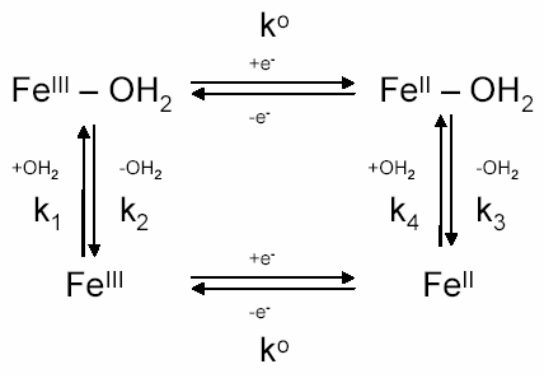

k^o for the five-coordinate heme ET reaction was experimentally determined to be 370 s^{-1}. For the six-coordinate heme ET reaction, a k^o value of 10 s^{-1} (consistent with previous observations for NOSs[24]) resulted in the best simulated voltammograms. A surface-confined system was modeled with the following parameters: capacitance = 4 μF, surface coverage = 5 x 10^{-11} mol/cm^2, electrode area = 0.07 cm^2, $E^o(Fe^{III/II})$ = -150 mV, $E^o(Fe^{III/II} – OH_2)$ = -250 mV. Values for k_1, k_2, and k_3 were entered into the simulation until a single set of rate constants was found that could adequately reproduce the experimentally derived voltammograms at 0.05, 1, and 8 V/s at pH 7 (**Figure A.3a**). For each simulation, k_4 was determined by the software. Using this procedure, values for k_1, k_2, and k_3 of 1 s^{-1}, 0.5 s^{-1}, and 100 s^{-1}, respectively, were able to accurately model the voltammograms in **Figure A.3a** (see **Figure A.5**). Notably, the simulation was insensitive for values of $k_3 > 100$ s^{-1}.

References and Notes

(1) Culotta, E.; Koshland, D. E. *Science* **1992**, *258*, 1862-1865.

(2) Alderton, W. K.; Cooper, C. E.; Knowles, R. G. *Biochemical J.* **2001**, *357*, 593-615.

(3) Aktan, F. *Life Sciences* **2003**, *75*, 639-657.

(4) Hurshman, A. R.; Krebs, C.; Edmondson, D. E.; Marletta, M. A. *Biochemistry* **2003**, *42*, 13287-13303.

(5) Direct electrochemistry of the neuronal nitric oxide synthase heme domain utilizing the surfactant film methodology (M. Bayachou, J.A. Boutros, *J. Am. Chem. Soc.* **2004**, 126, 12722) has been reported. Square wave voltammetry confirms that the $Fe^{III/II}$ potential shifts in the presence of H_4B. A proton-coupled ET mechanism accounts for the observed pH dependence of the potential.

(6) Rusling, J. F. *Acc. Chem. Res.* **1998**, *31*, 363-369.

(7) Immoos, C. E.; Chou, J.; Bayachou, M.; Blair, E.; Greaves, J.; Farmer, P. J. *J. Am. Chem. Soc.* **2004**, *126*, 4934-4942.

(8) Ma, H.; Hu, N. *Anal. Lett.* **2001**, *34*, 339-361.

(9) Zhang, Z.; Nassar, A.-E.; Lu, Z.; Schenkman, J. B.; Rusling, J. F. *J. Chem. Soc., Faraday Trans.* **1997**, *93*, 1769-1774.

(10) Fleming, B. D.; Tian, Y.; Bell, S. G.; Wong, L.; Urlacher, V.; Hill, H. A. O. *Eur. J. Biochem.* **2003**, *270*, 4082-4088.

(11) Presta, A.; Weber-Main, A. M.; Stankovich, M. T.; Stuehr, D. J. *J. Am. Chem. Soc.* **1998**, *120*, 9460-9465.

(12) Lvov, Y. M.; Lu, Z.; Schenkman, J. B.; Zu, X.; Rusling, J. F. *J. Am. Chem. Soc.* **1998**, *120*, 4073-4080.

(13) Bard, A. J.; Faulkner, L. R. *Electrochemical Methods*; Second Edition; John Wiley & Sons, Inc.: New York, 2001.

(14) Lin, R.; Immoos, C. E.; Farmer, P. J. *J. Biol. Inorg. Chem.* **2000**, *5*, 738-747.

(15) Wilker, J. J.; Dmochowski, I. J.; Dawson, J. H.; Winkler, J. R.; Gray, H. B. *Angew. Chem. Int. Ed.* **1999**, *38*, 90-92.

(16) Crutchley, R. J.; Ellis, W. R.; Gray, H. B. *J. Am. Chem. Soc.* **1985**, *107*, 5002-5004.

(17) Dawson, J. H.; Andersson, L. A.; Sono, M. *J. Biol. Chem.* **1983**, *258*, 13637-13645.

(18) Laviron, E. *J. Electroanal. Chem.* **1979**, *101*, 19-28.

(19) Presta, A.; Siddhanta, U.; Wu, C.; Sennequier, N.; Huang, L.; Abu-Soud, H. M.; Erzurum, S.; Stuehr, D. J. *Biochemistry* **1998**, *37*, 298-310.

(20) At 200 mV/s, the two cathodic peaks in E_1 collapse into a single peak, yielding a potential representative of the population distribution between $E_{p,c}(1)$ and $E_{p,c}(2)$ and permitting us to estimate a midpoint potential ($E_{1/2}$) for E_1.

(21) Munge, B.; Estavillo, C.; Schenkman, J. B.; Rusling, J. F. *ChemBioChem* **2003**, *4*, 82-89.

(22) Aguey-Zinsou, K.; Bernhardt, P. V.; Voss, J. J. D.; Slessor, K. E. *Chem. Commun.* **2003**, 418-419.

(23) Hurshman, A. R.; Marletta, M. A. *Biochemistry* **2002**, *41*, 3439-3456.

(24) Stuehr, D. J.; Santolini, J.; Wang, Z.; Wei, C.; Adak, S. *J. Biol. Chem.* **2004**, *279*, 36167-36170.

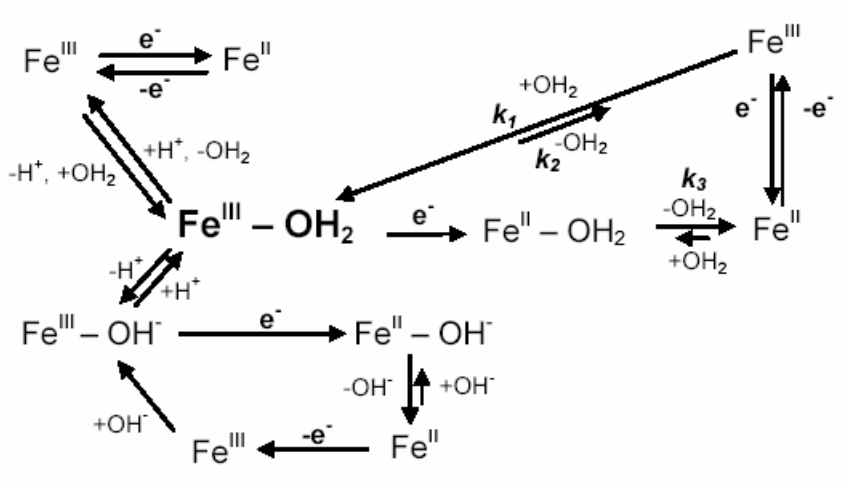
Fe^III
e^-
Fe^II
-e^-
+OH2
k1
k2
-OH2
Fe^III
e^-
-e^-
+H^+, -OH2
-H^+, +OH2
k3
-OH2
+OH2
Fe^III – OH2
e^-
Fe^II – OH2
Fe^II
-H^+
+H^+
Fe^III – OH^-
e^-
Fe^II – OH^-
-OH^-
+OH^-
+OH^-
Fe^III
-e^-
Fe^II

Scheme A.1.

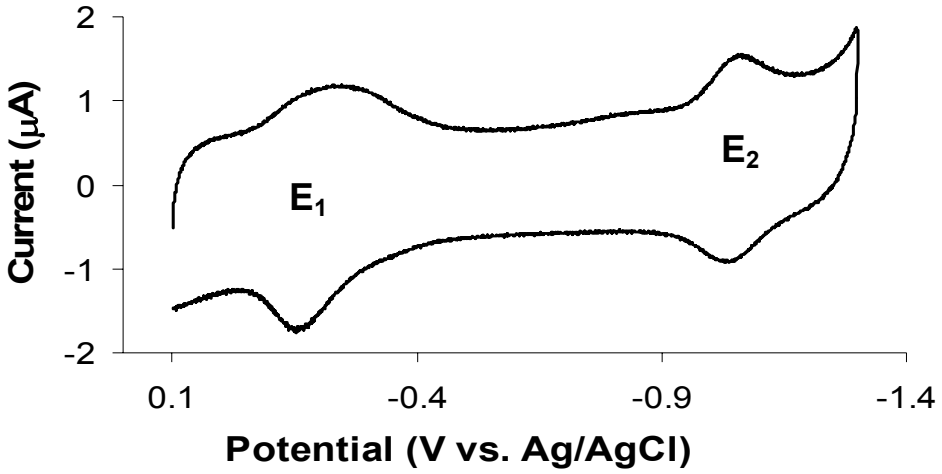

Figure A.1. Cyclic voltammogram of iNOS in DDAB on BPG (0.07 cm^2) at 200 mV/s in 50 mM KP_i/50 mM KCl/pH7.

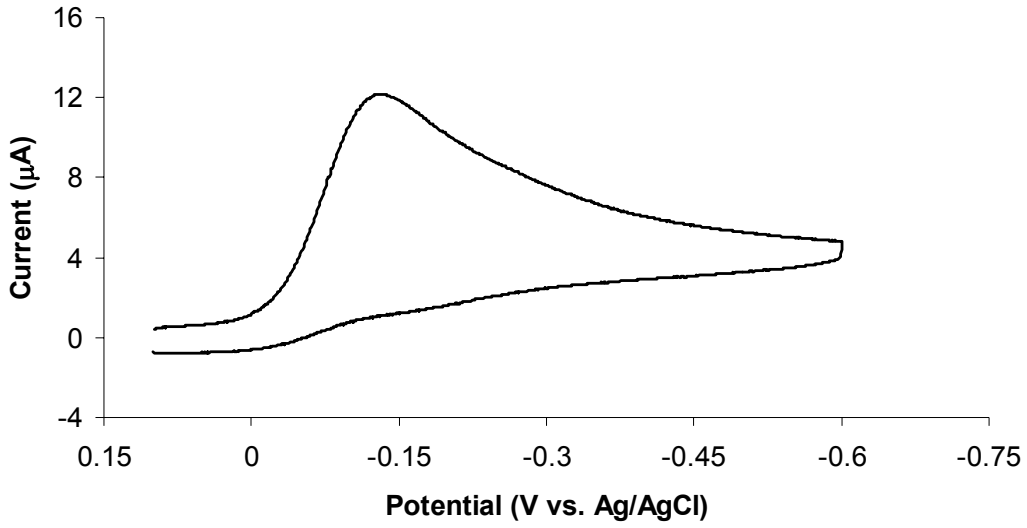

Figure A.2. Cyclic voltammogram of iNOS in DDAB on BPG at 200 mV/s in 50 mM KP_i/50 mM KCl/pH 7 and 94 μM O_2.

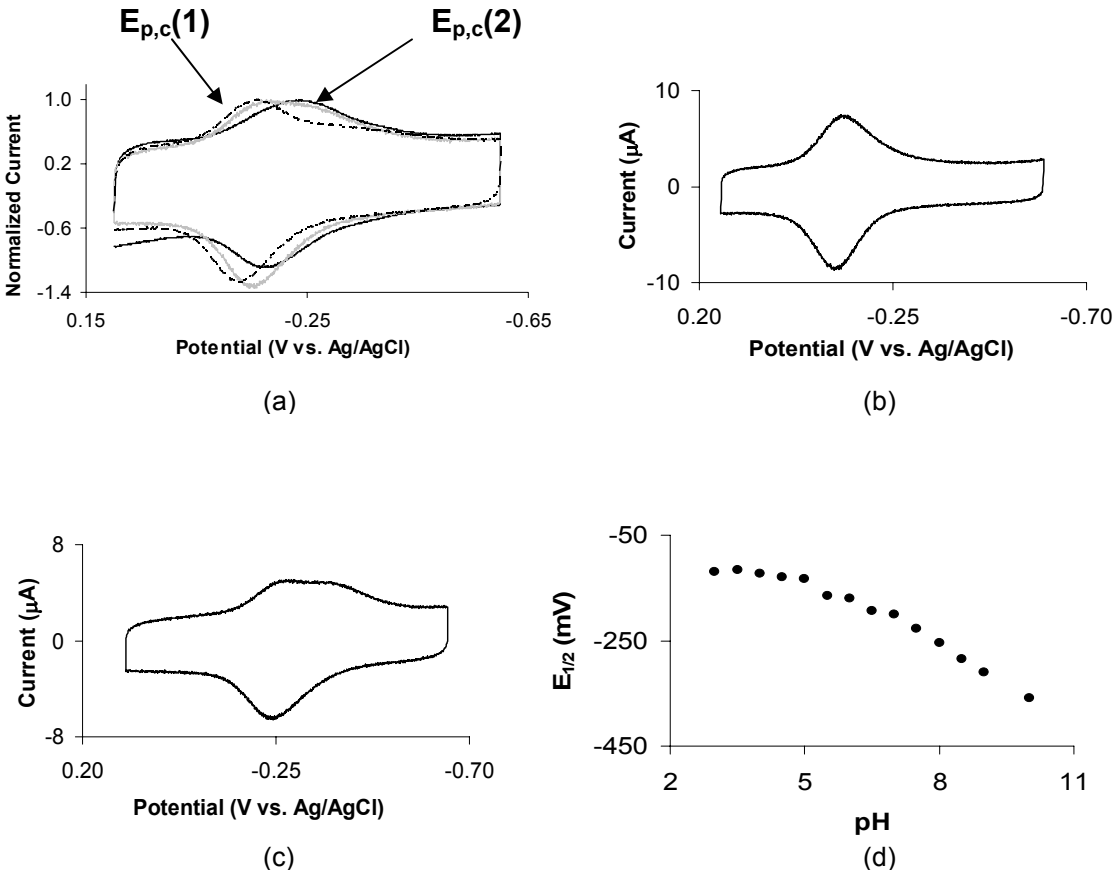

Figure A.3. Cyclic voltammograms of iNOS in DDAB on BPG in 50 mM KP_i/50 mM KCl a) at 0.05 (black), 1 (gray), and 8 (dashed) V/s, pH 7; b) at 1 V/s, pH 5; c) at 1 V/s, pH 9. d) Variation of the average $Fe^{III/II}$ midpoint potential with pH at 200 mV/s.

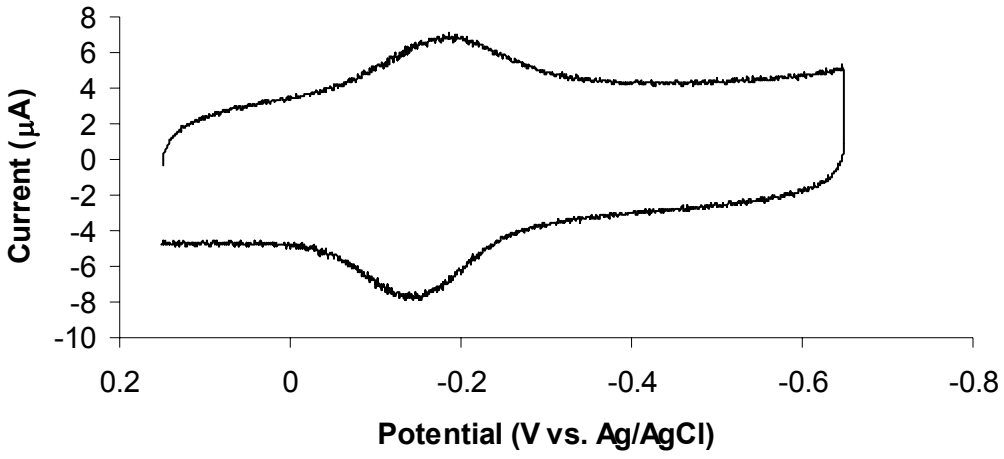

Figure A.4. Cyclic voltammogram of iNOS in DDAB on BPG in 50 mM KPi/50 mM KCl/pH 7 and 500 mM imidazole at 1 V/s. Note that only a single cathodic process is observed (cf. **Figure A.3a**).

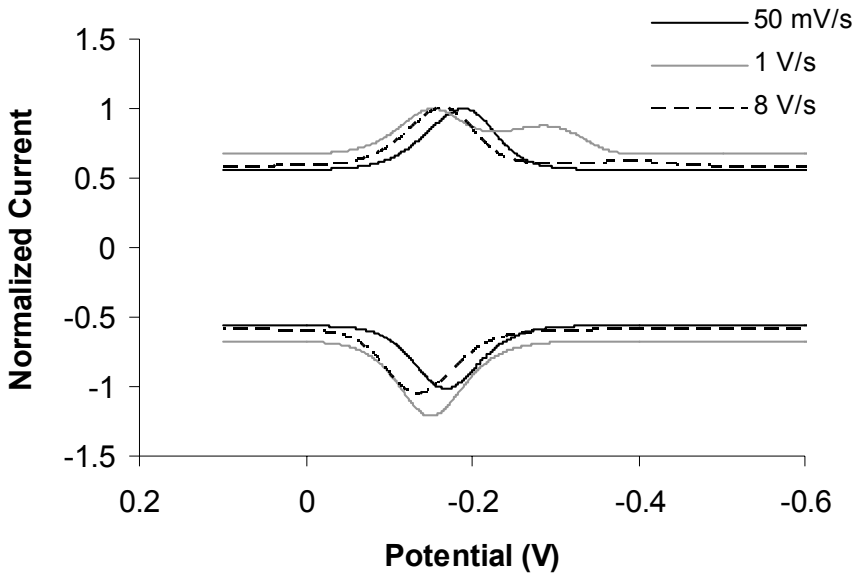

Figure A.5. Digitally simulated voltammograms at a) 0.05 (black), b) 1 (gray), and c) 8 (dashed) V/s for iNOS in DDAB films. Simulation details are listed in the Experimental Methods.